TAMPEREEN TEKNILLINEN YLIOPISTO
TAMPERE UNIVERSITY OF TECHNOLOGY

SAMULI TUOMINEN

PRINTED TEMPORARY TRANSFER TATTOOS FOR SKIN-MOUNTED ELECTRONICS

Master of Science Thesis

Examiner: Professor Matti Mäntysalo
Examiner and topic approved by the Dean of the Faculty of Computing and Electrical Engineering on 28th of March 2018

ABSTRACT

SAMULI TUOMINEN: Printed Temporary Transfer Tattoos for Skin-Mounted Electronics
Tampere University of Technology
Master of Science Thesis, 90 pages, 4 Appendix pages
September 2018
Master's Degree Programme in Electrical Engineering
Major: Electronics
Examiner: Professor Matti Mäntysalo

Keywords: printed electronics, release film, screen printing, skin-mounted electronics, stretchable interconnect, temporary transfer tattoo, thin film

Skin-mounted electronics has developed from thick bandage-like structures to thin tattoo-like films in the past years. However, the properties of the tattoos still need improvement with stretchability, transparency, conformability, conductivity and biocompatibility being the most important ones. In addition, the manufacturing methods of the tattoos need development. Overall, improvement of the tattoos and development of the manufacturing methods need development of the used materials.

The objective in this thesis is to fabricate and analyze temporary transfer tattoos. The aim is to achieve the mentioned properties by environmentally friendly, cheap and additive manufacturing methods. First, the thesis discusses theoretical background of stretchable interconnects and skin-mounted electronics. Stretchable interconnects are then printed on temporary transfer tattoo paper and the interconnects are electrically and mechanically characterized. Mechanical characterization and some of the electrical characterizations are done on the skin and in a mechanical test instrument. In addition, the tattoo paper and materials theoretically suitable for manufacturing the tattoos with the desirable properties are characterized.

The acquired sheet resistance of the tattoos was 41.7 mΩ/□. The maximum strain before breaking was 19.4 %, but the reliability of the result was not confirmed. The printed interconnects were not transparent due to the material that was used. Thickness of the tattoos was not measured, but one theoretical calculation resulted in a 1.9 μm thickness. Nevertheless, slight conforming of the tattoos was visually observed. The conductive inks proved to be difficult to handle and they need more development. In addition, the tattoo paper was not suitable for fabricating the tattoos due to the low heat resistance of the paper. Finally, the stretching test setups are not suitable for thin tattoos because of the firm contact that is required between the tattoos and the test instruments to obtain the results.

TIIVISTELMÄ

SAMULI TUOMINEN: Painetut siirtokuvatatuoinnit iholle kiinnitettävään elektroniikkaan
Tampereen teknillinen yliopisto
Diplomityö, 90 sivua, 4 liitesivua
Syyskuu 2018
Sähkötekniikan diplomi-insinöörin tutkinto-ohjelma
Pääaine: Elektroniikka
Tarkastaja: Professori Matti Mäntysalo

Avainsanat: iholle kiinnitettävä elektroniikka, ohutkalvo, painettava elektroniikka, siirtokuvakalvo, siirtokuvatatuointi, silkkipaino, venyvä johdin

Iholle kiinnitettävä elektroniikka on kehittynyt viime vuosien aikana paksuista laastarimaisista rakenteista ohuiksi tatuointimaisiksi kalvoiksi. Ominaisuudet, joista tärkeimpinä ovat venyvyys, läpinäkyvyys, mukautuvuus, sähkönjohtavuus ja bioyhteensopivuus, tarvitsevat kuitenkin vielä parantamista. Lisäksi tatuointien valmistusmenetelmät vaativat kehitystä. Kaiken kaikkiaan tatuointien ja valmistusmenetelmien kehittäminen vaatii käytettävien materiaalien kehittämistä.

Tämän diplomityön tarkoituksena on valmistaa ja analysoida siirtokuvatatuointeja. Tavoitteena on saavuttaa aiemmin mainitut ominaisuudet ympäristöystävällisillä, halvoilla ja additiivisilla valmistusmenetelmillä. Työ käsittelee ensin venyvien johdinten ja iholle kiinnitettävän elektroniikan teoreettista taustaa. Sitten venyviä johtimia painetaan siirtokuvatatuointipaperille ja johtimet karakterisoidaan mekaanisesti ja sähköisesti. Mekaaninen karakterisointi ja osa sähköisistä karakterisoinneista suoritetaan iholla sekä mekaaniseen karakterisointiin tarkoitetussa laitteessa. Lisäksi tatuointipaperi ja materiaalit, jotka sopivat ainakin teoreettisesti haluttuja ominaisuuksia omaavien tatuointien valmistamiseen, karakterisoidaan.

Valmistettujen tatuointien neliöresistanssi oli 41,7 mΩ/□. Suurin saavutettu myötymä oli 19,4 %, mutta tuloksen luotettavuutta ei kuitenkaan voitu varmistaa. Painetut johtimet eivät olleet läpinäkyviä johtuen käytetystä materiaalista. Tatuointien paksuutta ei mitattu, mutta erään teoreettisen laskelman mukaan paksuus olisi 1,9 µm. Tatuoinneilla oli myös havaittavissa lievää iholle mukautumista. Johtavat musteet osoittautuivat hankalaksi käsitellä ja tarvitsevat lisää kehitystä. Käytetty tatuointipaperi ei myöskään alhaisesta lämmönkestävyydestään johtuen soveltunut riittävän hyvin tatuointien valmistukseen. Lisäksi venytystestilaitteistot eivät soveltuneet ohuiden tatuointien testaukseen johtuen pitävästä kontaktista, joka laitteiston ja tatuointien välille vaadittiin tulosten saamiseksi.

PREFACE

This Master of Science thesis was done at Laboratory of Electronics and Communications Engineering at Tampere University of Technology. The work was done as a part of VitalSens and EpiPrint projects.

I would like to thank my instructor and the examiner of this thesis Matti Mäntysalo for all the guidance, feedback and the opportunity to take on this challenge. I would also like to thank all my co-workers, especially Ph.D. Thomas Kraft, for aiding me and providing valuable tips throughout the thesis.

Finally, I would like to thank my family and friends for supporting me throughout my studies.

Tampere, 17.9.2018

Samuli Tuominen

CONTENTS

LIST OF FIGURES

LIST OF ABBREVIATIONS AND SYMBOLS

4PP	4-point probe
Galinstan	alloy composed of gallium, indium and tin
CNT	carbon nanotube
CVD	chemical vapor deposition
CI	confidence interval
CuNP	copper nanoparticle
DMP-2850	Dimatix Materials Printer model 2850
DoD	drop-on-demand
ECM	Engineered Conductive Materials
EMS	Engineered Materials Systems Incorporation
EGaIn	eutectic gallium-indium
FDA	Food and Drug Administration
GPIB	General Purpose Interface Bus
IPA	isopropyl alcohol
et al.	Latin for at alia, and others
e.g.	Latin for exempli gratia, for example
i.e.	Latin for id est, in other words
1D	one-dimensional
ANOVA	one-way analysis of variance
PDMS	polydimethylsiloxane
PET	poly(ethylene terephthalate)
PMMA	poly(methyl methacrylate)
PVA	poly(vinyl alcohol)
p-value	probability value
rpm	revolution per minute
R2R	roll-to-roll
SEM	scanning electron microscope
AgNP	silver nanoparticle
AgNW	silver nanowire
TGA	thermogravimetric analysis
TPU	thermoplastic polyurethane
2D	two-dimensional
UV	ultraviolet
USB	Universal Serial Bus
0D	zero-dimensional

A_0	amplitude
A	area
G	conductance
σ	conductivity
I	current
P_0	incident power of light
l	length
P_T	power of light through a material
R	resistance
ρ	resistivity
R_S	sheet resistance
α	significance (level)

ε	strain
t	thickness
T	transmittance
V	voltage
w	width
x	x coordinate
y	y coordinate

1. INTRODUCTION

Electronics is a large field of science that comprehends anything from the behavior of individual charge carriers, usually electrons, to complicated electronic devices. However, this thesis concentrates only on a few small sectors in the field of electronics. How exactly it is divided in to smaller parts is not unambiguous but depends highly on the perspective.

Traditionally, electronics applications have composed of rigid components on rigid substrates. However, in the past years applications that are flexible and stretchable have rapidly emerged, and this trend continues in an increasing fashion. In addition, development of modern manufacturing methods (e.g. printing technologies), which is partially a reason for increasing number of flexible applications, is growing at a swift rate.

In electronics, there are countless different applications, and numerous ways to classify these applications. Home electronics, portable electronics, industrial electronics, automotive electronics etc. All these can be used to classify electronics applications by their use. In addition to these, there is an electronics type called wearable electronics, which is used to refer to electronics applications worn by the user. One of the most classic wearable electronics application is the wristwatch, and it is probably this application that has been the inspiration to the modern wearable electronics applications today. Many of the applications in wearable electronics industry are different kinds of wristbands and bracelets. However, wearable electronics have been developed even further, and applications laminated on clothes or even mounted directly on the skin have appeared.

The previous discussion presents different ways to divide the large field of electronics in to smaller parts. Rather than talking generally about “electronics”, people, and especially professionals, talk about printed electronics, flexible electronics, stretchable electronics, wearable electronics etc. to be more specific about subject at hand. The examples presented are actually relevant since they are used in this thesis: Printing technologies are used as the main manufacturing methods, and the fabricated temporary transfer tattoos are designed to be used on the skin. Hence, the title of the thesis is “Printed Temporary Transfer Tattoos for Skin-Mounted Electronics”. In addition, the fact that the fabricated temporary transfer tattoos are used on the skin sets certain requirements for their properties. However, these are discussed later in this thesis.

Printing technologies is an additive manufacturing method as opposed to subtractive methods such as photolithography. Additive means basically adding of material only where necessary, whereas subtractive means adding of material everywhere and then removing the excess. Additive methods have multiple advantages over subtractive methods

such as cost-effectiveness, being environmentally friendly, possibility to use a wide variety of materials and the possibility to manufacture complex structures with ease. Thus, printing technologies are widely used and studied in electronics manufacturing today.

Skin-mounted electronics have developed from thick bandage-like structures toward extremely thin, soft and transparent tattoo-like films. Probably the earliest work reporting these tattoo-like structures is by Dae-Hyeong Kim et al. [1]. They used a term “epidermal electronics” to refer to skin-mounted electronics with thicknesses, effective elastic moduli, bending stiffnesses and areal mass densities matching to the epidermal layer of human skin. However, their devices were not transparent and did not utilize the most beneficial materials. In addition, it is desirable to aim for structures that are even thinner, softer and lighter than human epidermis.

Later, Woon-Hong Yeo et al. [2] presented a method of fabricating and transferring a tattoo-like device on to a sheet of poly(vinyl alcohol) (PVA). The sheet of PVA was then placed on to the skin, and the PVA was dissolved with water leaving the device mounted on the skin. The other method to transfer the device on the skin was to use an elastomeric stamp. The device was first transferred on to the stamp, which was then placed on the skin. A glue layer sprayed on the skin guaranteed enough adhesion for the device, which then released from the stamp, leaving it mounted on the skin. This method resembles the transfer of a temporary transfer tattoo. However, in both methods it was necessary to use adhesive sprays to guarantee a sufficient adhesion between the device and the skin.

Recently, Alexander J. Casson et al. [3] reported electrodes inkjet printed directly on to a transfer tattoo paper. It was then possible to transfer the electrodes on to the skin by wetting the transfer tattoo paper. The authors used a thick 10 μm adhesive sheet between the electrodes and the skin to produce sufficient adhesion. According to the authors, the sheet was painless to remove and was approved by Food and Drug Administration (FDA). However, the thickness of the sheet allowed only a capacitive contact with the skin which is not suitable for high-frequency applications. In addition, the electrodes were printed using silver nanoparticles which are not suitable for manufacturing stretchable structures.

Most recently, Kabiri Ameri et al. [4] reported graphene based electronic tattoos that were extremely thin and transparent. That is, the visual appearance of the tattoos was close to ideal. In addition, there was no adhesives used due to the high conformability of the tattoos with the skin. Thus, the tattoos should be comfortable to the user. However, the manufacturing method was a subtractive method, which included some undesirable process steps. Also, the sheet resistance of the devices was quite high, which is not desirable in high-frequency applications.

This thesis focuses on fabrication of stretchable interconnects on temporary transfer tattoo paper by printing technologies. The aim is to produce structures with low thicknesses, low sheet resistances and high transparencies. In addition, using chemical adhesives for

mounting the temporary transfer tattoos is avoided. The fabricated structures and the used materials are electrically and mechanically characterized, and the results are analyzed. In addition, theoretical background of stretchable interconnects and skin-mounted electronics is discussed.

First, chapter 2 focuses on the theory of stretchable interconnects and different materials used in them. Second, chapter 3 discusses skin-mounted electronics, its objectives and electronic temporary transfer tattoos. Third, chapter 4 presents the materials and methods used in this thesis. Fourth, chapter 5 describes the conducted experiments including characterization of materials and fabrication and characterization of the fabricated temporary transfer tattoos. Fifth, chapter 6 presents and discusses the results of the experiments and observations made during the experiments. Finally, chapter 7 presents the conclusions made during the thesis and discusses how well different objectives set for the thesis have been achieved and then gives proposals for future works.

2. STRETCHABLE INTERCONNECTS

In general, electronic circuits consist of components, with specific functions, and interconnects that connect the components together. Thus, the interconnects act as signal and power routes. In stretchable electronics, the components are usually stiff and the stretchability of the systems is realized by implementing the interconnects stretchable.

Stretchability of interconnects means that the electrical conductivity should be maintained during the deformation of the interconnects. In other words, the electrical conductance should remain above certain value at all times. However, it is never completely unambiguous how high the conductance should remain when an interconnect is stretched, or how much it should be possible to stretch the interconnect before losing conductivity. These are basically dependent on the application and the requirements for the conductance and stretchability. It is for these reasons that the literature mentions stretchable interconnects with very different conductances and maximum strains. Let it be noted at this point that often, also in this thesis, interconnects are referred to as "conductors".

Before discussing the different strategies to achieve stretchable interconnects, it is important to have a basic understanding of the relation between conductance and strain of the interconnect. First, let us consider a conventional rectangular conductor, with a cross-sectional area A and length l, such as the one in figure 1.

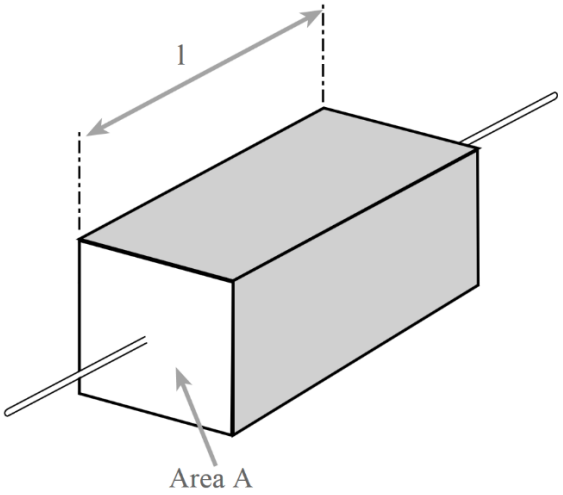

Figure 1. *An electrical conductor with a rectangular cross-sectional area A and length l [5].*

Depending on the material of the conductor, e.g. copper or silver, it has a resistivity ρ specific to that material. Now, the conductivity σ of the material is the reciprocal of the resistivity, and a conductance G, which is dependent on the dimensions of the wire as well as the conductivity, is the reciprocal of a resistance R. Usually, resistance is the

measure used to describe the electrical performance of a conductor instead of the conductance or conductivity, and this practice is used also in this thesis.

The resistance of a conductor is measured in ohms (Ω) and is mathematically defined as [5]

$$R = \rho \frac{l}{A} = \rho \frac{l}{wt}. \quad (1)$$

On the right-hand side of the second equality, the cross-sectional area A is represented as the product of the width w and thickness t of the conductor. Now, assuming that the width and length of the conductor are equal with each other, they can be eliminated from equation (1), and the equation can be reduced to express the sheet resistance of the conductor

$$R = \frac{\rho}{t} = R_S. \quad (2)$$

The assumption that the width and length of the conductor are equal, practically means that the top view of the conductor is a square. Thus, the resistance of the square measured from one edge to the opposite edge is exactly the sheet resistance of the square; just as equation (2) claims. This is probably the reason why the quantity is called sheet resistance and the unit is ohms/square or more commonly Ω/□.

In addition, adding squares one after another, a series connection of resistances is made, and a conductor consisting of these squares is formed. The total resistance between the front edge of the first square and back edge of the last square is the sum of the resistances of the squares, or in other words, the sum of the sheet resistances of the squares. Since the dimensions of the squares are equal, the total resistance of the conductor is the sheet resistance of one square multiplied by the number of squares. This means that the resistance of a conductor can be calculated if the sheet resistance of the conductor and the number of squares is known. The following equation relates closely to the previous explanation: By combining equations (2) and (1), the sheet resistance can be expressed with the resistance

$$R = \frac{\rho}{t}\frac{l}{w} = R_S \frac{l}{w} \Leftrightarrow R_S = R \frac{w}{l}. \quad (3)$$

Indeed, the length of the conductor divided by the width of the conductor gives the number of squares, which multiplied by the sheet resistance gives the resistance of the conductor. The equation can be used the other way too: The sheet resistance of a conductor with any length and width (assuming uniform width and thickness along the whole length) can be calculated if the resistance of the conductor is measured. In addition, since the resistance of the conductor results basically from the sheet resistances of series connected squares, the total resistance can be calculated even if the sheet resistances are not equal, as long as the average sheet resistance of all squares is known. Furthermore, the sheet

resistance can be calculated even if the width of the conductor is not uniform along the length, as long as the average width is known.

One of the key advantages of the sheet resistance over the conventional resistance is that the former quantity can be used to compare conductors with very different sizes, since the sheet resistance does not depend on the size of the square but only on the resistivity and thickness. Additionally, since resistivity is a material property and thickness can be considered as a property of a fabrication process, it is easy to use the sheet resistance as a tool in design when the used material and fabrication process is known. Furthermore, the sheet resistance can be directly measured using a 4-point probe (4PP) method, which is a suitable method for thin conductive layers and layers with a low resistance. 4PP method is discussed in more detail in chapter 4.3.1. [6]

When a conductor is stretched, the length of the conductor increases and from equation (1) it is obvious that also the resistance increases. In addition, due to Poisson's effect the transverse dimensions of the conductor decrease as the longitudinal dimension increases [7]. In other words, when the length of the conductor increases, the width and thickness of the conductor decrease. Again, from equation (1) it is obvious that decreasing the thickness and width of the conductor increases the resistance. Also, from equation (2) it can be seen that decreasing the thickness also increases the sheet resistance. Therefore, in general, stretching a conductor causes the resistance of the conductor to increase. However, the actual dependence between the resistance, or the sheet resistance, and the dimensions of the conductor in equations (1)–(3) holds only if the resistivity remains constant. Yet, this is not the case when considering conductors fabricated using nanocomposites, which are discussed in chapter 2.3.

The next subchapters discuss the different strategies to fabricate stretchable conductors. The manner of approach chosen is from the easiest concept to understand to the most complicated concept. That is, first, chapter 2.1 introduces intrinsically stretchable conductive materials i.e., materials that are conductive and stretchable at the same time. Second, chapter 2.2 discusses certain structures that are rendered stretchable by taking advantage of different geometries. This means that the used materials itself do not stretch at all. Finally, chapter 2.3 presents different types of nanocomposites that, in a way, combine the two previous methods of creating stretchable structures. Therefore, nanocomposites could be called semi-intrinsically stretchable structures.

2.1 Intrinsically stretchable conductive materials

In general, intrinsically stretchable conductive materials combine stretchability and conductivity. In principle, if rubber was electrically conductive material, it would be considered an intrinsically conductive material. This way, a regular rubber band could be used as a stretchable conductor. Even though the functioning principle of intrinsically stretch-

able materials is easy to understand, there are numerous challenges and problems associated with them, which limits their use. These materials are shortly discussed next for their potential as stretchable interconnects.

Liquid metals, such as mercury, and liquid metals based on gallium, such as eutectic gallium-indium (EGaIn) and an alloy composed of gallium, indium and tin called Galinstan, are special types of metals that are in liquid form in room temperature. They have a high reversible stretchability due to their liquid nature and a high metallic conductivity. However, the challenges are quite extensive. [8]

First, mercury is extremely toxic for human tissue [9] and even though gallium has low toxicity, some of its salts are poisonous [8, p. 4]. Second, liquid metals must be encapsulated, which is usually implemented by filling small microchannels with the metal, but fabrication of the microchannels is challenging. Third, patterning liquid metals by inkjet printing, and possibly by other a number of other printing technologies, is difficult due to the large surface tension and an oxide layer that gallium-based liquid metals spontaneously form on their surface [8, p. 5]. Fourth, liquid metals are not transparent. Fifth, using liquid metals in skin-mounted electronics could be dangerous since in liquid from the metal could easily enter the human body. Thus, it may not be possible to use liquid metals to fabricate electrodes designed to be directly in touch with the skin. [8] Liquid metals still need to be studied and these challenges need to be overcome before they can be used more practically in stretchable electronics. Also, using liquid metals safely in skin-mounted electronics, especially in applications where the liquid metal would make a direct contact with the skin, could be difficult.

In addition to liquid metals, conductive polymers are highly stretchable, transparent, biodegradable and can be made biocompatible, but the greatest limitation is their low conductivity. It can be increased by doping, but it is still a few orders of magnitude lower than the conductivity of silver or copper. [10] It is also unclear whether these materials are suitable to be deposited by printing technologies.

Graphene is a material with numerous superior properties with the most relevant for this thesis being the highest known electrical conductivity and lowest thickness of all materials and high optical transmittance (97.7 %). However, these properties can be achieved only with the purest samples of graphene, which is possible only in laboratory environment at the moment. [11] In addition, graphene has a high Young's modulus and stretchability of only 20 % [12, pp. 1532–1533]. Also, continuous graphene sheets cannot be fabricated by printing technologies. However, it is possible to use graphene in nanocomposites, which is discussed in chapter 2.3.3.

2.2 Geometrically rendered stretchability

Stretchability in general means that atoms in the crystal lattice of a material need to move in respect to each other, and e.g. metals, which are the most common electrical conductors, have strong interatomic bonds and moving the atoms is difficult. However, this problem can be overcome by shaping materials in to certain shapes. The shapes generally take advantage of a simple material property: Any material thin enough can be bent with fairly small effort [13]. By shaping a material in to a suitable shape, stretching the *system* (shape) occurs by actually bending the *material*. It should be noted here that the difference between a stretching material and a stretching system is important. This difference becomes clearer through this and the next chapter. Different stretchable shapes with maximum elongations and scalability are presented in figure 2.

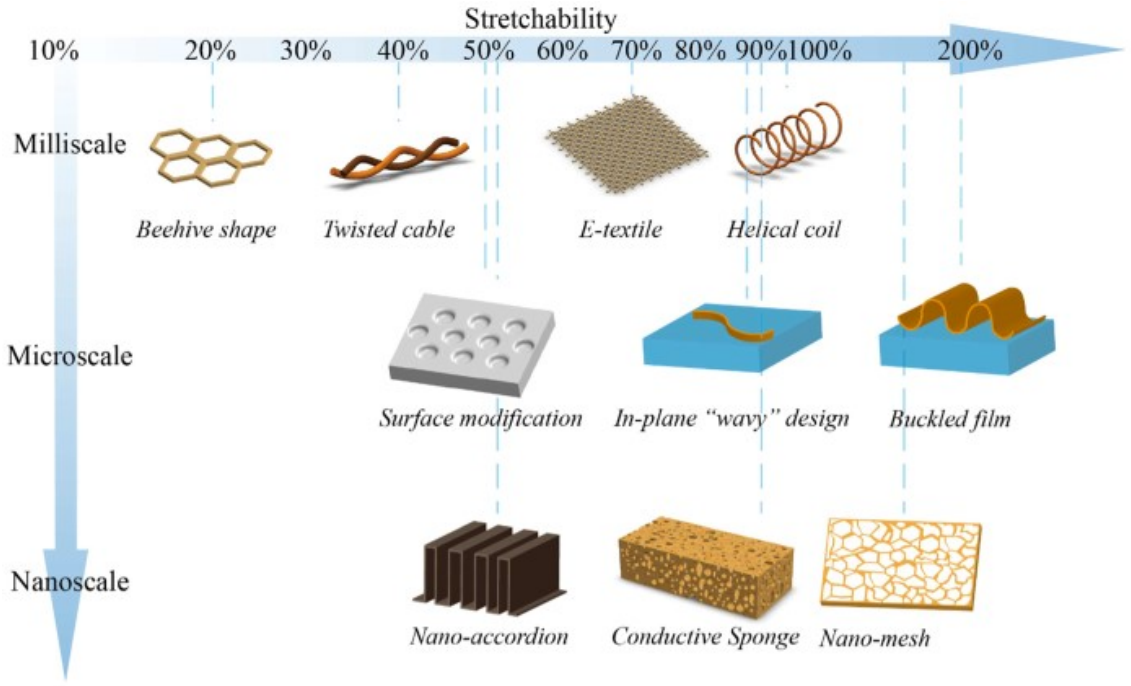

Figure 2. *Different stretchable structures and their maximum elongations with the structure size that can be achieved [14].*

One of the first strategies to make stretchable interconnects was to wind a conductor in to a helical coil. The coil then functioned like a spring making it possible to stretch and compress it. One familiar device using this strategy is a telephone, where the telephone receiver is connected to the base with a coil-shaped cord, which allows the receiver to be moved away from the base. [14] Here, the thickness of the coiled wire is important since thinner wire allows the coil to be stretched with less force. The problem with the helical coil is the scalability of size as well as the manufacturing scalability. It is difficult to fabricate coils with radiuses in the micro- or nanoscale. [14] In addition, integrating the fabrication of coils to e.g. roll-to-roll (R2R) processes for cost-efficient large-scale manufacturing is also difficult.

In addition to the helical coil, one widely used strategy is a buckled film. This strategy has two variations: pop-up structure, where the conductor is bonded to the substrate at specific locations only like in figure 2, and out-of-plane wavy structure where the conductor is in touch with the wavy surface of the substrate along the whole length of the substrate [15]. In this strategy, the bending of material as the system is stretched is more apparent than in the case of the helical coil. Figure 3 presents the tensile deformation of a buckled film system.

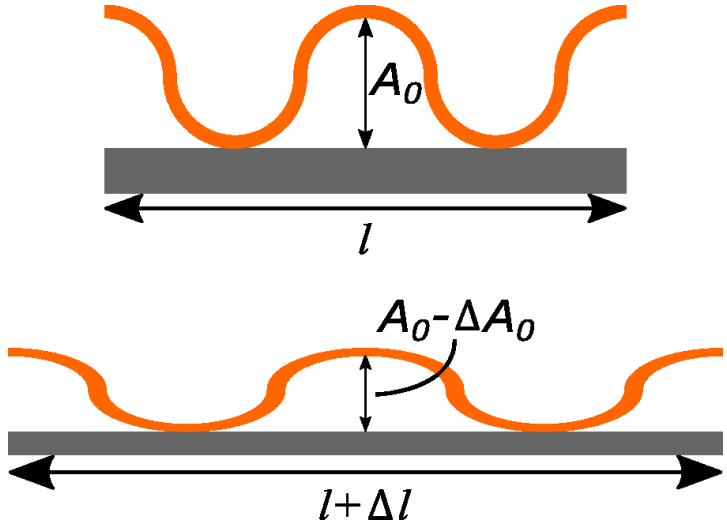

Figure 3. *A cross-section of a buckled film on a stretchable substrate before and after tensile strain.*

The buckled film (conductor) on a stretchable substrate in figure 3 is the system with an original amplitude and length A_0 and l, respectively. After the system is stretched to length $l + \Delta l$, the amplitude of the film decreases to $A_0 - \Delta A_0$. However, the length of the film along its surface still equals the length before the deformation. So, even though the system has stretched, the material (conductor) has not. The amplitude of the wavy structure has decreased, or in other words, the material has bent to become straighter. This kind of behavior has one major advantage: The original amplitude of the conductor can be freely selected, which results in desirable stretchability. However, the conductor does not have the same mechanical support along its length as the pop-up structure does. Furthermore, fabricating structures in layers, one basic strategy of electronics' miniaturization, is extremely difficult with both buckled film structures. In addition, pop-up structures cannot be fabricated using printing technologies, and out-of-plane wavy structures usually need pre-strained substrate, which is a problem when considering R2R processes.

One solution to the problems, that buckled film structures have, is using in-plane wavy structures instead. These are strategies utilizing the same type of material behavior as helical coils, only these are two-dimensional springs. Here the "stretching the system by bending the material" -behavior is also quite apparent. Figure 4 presents tensile deformation of an in-plane horseshoe-like conductor on a stretchable substrate. There are also other types of meander shapes in addition to the horseshoe, but they usually do not show

as high stretchability as the horseshoe does [16]. It is one of the many material properties that sharp corners experience high stresses and cause the first fractures. However, the horseshoe has only rounded curves, which is probably the reason for better stretchability over the other shapes.

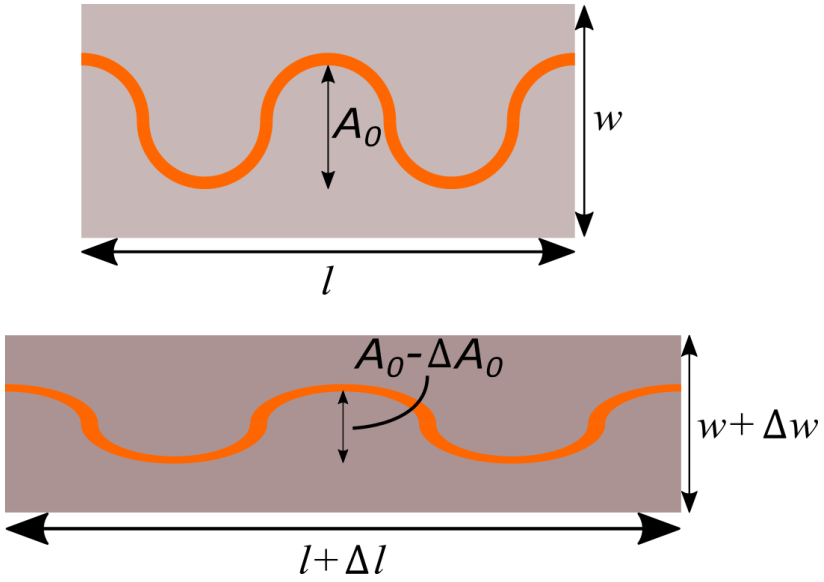

Figure 4. *Top view of a horseshoe-like in-plane wavy structure before and after tensile strain.*

In this case, the original amplitude of the conductor and length and width of the total system are A_0, l and w, respectively. After stretching the system to length $l + \Delta l$, the amplitude of the conductor decreases to $A_0 - \Delta A_0$, and due to Poisson's effect, the width of the system decreases to $w - \Delta w$. The idea here is similar to the buckled film: Stretching the system causes the conductor to straighten by bending. It is not completely clear whether the mechanics of the deformation are the same as in the case of the helical coil, since now the conductor is completely bound to the substrate, but the helical coil is a freestanding structure. However, the Poisson's effect could be the reason forcing the conductor to bend and straighten. The maximum strain that this kind of in-plane structure can exhibit without fracturing is only 8 % [16]. The problem with the structure is that the substrate is stretching evenly everywhere, and even if the conductor bends due to its shape, local microscopic strains of the substrate under the conductor causes the material to stretch.

The stretchability of the in-plane wavy structures can be improved by fractalizing the conductor [17]. In other words, the conductor is divided in to smaller and smaller parts and each part is implemented by using meander shapes. This is presented in figure 5.

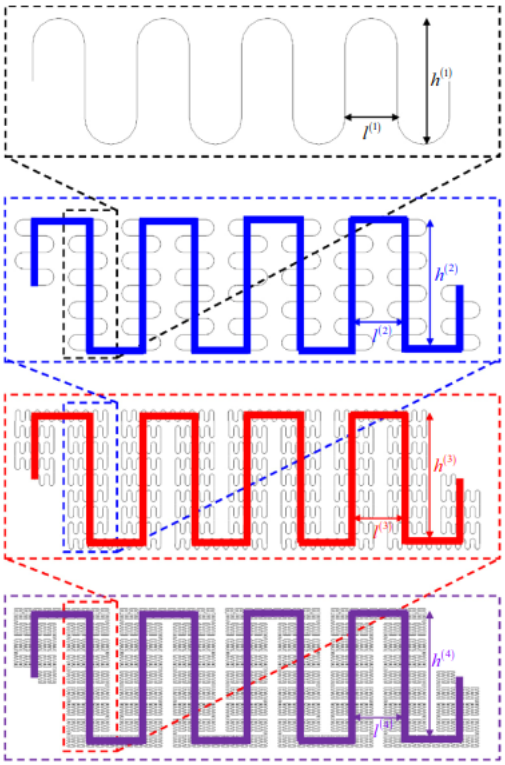

Figure 5. *Fractalizing an in-plane conductor using a horseshoe-like shape. First order iteration on the top and then second, third and fourth iterations when going from top to bottom [17].*

In the fractal decomposition of the conductor, the local strains, that would otherwise stretch the conductor material, only cause bending of the smaller conductors. According to Zhang et al., increasing the number of iterations in the fractal design increases the stretchability of the system [17]. However, the problem with this design is the absolute resistance it offers. There are long sections of narrow lines in the design, and according to equation (1), this increases the resistance of the interconnect. Another problem is the producibility of the interconnects. Assuming that two components are close to each other and could be connected with a straight line, using the fractal design to decompose that line into smaller parts would require so small line widths and gaps in the first iteration interconnect, that it would not be possible to fabricate them. This can be presented in the other way too: Assuming even the smallest possible line width and gap in the first order iteration producible by chosen method, the total area coverage in the fourth iteration would be extremely high increasing the resistance to high values.

Figure 2 presents also other types of stretchable structures, but they are not discussed as they all rely on to bending the material for system stretchability, and the general problems regarding the structures geometrically rendered stretchable were already presented in the previous discussion. Next chapter discusses nanocomposites, which are partially stretchable materials, but also rely on benefits offered by different geometries.

2.3 Composite nanomaterials

Composite nanomaterials, or nanocomposites, are materials consisting of two (or more) functional components: a polymer matrix and conductive solid particles. The function of the polymer matrix is to bind the conductive particles and act as the stretchable component. On the other hand, the conductive particles also contribute to the stretchability by being able to move or turn in respect to each other when the nanocomposite is stretched. The conductivity is maintained by the contact area between the conductive particles. The advantage of nanocomposites over geometrically rendered stretchable systems is the small space. When geometrically rendered stretchable systems need to use large surface areas or out-of-plane dimension, nanocomposites do not. This allows stacking of nanocomposite layers, which is not possible for geometrically rendered stretchable systems.

The relation between strain and resistance was already discussed previously, but a constant resistance was assumed. However, in nanocomposites the conductive particles move and change position, and this effectively changes the structure of the composite and the resistivity with it [18].

Suikkola et al. [18] have developed a regression model for the dependence between normalized resistance and strain of a certain screen printed conductor. The model is somewhat relevant to this thesis since the same ink is used to print the conductors in both works. The authors also present a residual of the normalized resistance as function of strain. The regression model and its residuals as a function of strain are shown in figure 6.

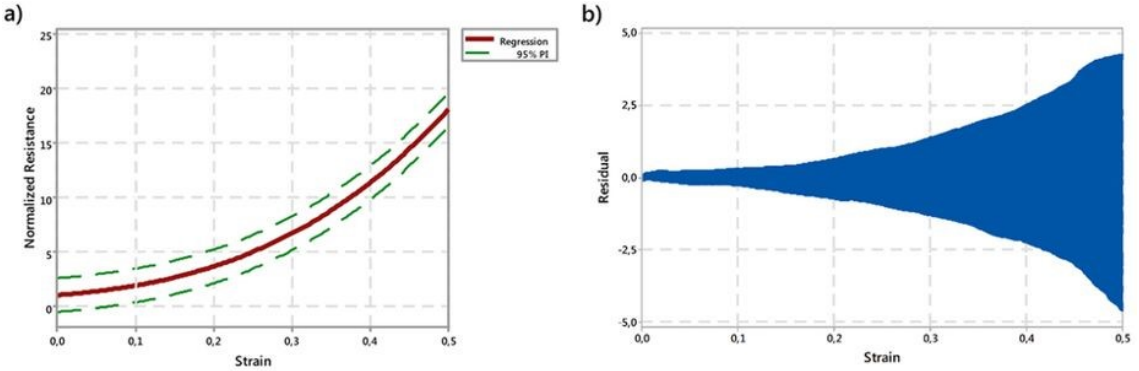

Figure 6. *a) A regression model of certain screen printed conductor and b) the residuals of the regression model as a function of strain [18].*

In the regression model the normalized resistance as a function of strain follows a cubic equation

$$\frac{R}{R_0} = 64.5269\varepsilon^3 + 24.4836\varepsilon^2 + 5.759\varepsilon + 1, \quad (4)$$

where R_0 is the initial resistance of the conductor and ε is the strain of the conductor. In figure 2 b), residual means the difference between an observed normalized resistance value and a fitted value shown in the regression model. The interesting part in the residual graph is how unpredictable the actual resistance of a conductor can get when strain increases. This is quite expectable though, as the movement and shifting of the conductive particles in a conductor and thus, the actual resistivity is extremely difficult to predict as the conductor is stretched.

However, under tensile strain the particles move farther away from each other in the conductor and thus, the contact areas between different particles diminish, and the length of the current's path increases at the same time. In addition, the amount and size of the particles remain constant and thus, even if the resistivity might occasionally decrease due to benign position of the particles, the overall resistivity increases. This is because the volume of the conductor increases when stretched, even though Poisson's effect decreases the cross-sectional area, and the increased volume is filled with the polymer material of the conductor. In conclusion, according to equation (1), the increasing resistivity and length as well as the decreasing cross-sectional area causes the cubic growth of a conductor fabricated using a metal–polymer composite.

Even though nanocomposites are solid materials, it should be noted that nanocomposites are usually in the form of solutions, or inks, *during deposition* to substrates since printing technologies use materials mainly in liquid forms. For this reason, nanocomposite inks include components that are not functional after the nanocomposite ink is deposited and cured. These non-functional components include solvents and surfactants that are used to control the viscosity and surface tension of the ink; two important parameters when considering the printability of the ink. In this thesis, the formulation of inks is not in focus and thus, it is not discussed any further.

The most interesting property of the nanocomposites in ground of this thesis is the dimensions of the conductive particles. Generally, the nanocomposites are divided in to three groups based on the dimensions: zero-dimensional (0D), one-dimensional (1D) and two-dimensional (2D) nanomaterials. 0D nanomaterials include metal nanoparticles that are in nanometer scale in all three dimensions. 1D nanomaterials include high aspect ratio metal nanowires and carbon nanotubes that are in nanometer scale in two dimensions but exceed the nanometer scale in the third dimension. Finally, 2D nanomaterials are metal and graphene flakes that are in nanometer scale in one dimension but exceed the nanometer scale in the other two dimensions.

The next subchapters discuss the different types of nanocomposites, their properties, pros and cons. The idea is to give a clear understanding of what these materials are best suitable for, and to argue why specific materials would be best suited for using in this thesis. In addition, the state-of-the-art of the nanocomposites is explained. It should also be noted

that the discussion focuses on the actual conductive particles rather than the polymer material, since the particles are the limiting factor when it comes to stretchability and conductivity of a nanocomposite.

2.3.1 0D nanomaterials

Metal nanoparticles, such as silver nanoparticles (AgNP) or copper nanoparticles (CuNP), are 0D nanomaterials, which means that they are relatively small in all three dimensions. Placing high number of these particles in to a small volume results in relatively large contact area and thus, large conductance between the particles. In addition, the smaller the particles the larger the total contact area between the particles. This results from the increased total surface area due to the cutting surfaces when large particles are cut in to smaller ones. This way the total volume of conductive particles remains the same, which is important when considering the stretchability. That is, high volume of conductive particles results in high conductivity but small stretchability due to increased stiffness and vice versa.

However, the problem with nanoparticles is low stretchability in any case. This results from the geometry of the particles: Since they are 0D particles, they cannot be arranged in such positions in respect to each other, that they could be moved far away while maintaining conductivity. In other words, when a nanoparticle-based conductor is stretched, the contact area between the nanoparticles decreases rapidly as the distance between them increases resulting in the loss of conductivity at low strains.

Yao and Zhu reported in their review of stretchable materials a number of works achieving high strains with nanoparticles [19]. However, all these works rely on either the geometry of the conductors or using 1D fibers and 2D sheets as a base for the stretchability. In other words, the stretchability of the structures does not rely on the stretchability properties of the actual nanoparticles. Thus, even though metal nanoparticles offer high conductivity, they cannot be used in stretchable interconnects without relying on the geometry of the conductor (this was already discussed) or using 1D and 2D materials, which are discussed in the next two subchapters.

2.3.2 1D nanomaterials

1D nanomaterials such as silver nanowires (AgNW) and carbon nanotubes (CNT) are high aspect ratio materials. In other words, their length can be two or three orders of magnitude larger than their diameter [19, p. 1491]. When such materials are deposited on to a substrate, they spontaneously form a mesh-like structure. When the structure is stretched, the nanomaterials can slide or rotate in respect to each other while maintaining conductivity. When the strain is released, the nanomaterials turn back (in case of rotation) or tend to buckle (in case of sliding) rather than slide back. Zhu and Xu [20] demonstrated this behavior with CNTs and is presented in figure 7.

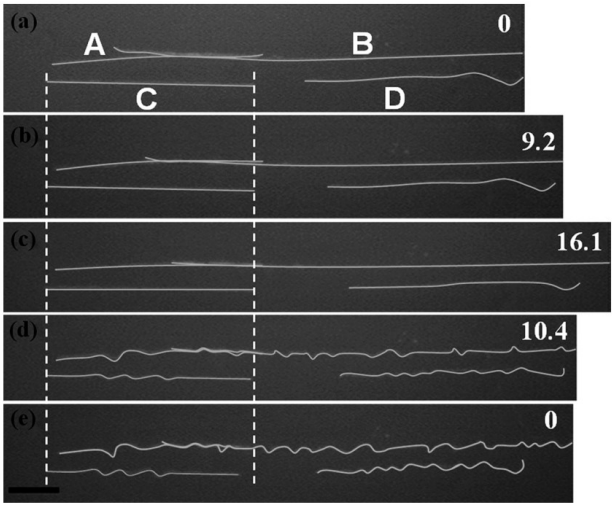

Figure 7. *Four CNTs marked A, B, C and D under different strains (shown on the right in percentage) [20].*

In the above figure, the sliding of the CNTs is apparent when observing the gap between CNTs C and D, or when observing the amount of overlap of CNTs A and B. When the CNT composite is stretched ((a) through (c) in the figure), the CNTs clearly slide away from each other. In addition, the conductivity between CNTs A and B is maintained through their contact area. However, the size of the contact area decreases as the composite is stretched resulting in increasing resistance. When the strain is released ((c) through (d) in the figure), the CNTs buckle rather than slide back in to their original positions. Zhu and Xu also report that when the composite is cyclically stretched, the resistance during each stretching cycle remains essentially constant to the amount of strain from the previous stretching cycle and starts to increase only after exceeding the previous strain. This is due to the buckled CNTs first straightening before starting to slide again and is similar to the behavior of stretching a buckled film on a stretchable substrate as discussed in chapter 2.2. It is not sure whether the buckling can occur also with other materials in addition to CNTs, but theoretically there should not be restrictions. According to Euler's buckling theory [21], load required for buckling is affected only by the length, Young's modulus and moment of inertia of a column-like particle and thus, it should be possible to buckle different metal nanowires.

Kim et al. report a AgNW structure where the stretchability of the nanowire network occurs by rotation of the nanowires [22]. Fabrication process of the nanowire network is presented in figure 8 and the network under tensile strain in figure 9.

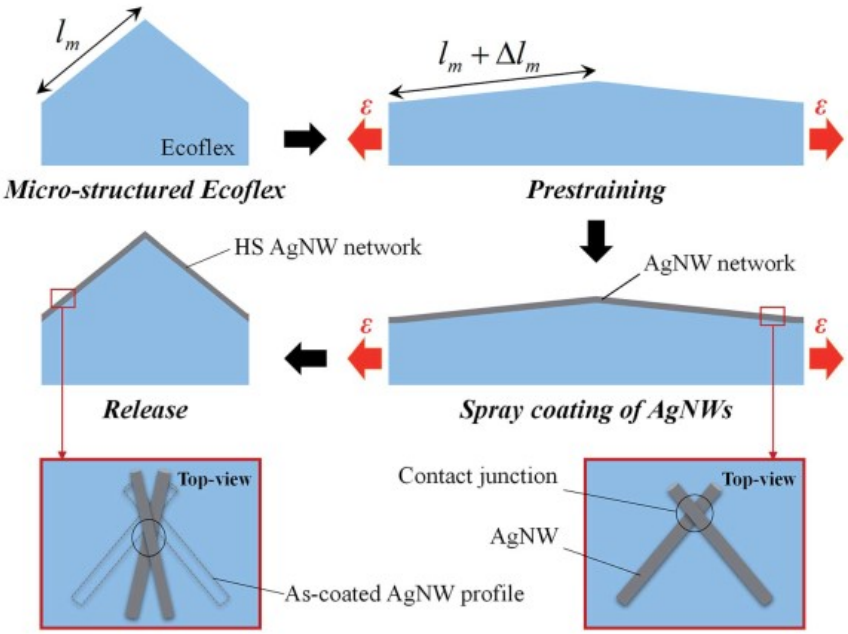

Figure 8. *Fabrication of a AgNW network on a pre-strained Ecoflex substrate [22].*

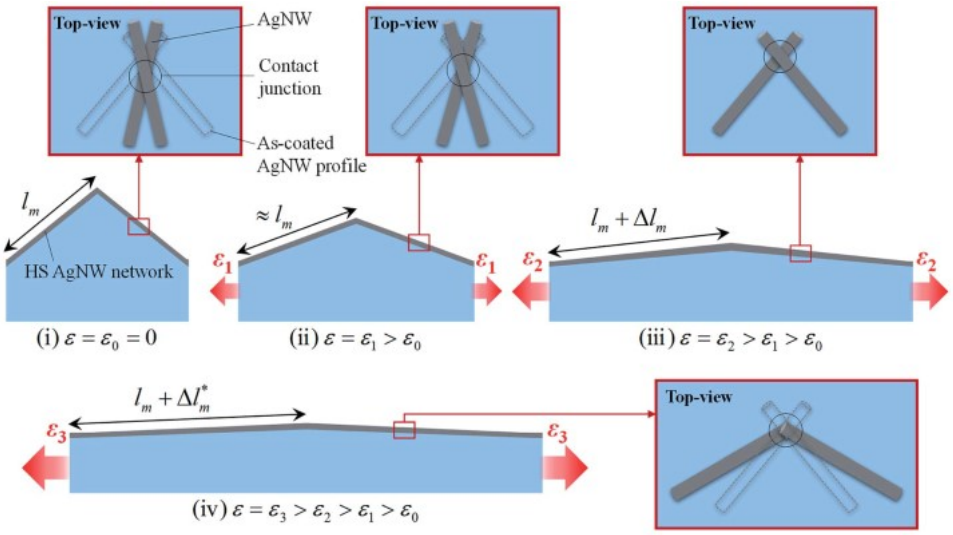

Figure 9. *A AgNW network on Ecoflex substrate under different levels of tensile strain [22].*

Figure 8 shows how the AgNWs rotate in to an almost vertical alignment when the pre-strained substrate is released, and figure 9 shows how the AgNWs rotate and approach a horizontal alignment under tensile strain. This strategy uses pre-strained and micro-structured substrate, and especially the pre-strain seems to have high impact on the stretchability, since the more vertical the original alignment of the AgNWs is the more they can rotate and approach the horizontal alignment. Using pre-strain is not desirable, but it

should be possible to use the same strategy without pre-strain to fabricate stretchable nanowire networks. However, in this case the stretchability would be lower. Kim et al. report that their strategy allows strains of over 700 % [22], so it could be possible to achieve still high strains even without pre-strain.

The disadvantage of the 1D nanomaterials is the low conductivity when compared to the 0D nanomaterials. This results basically from the small contact area between the 1D particles. More accurately, Daniel Langley has studied effects of percolation on the different properties (electrical properties included) of AgNWs. Langley reports, that the resistance of a AgNW network increases as the length and diameter of the individual AgNWs decrease. The decrease in resistance due to decrease in diameter results basically from equation (1). The effect of AgNW length on the resistance is based on the tendency of longer AgNWs to form junctions, and thus electrical pathways for electrons, with each other more probably than short AgNWs. This is the basic observation of the percolation theory. [23]

In their review, Yao and Zhu [19] report multiple works with sheet resistances from 8–50 Ω/□, which are still sufficient sheet resistances. In addition, these structures have high transparency, which is another desirable property when considering skin-mounted electronics. Transparency is discussed in more detail in chapter 3.1.4.

2.3.3 2D nanomaterials

2D nanomaterials are flake-like materials that are in micrometer scale in length and width but that are in nanometer scale in thickness. Due to the large surface area of the particles and thus, the large contact area between them, it is possible to create structures that are highly conductive and highly stretchable. However, due to the large surface area of the flakes, it is not possible to fabricate transparent conductors.

Araki et al. report fabrication of Ag flake conductors with a stretchability of 600 % and a resistivity of 2.4 Ω·cm at that strain [24]. More recently, Matsuhisa et al. report Ag flake conductors with a resistivity of only 5.5 mΩ·cm at a strain of 215 % [25]. In addition, according to Matsuhisa et al., by the time of the publication of their work the resistivity of their conductors was the lowest reported among conductors that can be stretched more than 150 % [25]. Graphene was already discussed in chapter 2.1, but it should be mentioned here that in addition to metal flakes, graphene flakes are also used in nanocomposites. The interest of graphene relies on the already discussed high theoretical conductivity and transparency. So, at least in theory it should be possible to fabricate transparent conductors with 2D nanomaterials, if the used conductive particles are thin graphene flakes.

3. SKIN-MOUNTED ELECTRONICS

Devices used in skin-mounted electronics focus mainly on measuring or supporting the many different functions of a human body. Typically, rigid electrodes are mounted on the skin via adhesives with conductive hydrogels between the skin and the electrodes to guarantee a sufficient electrical contact. Figure 10 shows typical medical electrodes.

Figure 10. *Medical electrodes with a metal button in the middle for connecting cables for different body measurements [26].*

Medical electrodes like the ones in figure 10 have low contact impedances due to the hydrogel that conforms with the skin and increases the contact area between the skin and the electrode providing low noise high quality measurement signals. However, there are numerous problems with these electrodes regarding the use of the hydrogel, use of adhesives, thickness and stiffness of the electrodes etc. The next subchapters first discuss the objectives for skin-mounted electronics and then discuss electronic temporary transfer tattoos as a possible solution for the different problems. Finally, the state of the art of these tattoos is presented and discussed.

3.1 Objectives for skin-mounted electronics

When something is mounted on human skin, multiple considerations need to be made. This is the case also for electronics. First, electronics should be stretchable since it experiences deformation as the skin stretches. Second, electronics should be biocompatible since human health and well-being play a critical role. Third, electronics should conform to the surface of the skin to create as much contact area as possible with the skin. Fourth, electronics should be transparent since transparency improves privacy of the user. Finally, electronics mounted on the skin should feel as comfortable as possible.

This chapter discusses these objectives looking to answer questions such as, why are these aspired, how are the objectives achieved and what are the current states of these objectives

in skin-mounted electronics. Each chapter discusses one of the aforementioned objectives. Let it be noted that comfortability is achieved with adhesive-free structures as well as low device thicknesses, properties important for conformability and biocompatibility, and thus, comfortability is discussed along these properties and does not have its own subchapter.

3.1.1 Stretchability

Stretchability is probably the most important single property of a skin-mounted electronic device; if it is not stretchable, it is most likely not functional. Human skin stretches to approximately 30 % elongation depending on the anatomical location [27]. Thus, an electronic device mounted on the skin should stretch to at least that strain. Otherwise, the device will either fracture, causing an electrical malfunction, or delaminate from the skin. On the other hand, no stretchability higher than 30 % is necessary.

Depending on the application and complexity of the device, there might be other requirements for stretchability in addition to the 30 % minimum elongation. Since this thesis concentrates only on stretchable interconnects mounted on skin, the only objective for stretchability is to have it at 30 % elongation. Strains in this range are quite easy to achieve with most materials used in stretchable electronics, including materials discussed in chapters 2.3.2 and 2.3.3. Furthermore, there are already demonstrations of skin-mounted electronics using meander shaped metal traces and chemical vapor deposition (CVD) grown graphene [4, 2].

3.1.2 Biocompatibility

Biocompatibility is a concept that does not have any established definition. In essence, it refers to a situation where a material has to perform in such a way that it produces an appropriate host response. In other words, an appropriate response from human tissue to a material needs to be defined in every application, and the material has to produce that and only that response. Furthermore, this means that generally a material cannot be said to be biocompatible, since biocompatibility is not a material property but needs to be defined individually in each application. [28, p. 9]

In the case of skin-mounted electronics, biocompatibility refers to the response of the tissue from the host's body to the materials used in the electronic devices mounted on skin. Furthermore, since there are usually multiple materials used in a skin-mounted electronic device, biocompatibility can be used to refer to the response of the body to the whole device.

The electronic devices considered in this thesis do not have any specific functionalities other than being conductive and stretchable. This means that an appropriate body's response to the devices is that there is no response at all. Thus, the skin-mounted electronic

devices are considered biocompatible if they do not produce any response from the body of the host. Also, whenever a material is considered biocompatible in this thesis, biocompatibility of the material is defined as follows: A material does not produce any response from the human body when in contact with the skin.

So far, skin-mounted electronics has mostly relied on adhesives for attaching devices on the skin [1]. However, chemical adhesives are not usually biocompatible since they can produce numerous problems such as skin irritation, allergic reactions, redness and even tearing of the skin. Also, removing the device from the skin can be very painful. [3] These are all unwanted responses from the skin and should be eliminated. For these reasons, ways of attaching devices on the skin without adhesives are studied.

Additionally, since human health is the main concern when developing skin-mounted electronics, using toxic materials must be avoided even if the materials are not in direct contact with the skin. This kind of safety measure should be used to make sure that if the device does not work properly, there is no chance for major health issues.

3.1.3 Conformability

Conformability can be understood as a measure to how large is the true contact area in respect to the nominal contact area between a thin film and the skin. Nominal contact area is the actual surface area of a thin film since, as the conformability is observed on a macroscopic level, the thin film appears to be completely in contact with the skin. In other words, the contact area between the thin film and the skin *appears* to be the whole surface area of the thin film. However, true contact area is the microscopic contact area between the thin film and the skin. Different true contact areas are presented in figure 11 resulting in different conformabilities of the thin film.

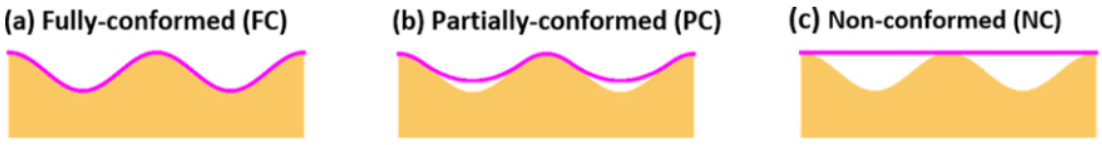

Figure 11. *A thin film a) fully conformed, b) partially conformed and c) nonconformed on skin [29].*

From figure 11 it is obvious that the maximum true contact area equals the nominal contact area. From this, it follows that conformability is 100 % for a fully conformed thin film and close to zero for a nonconformed thin film. The importance of the true contact area arises when observing the electrical performance of a device as well as the adhesion of a thin film to the skin. Both of these require that the thin film is much closer to the skin as it appears to the naked eye; that is, the true contact area should be as high as possible.

As stated, high conformability is necessary for two reasons. First, contact impedances are minimized between the skin and an electrode printed on a thin film, if the true contact area is as large as possible (electrical performance). Second, adhesion without chemical adhesives is sought for biocompatibility reasons, and the adhesion is formed due to intermolecular forces known as van der Waals interactions. [3] These interactions form spontaneously between different molecules, but only if they are close enough to each other i.e., the distance between the molecules has to be in nanometer scale [30]. Surface roughness of human skin is tens of micrometers; around thousand times larger than the longest possible distance for van der Waals interactions to form [31]. Thus, for a sufficient adhesion between a thin film and the skin, it is necessary to have the true contact area as high as possible.

Conformability requires the film mounted on the skin to bend. For soft bending to occur, the film needs to be thin. It is has already been stated that the bending stiffness of a thin film decreases as the thickness of the thin film decreases. This allows the thin film to bend with as little effort as possible, which further allows the thin film to conform on the skin on the microscopic level.

There are already publications reporting high or full conformability achieved with low film thicknesses [4, 2]. In addition, there exists a theory for calculating the largest allowed thickness for a thin film to fully conform on elastic membrane [29]. According to the theory and research by Kabiri Ameri et al. [4], the largest film thickness for a poly(methyl methacrylate) (PMMA) thin film to fully conform on human skin is 510 nm. The theory for full conformability states that there are multiple variables that determine the conformability [29]. For this reason, the critical film thickness basically depends on the material of the thin film as well as the material of the membrane that the thin film is mounted on.

3.1.4 Transparency

Unobtrusiveness is a desirable property in wearable electronics. However, electronics laminated on skin cannot be concealed in a similar way that electronics laminated in textiles can. Electronics mounted on the skin can be concealed under clothing in many situations, but for example a device mounted on a person's forearm is visible if the person is not wearing a shirt with long sleeves. Obviously, if the person does not want other people to notice the skin-mounted device, wearing a long-sleeved shirt is the only practical way of concealing the device. However, having to do this at all times is a great limitation to daily social life.

Virtually, the only way to create an unobtrusive skin-mounted electronic device is to make the device transparent. There are some highly transparent polymers [32, p. 89] and since they are also flexible, and some are even stretchable, they are potential substrate materials for skin-mounted electronics. Thickness of the film is also important since thinner films are more transparent [32, p. 89].

The more challenging objective is to make the actual conductive paths transparent. Again, thickness of the material inversely affects the transparency [33, p. 1497]. However, there is another way to increase transparency of the printed traces. Transparency is a direct consequence of a high light transmission through a material. This light transmission is described by transmittance which is defined as

$$T = \frac{P_T}{P_0} \times 100\ \%, \tag{5}$$

where P_T is the power of light through the material and P_0 is the incident power of light arriving at the surface of the material [34, p. 52]. For a conductive trace to have a high transmittance, it can be patterned in to a mesh-like structure where light can travel through the "holes" in the structure [33, p. 1497]. Thus, nanomaterials with high aspect ratios such as carbon nanotubes and metal nanowires, that can be patterned in to these kind of structures, are fine materials for transparent electronics. Furthermore, as discussed before, a graphene monolayer has a transmittance of 97.7 %. In addition, every additional layer decreases the transmittance by 2.3 % [35]. For this reason, thin graphene layers as conductive traces are highly transparent.

3.2 Electronic temporary transfer tattoos

Temporary transfer tattoo is a structure that can be transferred from one surface to another and removed whenever wanted. On the contrary, the ink used to make a permanent tattoo is struck under the skin and thus, cannot be removed as easily. Normally, the material used to carry the temporary transfer tattoo before transferring is paper. Thus, the term temporary transfer tattoo paper is often used.

Temporary transfer tattoo paper is a structure usually consisting of three layers: a backing paper, a release film and some kind of release coating between the two. The purpose of the backing paper is to support the thin release film making it possible to print on it, and the release coating allows an easy detachment of the release film from the backing paper. The release film carrying the printed pattern can then be transferred on to the skin (or any other surface given that there is sufficient adhesion) and is called a temporary transfer tattoo. [36] However, sometimes the release film with the printed pattern is referred to as a transfer tattoo even before transferring it to the skin. Since this thesis does not discuss permanent tattoos after this point, temporary transfer tattoos are sometimes referred to as transfer tattoos or even just tattoos.

3.2.1 Printing resolution of electronic transfer tattoos

The main difference between an electronic and a traditional transfer tattoo is the characteristic of the printed image. The traditional transfer tattoos have graphical images printed on them, but the electronic transfer tattoos have electronic circuits printed on them. This

sets certain requirements for the printing quality. The images printed on the traditional transfer tattoos just need to be printed with high enough resolution for a human eye not to detect any possible discontinuities in the image, as opposed to the electronic transfer tattoos that need to have high enough printing resolution to ensure electrical conductivity.

The resolution of a human eye is approximately 0.04 mm at best, that is, if two points are less than 0.04 mm away from each other, the human eye will not recognize them as two different points [37]. This means that in a graphic transfer tattoo, there could be a 0.04 mm gap between every adjacent ink droplet and human eye would see a perfect continuous image. Figure 12 shows what such an image would look like when magnified, and how naked human eye sees the same image.

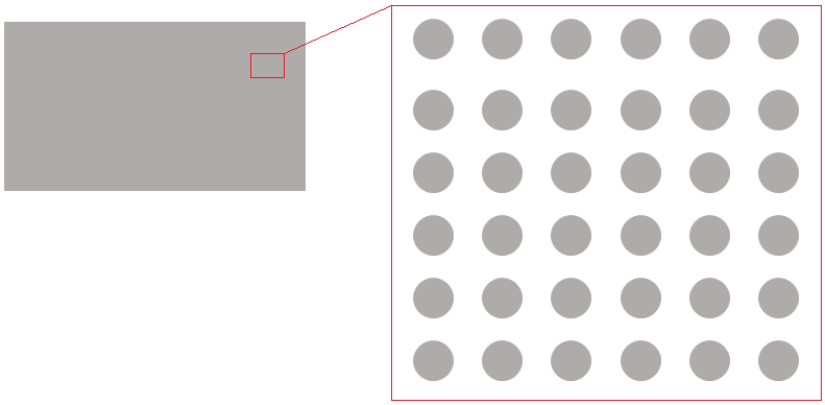

Figure 12. *Sufficient printing resolution for human eye in the image on the left and magnification of the same image on the right.*

In figure 12, the grey rectangle has sufficient resolution for human eye; there is no detectable discontinuities in the image. On the right side of figure 12, the magnification of the grey rectangle reveals gaps between grey droplets. If these gaps are smaller than 0.04 mm, human eye sees the rectangle as shown in figure 12. However, if the grey droplets were conductive ink, the gaps are too large for electrical conductivity between the droplets and thus, the printing resolution would not be sufficient for an electrical transfer tattoo.

In this thesis, printing methods have been chosen for the fabrication of transfer tattoos since they are widely used in today's electronics manufacturing and possess high resolution ink deposition quality. There are other reasons for choosing printing methods, but these are discussed in more detail in chapter 4.

3.2.2 Mechanics of transferring an electronic transfer tattoo

After printing the wanted electronic pattern on the tattoo paper, the tattoo is transferred on the skin. Let it be noted that a tattoo can be transferred on other substrates also, and in this thesis some experiments include tattoos being transferred on substrates other than

skin, but since focus is on skin-mounted electronics, the skin is considered the substrate for tattoos unless stated otherwise.

A transfer tattoo is transferred by placing the transfer tattoo paper print-side down on the skin, wetting, pressing against the skin and finally removing the backing paper. Figure 13 presents the transfer process.

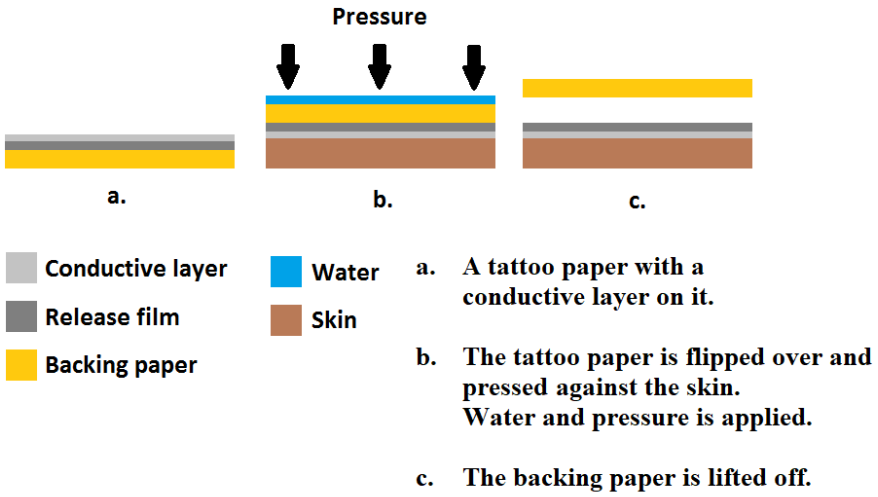

Figure 13. *Transfer process of a temporary transfer tattoo.*

As the transfer tattoo paper is placed on the skin, a nominal contact area is formed between the two as discussed in chapter 3.1.3. By applying water on the backing paper, it begins to absorb the water, which moves toward the release coating in a diffusion-like manner. This causes the release coating to wet, and the adhesion between the release film and the backing paper weakens. It is not exactly sure how the release coating functions, but it could be e.g. water-soluble material. Furthermore, by applying pressure on the backing paper, the pressure transmits to the water causing it to penetrate to even the smallest surface figures of the skin due to the extremely small size of water molecules. Since the release film is between the water and the skin, and the bending stiffness of such a thin film is low, the water can press the release film against the skin allowing it to achieve high conformability.

As the release film is pressed against the skin, conformability increases continuously. In other words, at first the conformability is near zero when the transfer tattoo paper is placed on the skin. Then the release film begins to conform to the skin from the top of the skin's surface toward the bottom. This can be understood by looking at figure 11. The conforming of the release film occurs from the nonconformed state, presented in figure 11 c), toward the fully conformed state in figure 11 a). Between the two states, the release film is partially conformed, and the conformability increases from near 0 to 100 %. However, the final conformability depends on the different properties discussed at the end of chapter 3.1.3, and might not reach the fully conformed state at all.

The mechanics of the release film's conforming are not quite clear. As the release film is pressed against the skin, the forces acting on the film as well as the friction between the film and the skin hinder the movement of the release film. Basically, there are two possibilities: The release film either becomes fixed in respect to the skin causing it to conform by stretching, or the release film does not become fixed causing it to slide on the surface of the skin. These mechanics are clarified in figure 14.

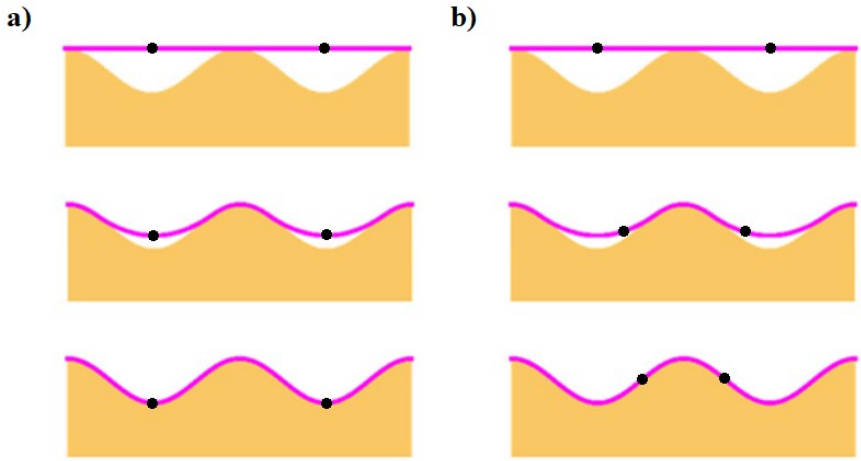

Figure 14. *The release film of a temporary transfer tattoo a) stretching while conforming and b) sliding while conforming, adapted from [29].*

In figure 14 a), the horizontal position of the black points on the release film is fixed. This means, that the distance of the black points along the surface of the release film needs to increase while it conforms to the surface. Thus, the release film needs to stretch. In figure 14 b), the horizontal position of the black points is not fixed and they move closer to each other in the horizontal direction. The distance of the black points along the surface of the release film remains the same through the steps. Thus, the release film needs to slide on the surface of the skin. In addition, since the adhesion between the release film and the skin increases as the true contact area increases, it is likely that at some point the adhesion is large enough to prevent the release film from sliding and it has to stretch to conform further. So, conforming the release film on the skin probably includes both of the basic mechanics.

The importance of these mechanics are not clear are they are not studied in this thesis. However, it should be noted that stretching of the release film while transferring it, lowers the maximum strain the release film can take after the transfer. This limits the applicability the tattoo. For example, if a maximum allowed strain for a conductor is 40 % and the transfer process increases the strain to 10 %, the conductor can be stretched by only 30 % on the skin. This should be considered in design process of tattoo applications. In addition, sliding of the release film causes it to wear due to friction, which could be hazardous to extremely thin films. Finally, it should be noted that the surface of the skin is not as uniform as figure 14 might let understand, and in reality the surface topography of the skin does not remain constant when pressure is applied on it. However, the mechanics

presented in this chapter can still be used as a guideline and give the basic idea of what should be considered when designing electrical transfer tattoos.

3.2.3 State of the art

There are some works that report tattoo-like electronic devices with some being extremely thin and even transparent as discussed in chapter 1. The graphene based tattoo sensors by Kabiri Ameri et al. [4] are probably the closest to the ideal tattoo-like device. One of these sensors mounted on skin is presented in figure 13.

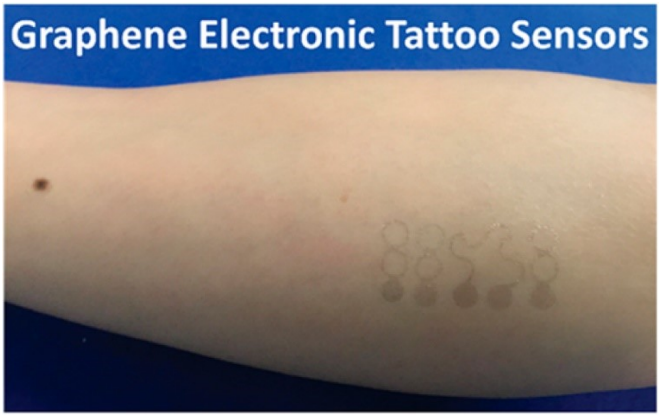

Figure 15. *A graphene based electronic transfer tattoo by Kabiri Ameri et al. [4].*

It is obvious from the figure above, that the transmittance of the tattoo is quite high. The tattoos by Kabiri Ameri et al. are also fully conformable, transparent, quite stretchable and are mounted without adhesives. However, the sheet resistance, which is close 2 kΩ/□, is far from desirable. Also, the fabrication process uses multiple process steps and one of them is etching copper, which is not desirable. [4] In this thesis, printing technologies were selected to remove the unnecessary and unwanted process steps along with other benefits.

So far, all the works that have reported these tattoo-like devices have used some commercial tattoo paper as a substrate. The problem is that these tattoo papers are designed to be used with normal water or oil based inks in normal inkjet printers with no post-treatments after printing. Therefore, there could be numerous problems when printing electronic transfer tattoos. First, the inks used usually include strong chemicals as solvents which might damage the tattoo paper. Second, printing with desired resolution demands good ink-substrate behavior which the tattoo paper might not fulfill. Third, post-treatments with heat or light could ruin the tattoo paper. In addition, often pre-treatments of the substrate are used before printing to ensure high printing quality, but it is possible that the pre-treatments also damage the tattoo paper.

4. MATERIALS AND METHODS

This chapter presents and argues chosen materials and methods. Printing methods were chosen in general because of their state of being environmentally friendly, scalability, cost-efficiency and the simple reason that they are widely used in electronics research and manufacturing. Some methods were also chosen after characterization of materials, discussed in chapter 5.1, showed that some materials cannot be processed with any initially chosen printing method. Characterization methods were chosen based on their advantages in thin film characterization and simply what was available.

Chosen methods affect the chosen materials, as not all the materials discussed in chapter 2 are suitable for printing. Also, there are material characteristics independent of deposition method that were discussed in chapter 2, and since not all materials have these characteristics, they are discarded at this stage.

4.1 Materials

The materials section presents the materials used in this thesis, which are divided in different types. Inks include conductive inks and dielectric inks, and substrates used are the temporary transfer tattoo paper and microscope glass slides.

Four conductive inks were initially chosen to be used in this thesis: one AgNW ink, one CNT ink, one graphene flake ink and one silver flake ink. There is also one silver nanoparticle ink just to test the inkjet printability and stretchability of the ink. In addition, the dielectric inks include one commercially available ink and one self-made ink.

4.1.1 Conductive inks

When selecting conductive inks, some specific properties were observed. Since the inks are printed on the temporary transfer tattoo paper, the inks should have low curing temperatures as it is assumed that the heat resistance of the tattoo paper is quite low. Furthermore, high conductance and high optical transparency are desirable properties of the printed layers, so transparency and sheet resistance of the inks were also observed. Conductive inks and their relevant properties are presented in table 1. All the information in the table is obtained from the datasheets of the inks or the websites of the inks' manufacturers [38–42].

Table 1. *Properties of chosen conductive inks.*

Ink	Sheet Resistance (Ω/□)	Transparency (%)	Curing Temperature (°C)
AgNW	50–100	>99	110
CNT	~(20–700)·10^3	N/A	80
Graphene	4·10^3	N/A	100
NPS-JL	0.060	N/A	120
CI-1036	<0.010	N/A	120

The AgNW ink was purchased as an inkjet-printable ink from Novarials Corporation. The AgNW ink has all the desired properties; however, according to the manufacturer the suggested layer thickness is 15–20 µm [38]. As discussed previously, sheet resistance and transparency of a thin film depends on the thickness of the thin film. Thus, it is reasonable to assume that the given theoretical values presented in table 1 apply for the suggested film thicknesses only. In this thesis, the coatings made with the AgNW ink will be below the suggested thickness range, and therefore the theoretical values could deviate from the measured values.

The CNT ink was purchased also as an inkjet-printable ink from NanoLab Incorporation. The ink has low curing conditions, but according to the measurement data provided on the ink's datasheet, the sheet resistance is high and the deposited layer is not transparent [39]. However, as transparency depends on the layer thickness, it is possible that the statement about the deposited layer not being transparent is related to a layer with high thickness. In addition, in theory CNTs should produce a transparent mesh-like network, and for that reason the CNT ink was selected.

The graphene ink was purchased as an inkjet-printable ink from Sigma-Aldrich. The ink has a reasonable sheet resistance and low curing temperature, but there is no information on the transparency. Thin graphene sheets are optically transparent, and since the ink contains graphene flakes that are 2D nanomaterials with a low thickness, the graphene ink was selected.

NPS-JL is a silver nanoparticle ink from Harimatec Incorporation. This ink belongs to the NPS-J series of inkjet-printable inks, and NPS-J is also a separate ink. The greatest difference between the NPS-J and NPS-JL is that the latter has a curing temperature of only 120 °C, which is suitable for the tattoo paper. However, NPS-JL is not transparent and not stretchable and thus, it is not suitable for fabricating transfer tattoos. Nevertheless, NPS-JL has been used in inkjet printing before and thus, it can be used to characterize the properties of inkjet printing as a manufacturing method in case the other inks fail.

Finally, CI-1036 is a screen-printable silver flake ink belonging to Engineered Conductive Materials (ECM) brand from Engineered Materials Systems (EMS) Incorporation. This ink is stretchable and highly conductive but not transparent, and screen printing as a method might produce too thick layers to fully conform to the skin. However, high conductivity, high stretchability and reliability of the ink with screen printing are reasons for selecting this ink.

4.1.2 Dielectric inks

DI-7540 is a screen-printable dielectric ink from EMS [43]. This ink is stretchable and designed to function with the CI-1036 ink. DI-7540 is also ultraviolet (UV)-curable so it should be suitable to be used on the tattoo paper. The ink has a sheet resistance of over 1000 MΩ so it can provide excellent insulation. However, the recommended film thickness when printed on silver is 36 µm, which increases the total thickness of the printed layers. [43] This in turn decreases the conformability of the transfer tattoos.

The other dielectric ink is a self-made PMMA ink. This ink was formulated by mixing 0.343 g of PMMA powder [44] by Alfa Aesar to 10 mL of toluene [45] purchased from VWR Chemicals. After mixing the two components, the solution was stirred on a magnetic stirrer for at least 24 hours before applying.

4.1.3 Substrates

Temporary transfer tattoo paper by Silhouette [46] was used as a substrate in most experiments. There is no information about the thermal properties of this particular tattoo paper, but a thermogravimetric analysis (TGA) of another tattoo paper, presented in figure 16, and heating tests by Sanchez-Romaguera et al. [47] suggest that the paper should not be used in temperatures higher than 135 °C.

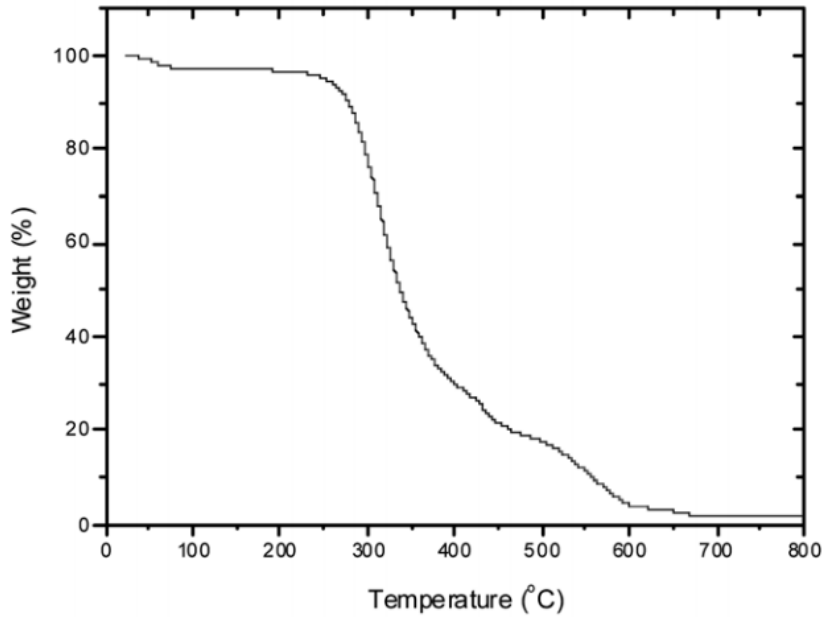

Figure 16. *Thermogravimetric analysis of certain transfer tattoo paper [47].*

The graph above shows an initial weight loss of the tattoo paper up to 100 ℃ apparently due to the loss of adsorbed moisture. After 225 ℃ up to 685 ℃, the weight loss occurs due to the decomposition of the tattoo paper's various components. This suggests that it should be safe to heat the tattoo paper up to a temperature of 225 ℃. However, the heating tests conducted by Sanchez-Romaguera et al. show that the tattoo paper starts to change color after 15 minutes at 150 ℃. Furthermore, 8 hours at 140 ℃ did not cause the tattoo paper to change color and thus, to be safe, Sanchez-Romaguera et al. decided to use 135 ℃ as the maximum curing temperature. [47] This temperature is also considered the maximum curing temperature in this thesis. Otherwise, the paper might start to change its color resulting in possible changes in the properties such as transferability.

A sheet of the tattoo paper along with a sheet of an adhesive film that is packed with the tattoo paper is presented in figure 17. Originally, the adhesive sheet was supposed not to be used. The tattoo paper sheets and the adhesive sheets are 216 mm x 279 mm in size. Thicknesses are unknown.

Figure 17. *A sheet of tattoo paper on the left and a sheet of an adhesive film on the right.*

Microscope glass slides by Corning Incorporated were used as a substrate material in some of the spin coating experiments. The slides are 75 mm x 25 mm in size. Thickness varies from 0.96 mm to 1.06 mm. The glass slides were cut in three for the experiments allowing square shaped coatings.

4.2 Fabrication methods

In this thesis, multiple methods were used to fabricate the transfer tattoos. Originally, inkjet printing was the primary fabrication method, but it was necessary to change the primary method to screen printing and to use also spin coating. Reasons will become clear later.

The following subchapters discuss these fabrication methods to give a general understanding of their operating principles and properties. Each chapter also discusses the advantages of the printing methods and presents reasons for choosing the methods used in this thesis.

4.2.1 Inkjet printing

Inkjet printing is a digital printing method which means that a digital image is used as the source for the printed patterns. The used ink is stored in an ink cartridge and the ink is jetted on the used substrate which is placed on the printing table of the printer. The printer used in this thesis is Dimatix Materials Printer model 2850 (DMP-2850) by Fujifilm [48], which is presented in figure 18.

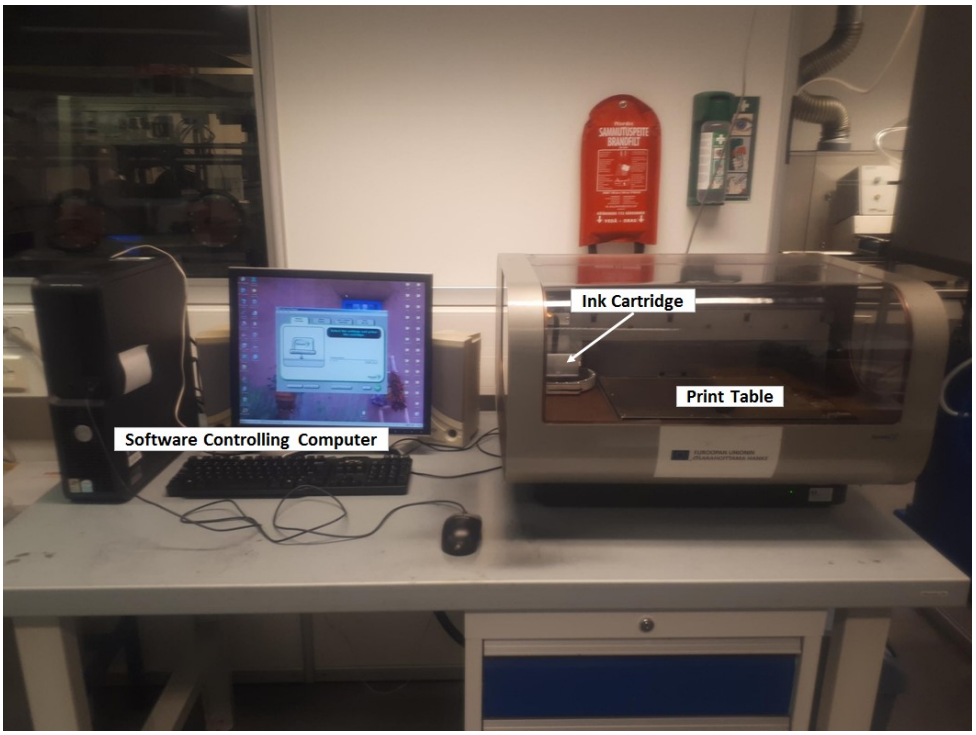

Figure 18. *DMP-2850 inkjet printer by Fujifilm used in this thesis.*

The ink cartridge has a piezo-driven jetting device, which means that a piece of piezoelectric material expands and compresses under a varying voltage. When the material expands, it forces an ink droplet out of the nozzle of the ink cartridge, and when the material compresses, it pulls more ink from the ink chamber of the cartridge to the nozzle ready for jetting the next droplet. This kind of printing, where ink droplets are jetted only when necessary, is called drop-on-demand (DoD) printing. [49]

The fact that inkjet printing is a digital printing method makes it possible to change the pattern anytime without the need to change settings of the printer or the need to use any external patterning equipment. The wasted amount of ink is also very minimal making the method cost-effective. It is possible to print thin layers, down to 100 nm, with inkjet printing, which is advantageous when considering the printing of the transfer tattoos that need to be thin [50]. Inkjet printing is also scalable process i.e., it is possible to scale it up to industrial manufacturing making inkjet printing an interesting fabrication method, even though in this thesis the scalability is not the main concern.

However, inkjet printing has slow printing speed when compared to e.g. screen printing. In addition, clogging of the nozzles of the ink cartridge is a common problem with inkjet printing as well as drying of the nozzles if the cartridge is unused for long periods of time. It is also not possible to use one cartridge for multiple different inks without getting the inks mixed, so every ink requires its own cartridge, and only one cartridge can be used at a time.

4.2.2 Screen printing

Screen printing is a printing method where ink is pushed through a patterned screen to a substrate under the screen. This way the pattern on the screen is “transferred” on the substrate. First, ink is added on the screen by hand. Second, the ink is spread over the pattern by a metallic squeegee. Third, a rubber squeegee is used to push the ink through holes that form the pattern. Finally, the pattern is formed on the substrate. The device used in this thesis is a semi-automatic screen printer SFC-300 by TIC which is presented in figure 19.

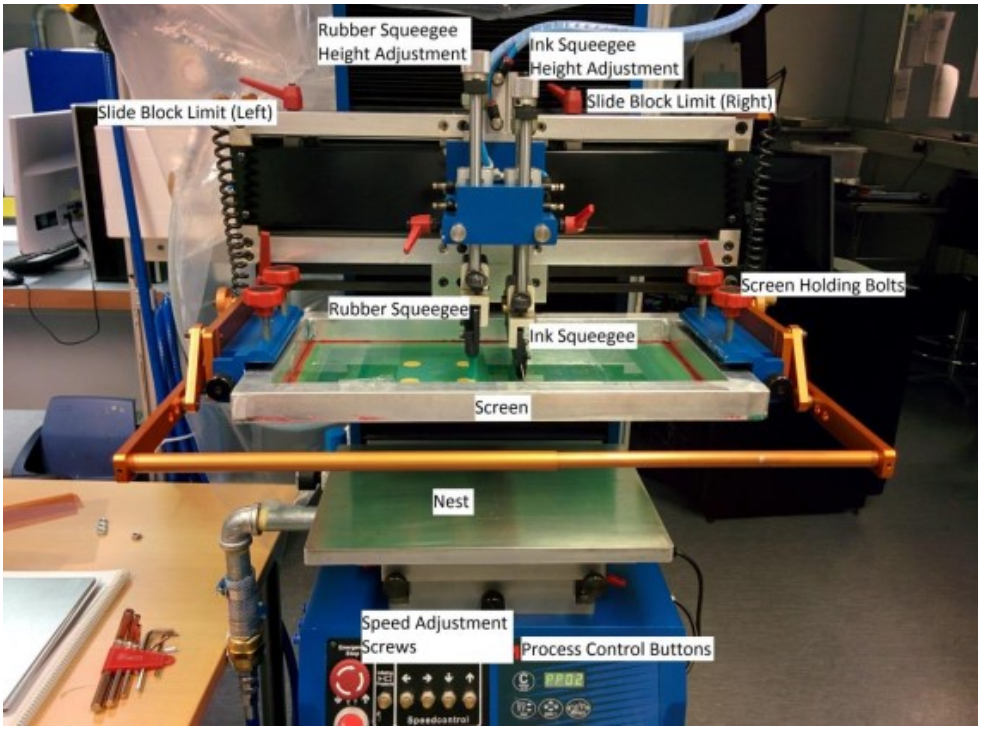

Figure 19. *SFC-300 screen printer by TIC used in this thesis [51].*

In the figure above, some relevant parts of the printer are marked. The parts are used to control e.g. pressures and speeds of the squeegees, and the size of the area where the ink is spread.

Screen printing is a relatively fast printing method when printing large patterns. Although it depends on the speed of the squeegees, it is still far faster method than inkjet printing. However, screen printing requires separate screen for each pattern which increases costs and consumes time to change the screens between different prints. It is also time consuming to set up the screen printer and clean the used screens after printing. In addition, the layer thicknesses are approximately 10 um at minimum, which could be too high for full conformability of the printed layers [52].

4.2.3 Spin coating

Spin coating is a deposition method where a substrate is rotated on high speed to spread a solution on the substrate by centrifugal force. The substrate is placed on a holder inside the spin coater, and a vacuum is usually used to keep the substrate in place. The speed used to rotate, the acceleration used to achieve the final speed and the time used to run the program, are set on the control panel of the spin coater. The control panel can also be used to add multiple steps where each step may have different speeds, accelerations and times. This way the spin coater may be used to run complicated coating programs if necessary. In this thesis however, only one step is used. After placing the substrate and adjusting the desirable settings, the used solution is drop casted on the substrate, and the set program is then run. The solution spreads on the substrate and eventually off the edges. [53]

Due to high speeds usually used in the process, the air flow above the substrate causes the usually volatile solvent in the solution to evaporate, increasing the viscosity of the solution until it no longer can be moved by the centrifugal force [53]. After this, the coating is complete. Model WS-650SZ-8NPP/LITE spin coater by Laurell Technologies Incorporation [54] used in this thesis is presented in figure 20.

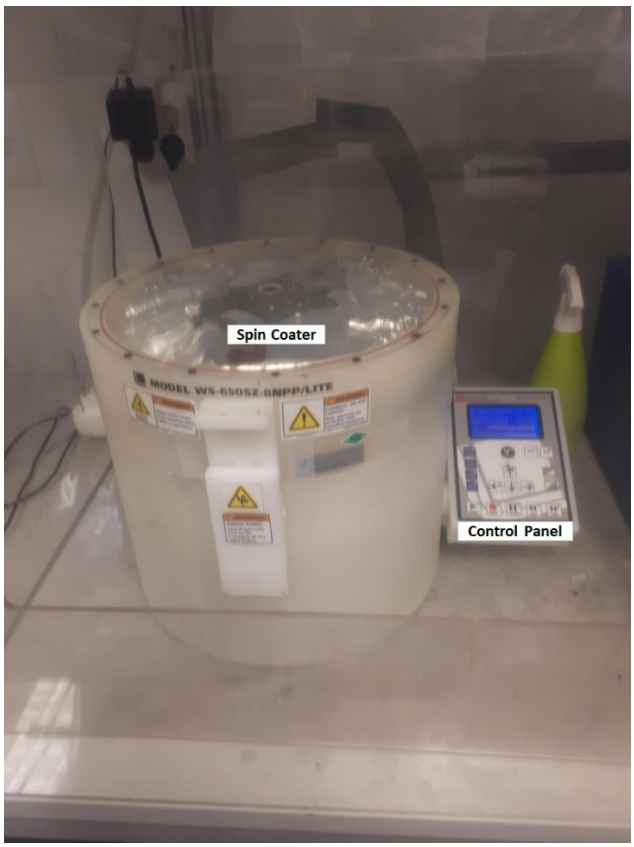

Figure 20. *Model WS-650SZ-8NPP/LITE spin coater by Laurell Technologies used in this thesis.*

Uniformity and thickness of the coating are the most important properties. Coating thickness can be managed by changing the rotation speed and acceleration. Acceleration is also important when considering the uniformity of the coating. Due to possible topographic features from e.g. previous processes, the solution may not uniformly spread around the surface of the substrate. The final speed phase provides a radial force to the solution, while the acceleration phase adds a twisting force, which may aid in the uniform spreading of the solution. [53]

Spin coating is a suitable method for creating extremely thin coatings. It is also very easy to use method, even though planning a suitable coating program with different speeds and accelerations could be time consuming. The problem of spin coating is the amount of waste it produces. The method requires relatively large amount of solution in respect to the size of the coating. The other problem is that spin coating is not suitable for creating patterned layers. Thus, other methods of patterning need to be considered for spin coated layers. This adds unnecessary steps to fabrication process when compared to screen printing and inkjet printing.

4.3 Characterization methods

Actual samples as well as samples fabricated during the material characterization process were electrically and mechanically characterized using multiple setups and instruments. These methods were selected considering their suitability for characterization of thin films. In addition, these methods were the most suitable methods available.

The purpose of the following subchapters is to discuss the used characterization methods. The primary principles of operation are presented, and pros and cons are reviewed. Also, there are some characterization methods, e.g. a multimeter, that are used only little and thus, are not discussed in detail.

4.3.1 4-point probe method

4PP method consists of a probe station and Keithley 2425 Sourcemeter. Four wires are connected to the appropriate terminals of Keithley 2425 Sourcemeter and to the terminals on the outside of the probe station. Then the actual probes inside the probe station are connected to the appropriate terminals on the inside of the probe station. With this setup, a connection between the probes and Keithley 2425 Sourcemeter is established. The probe station and Keithley 2425 Sourcemeter with the necessary connections are presented in figure 21.

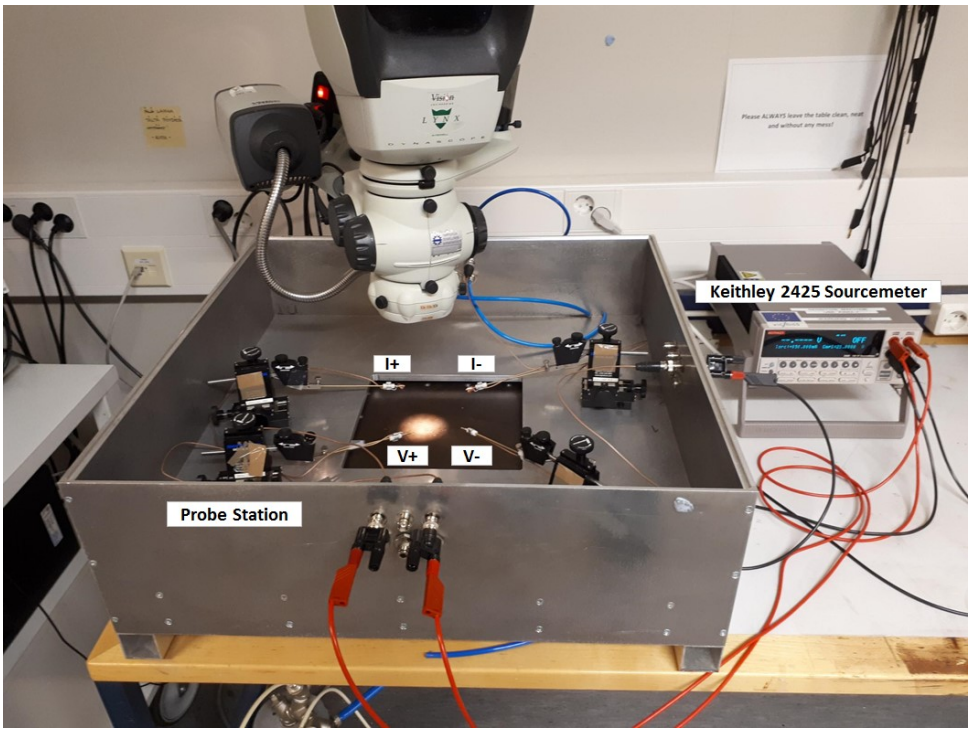

Figure 21. *The 4-point probe measurement setup used in this thesis.*

The idea of 4PP method is to use two probes for current conduction and another two for voltage measurement. The current probes and voltage probes are marked in figure 21. Positive current probe means that the current flows *from* that probe to the pattern under measurement, and negative current probe means that the current flows *to* that probe from the pattern.

The advantage of 4PP method is its suitability for measuring thin films. In addition, since current is fed to the pattern and voltage is measured using different probes, the contact resistances can be eliminated. Thus, measuring low sheet resistance values accurately is possible. However, in 4PP measurements the surface area of the sample needs to be relatively large, and thickness no more than 40 % of the probe spacing. Basically, this means that the sample needs to be thin in respect to the surface area. If these requirements are not fulfilled, correction factors need to be used. [6]

4.3.2 Electrical characterization of stretched tattoos

Electrical characterization of the fabricated tattoos used in tensile tests was conducted using Keithley 2425 Sourcemeter combined with a LabView data logger running on a laptop. The laptop is connected to Keithley 2425 Sourcemeter with a General Purpose Interface Bus (GPIB)–Universal Serial Bus (USB) -cable. The setup is presented in figure 22.

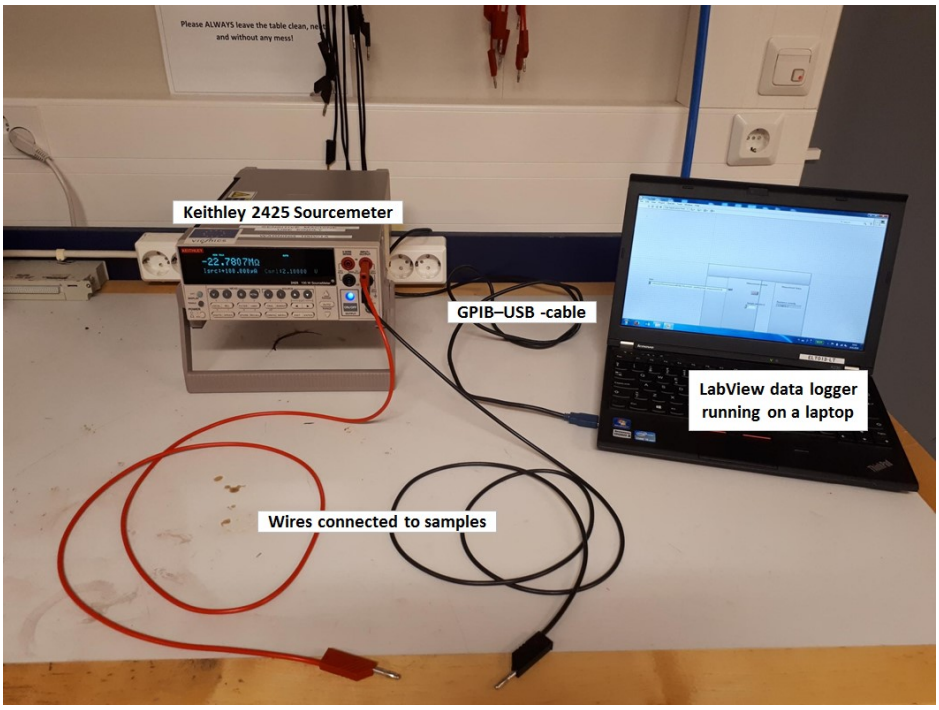

Figure 22. *The setup used to measure and log resistance values of stretched tattoos.*

Keithley 2425 Sourcemeter uses 2-probe method to measure the samples in this setup. This method is used since conductors with just two pads are easy to use in tensile tests. The LabView data logger saves resistance measurement data in to a text file and the data saving frequency can be varied. So, if the strain rate of the sample is high, the data saving frequency should be high as well. This ensures that there are enough saved data points during the deformation. On the other hand, the data transfer rate of GPIB–USB -cable is limited and thus, only moderate saving frequencies should be used. In this thesis, all tests used a 5 points per second saving frequency.

4.3.3 Instron 4411 tensile strength tester

Instron 4411 tensile strength tester was used for the mechanical and some of the electro-mechanical characterizations of the stretched samples. The device is designed to be used for mechanical characterization of materials and provides a possibility to either stretch or compress samples. In this thesis, samples are only stretched though. Instron 4411 tensile strength tester is presented in figure 23.

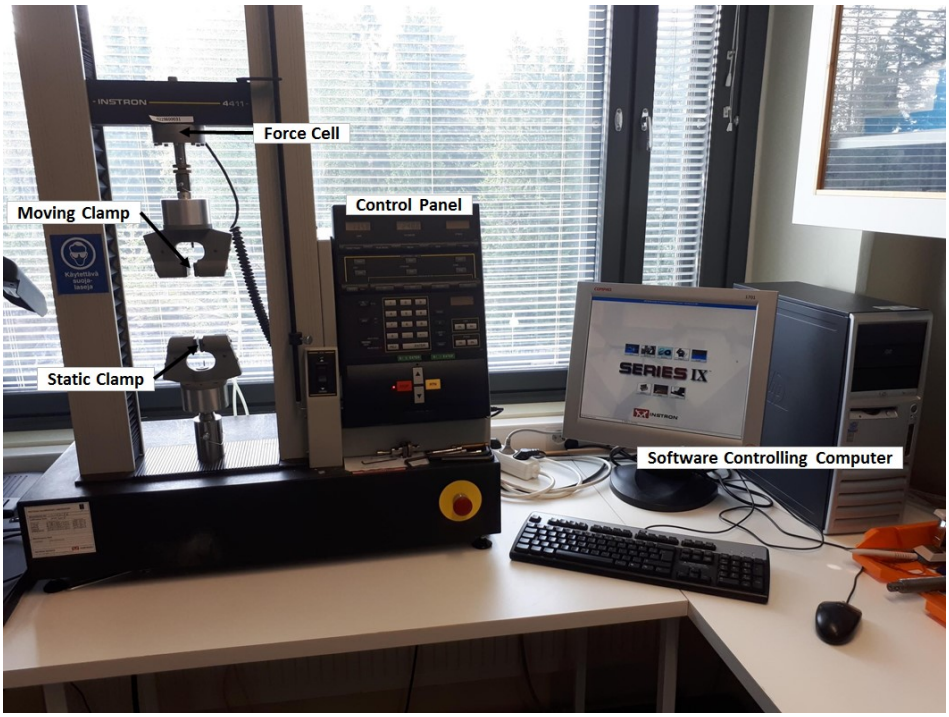

Figure 23. *Instron 4411 tensile strength tester.*

The basic operating principle of the device is to stretch a sample attached to the two clamps and measure and save the force and strain exerted on the sample. The device is a computer-controlled and the measurement data is saved on the computer in to a text file. Test settings such as strain rate, grip distance, data saving frequency etc. can be set on the computer software controlling the test.

One advantage of using Instron 4411 in a tensile test is the constant strain rate that is automatically maintained. This cannot be guaranteed in on-skin tests. This method also automatically measures the force and strain of the sample. Disadvantages are mainly the effects of the clamps on thin films. For example, the clamps can easily produce stress concentrations and discontinuities in stretchability of the samples causing their premature tearing.

5. EXPERIMENTS

This chapter describes characterization of the new materials as well as fabrication of samples for main experiments and characterization of these samples. The experimental section consists of three parts: characterization of materials, fabrication of samples for main experiments and characterization of these samples. Before the actual samples for main experiments can be fabricated, it is mandatory to find suitable methods for the fabrication process, which practically means testing the materials with different methods. Flowchart for the material characterization process is presented in figure 24.

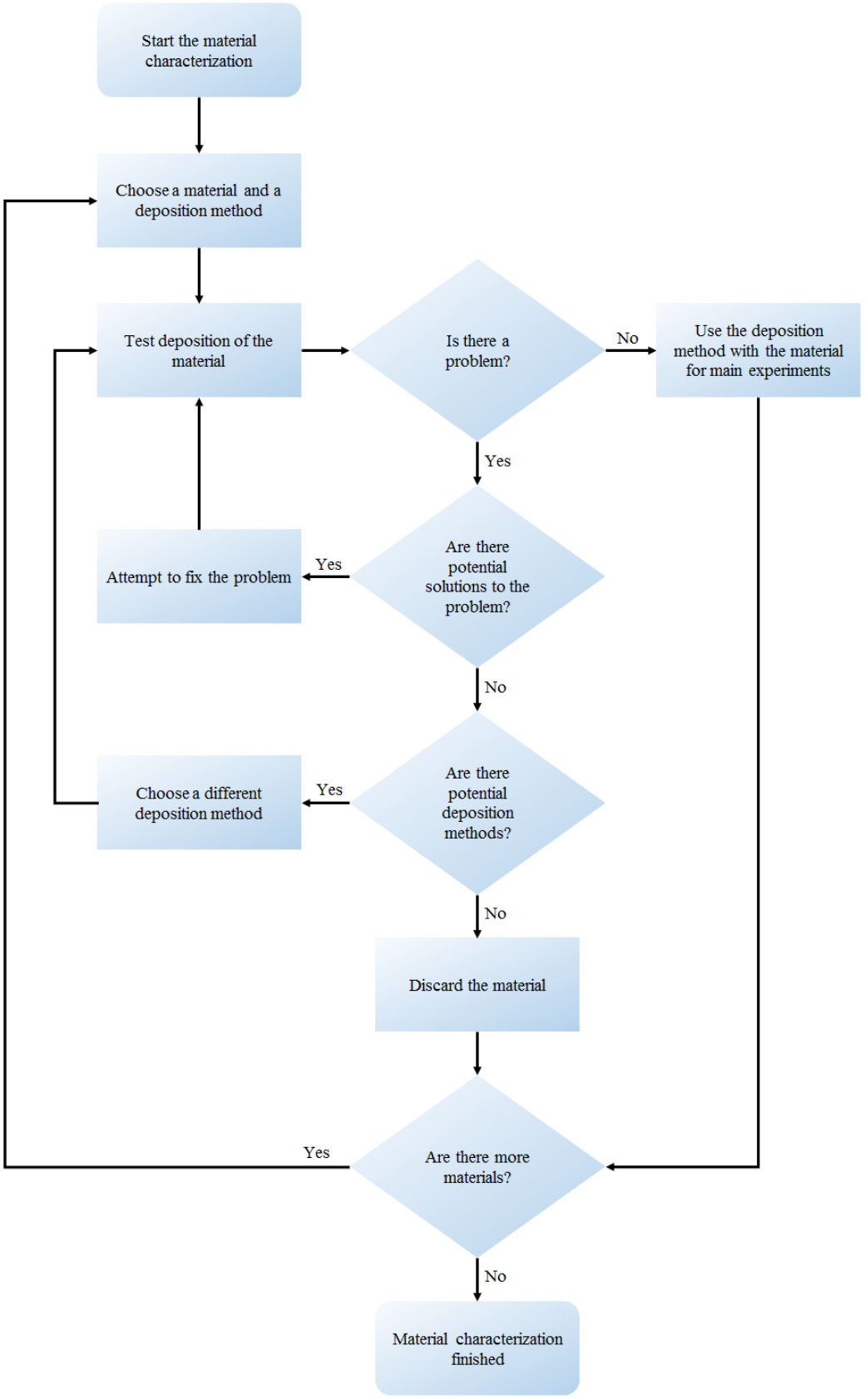

Figure 24. *A flowchart for choosing and eliminating materials during the material characterization process.*

The flowchart used in the material characterization process describes the choosing process in general, so it can be used basically in any kind of material choosing process or applied to other kind of processes. However, the strict requirements for each step in the process are not presented in the flowchart e.g., there is no information on different possibilities for attempting to fix encountered problems.

5.1 Characterization of new materials

Before it is possible to do any main experiments, materials need characterization. In this thesis, multiple materials were used that have not been used together before. Thus, the materials need to be tested out in different situations to see what can be done with them. The results of the characterization step in the experiments determine what kind of main experiments are done.

The flowchart in figure 24 is the general guideline for the process. The different methods used in each step of the process are chosen based on the expertise and knowledge of people associated with this thesis, as well as information found in literature. However, only as many different attempts to fix problems and test different deposition methods were used as was possible or considered worthy.

5.1.1 Temporary transfer tattoo paper

The main concern with the tattoo paper is the heat resistance. The inks need thermal curing and the dielectric ink DI-7540 needs UV curing, which also heats the substrate. Most of the different characterization processes also test the tattoo paper, so it is not necessary to conduct individual tests for all the properties of the paper.

The heat resistance test for the paper is quite simple. Four pieces of tattoo paper were cut and taped on separate aluminum plates. The pieces were then baked in an oven for 20 minutes. However, the temperature was different for each piece. The temperatures were 100 °C, 120 °C, 140 °C and 160 °C. After the baking process, the color of the pieces was examined. The results are briefly analyzed in chapter 6, but it was these results that were used to conclude that 20 minutes to 30 minutes at 120 °C should be the highest time-temperature combination.

5.1.2 Inkjet printability of NPS-JL and the new inks

The AgNW ink from Novarials was purchased as inkjet-printable ink, so it was first test printed with the Dimatix inkjet printer. The problem with inkjet printing was the extremely poor printability of the ink. At first, there was no clear droplets forming, only some obscure splashing of the ink, and after maybe 10 to 20 seconds, there was no ink coming out of the nozzles at all. The first possible solution to the problem was to test

different voltage waveforms, purging the nozzles and wetting the nozzles with ethanol moistened cleanroom paper. However, none of these improved the printability of the ink.

Degassing and filtration of the ink was done as a second possible solution to the problem. The ink was first degassed under -0.8 bar vacuum for 120 minutes and then filtered using a 0.45 µm filter. However, filtering the ink became also a problem as the ink was extremely "heavy" to inject through the filter. This was most likely caused by the AgNWs in the ink being too large and clogging the filter. Thus, the filtration step was removed from the problem solving process. After the ink was degassed, it was test printed again. However, there was no improvement in the printability of the ink.

Third possible solution tested was sonication of the ink, even though the manufacturer does not recommend this. The sonication was executed by placing an ink filled cartridge in to a pool of water and letting ultrasonic waves run through it. During the sonication, ink started to flow out of the nozzles clearing possible clogs, and the printability of the ink was tested again. However, there was still no improvement.

At this point it was concluded that there seems to be no clear solution to improve the printability of the ink. Furthermore, based on experience, the cause of the problem could be water that is used as the solvent of the ink. For sufficient droplet formation, the ink needs to wet the nozzle plate of the printer. However, water may not achieve sufficient wetting for some reason. Another possible, and also likely, reason is the clogging of the nozzle. The AgNWs are usually in micrometer range in length, but the largest recommended particle size for the Dimatix printer is approximately 0.2 µm.

The above described characterization procedure was also performed for the CNT ink from NanoLab and graphene ink from Sigma-Aldrich, which were also both purchased as inkjet-printable inks. Both of the inks also had water as a solvent and the printability was just as poor for both of them as it was for the AgNW ink. The differences were that the CNT ink was actually forming clear droplets for maybe 10 seconds but then stopped, and purging the nozzles when using the graphene ink completely emptied the cartridge. Since the purchased graphene ink container was only 5 mL, it ran out after the inkjet printability tests and thus, it was discarded.

The NPS-JL ink was also inkjet printed, and there were virtually no problems. This test was conducted to confirm the functionality of the inkjet printing as a deposition method. Five conductors, 50 mm x 2 mm in size, were printed and the electrical conductivity was confirmed. After printing, the conductors were transferred on to a poly(ethylene terephthalate) (PET) film with the ends of the conductors being connected to copper tapes attached to the PET film. It was confirmed that the conductivity was lost after the transfer and observation through microscope showed visible fractures in the conductors near the copper tapes. The small local strains due to the difference in height between the PET film and the surface of the copper tape caused the fractures resulting in loss of conductivity. It

was concluded that the nanoparticle-based ink is not suitable for stretchable applications, as was already expected before the test. Thus, the NPS-JL ink was discarded.

5.1.3 Spin coating, lifting and transferring of PMMA

Spin coating of the PMMA solution was done by first drop casting the solution on a glass substrate and then using different accelerations and spinning speeds to see if a continuous film can be produced. This test was done to see if it was possible to use the PMMA film as a carrier film for lifting a conductive ink layer.

The highest speed and acceleration used was 1500 revolutions per minute (rpm) and 200 rpm/s, respectively. The films coated were highly transparent, so it was difficult to examine if an acceptable film was formed. Figure 25 presents a spin coated PMMA film on top of a microscope glass slide.

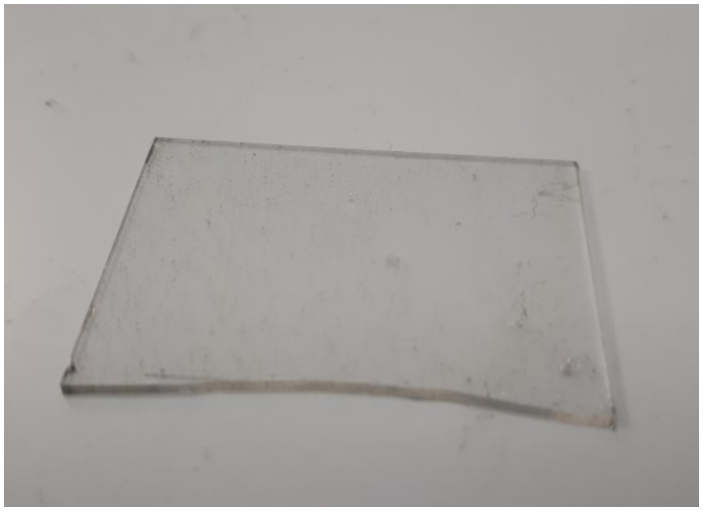

Figure 25. *A spin coated PMMA film on top of a glass slide. The PMMA film is extremely thin and highly transparent, so spotting the difference between the glass slide and PMMA film is not possible.*

After spin coating the PMMA films, but before the lift and transfer process, it is necessary to do some preparations to the tattoo paper because the backside of the paper must not get wet. Thus, the tattoo paper was placed on a PET film backside down and then the edges of the tattoo paper were sealed with scotch tape. Figure 26 presents a prepared piece of tattoo paper.

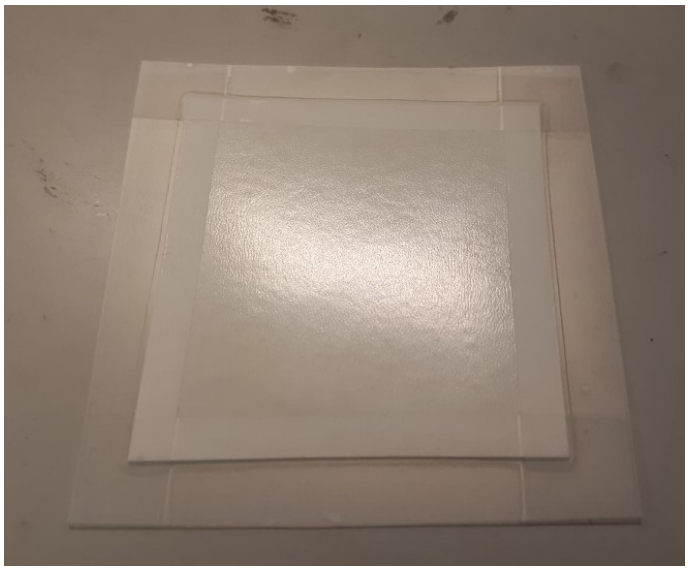

Figure 26. *A piece of tattoo paper covered with a PET film from the back and scotch tape from the edges to prevent the backing paper from wetting.*

After the necessary preparations were done, one glass slide at a time was placed on the surface of water in a suitable container. The water started to penetrate in between the PMMA film and glass, resulting in the PMMA film lifting and floating on the surface, while the glass slide sank underwater. This is due to the tendency of the water to wet the high surface energy glass slide and repelling the low surface energy PMMA film. The successful lifting of a film from the glass slide was considered as a confirmation for a successful spin coating of PMMA. Figure 27 presents the process steps of lifting and transferring the lifted PMMA film on to a piece of tattoo paper.

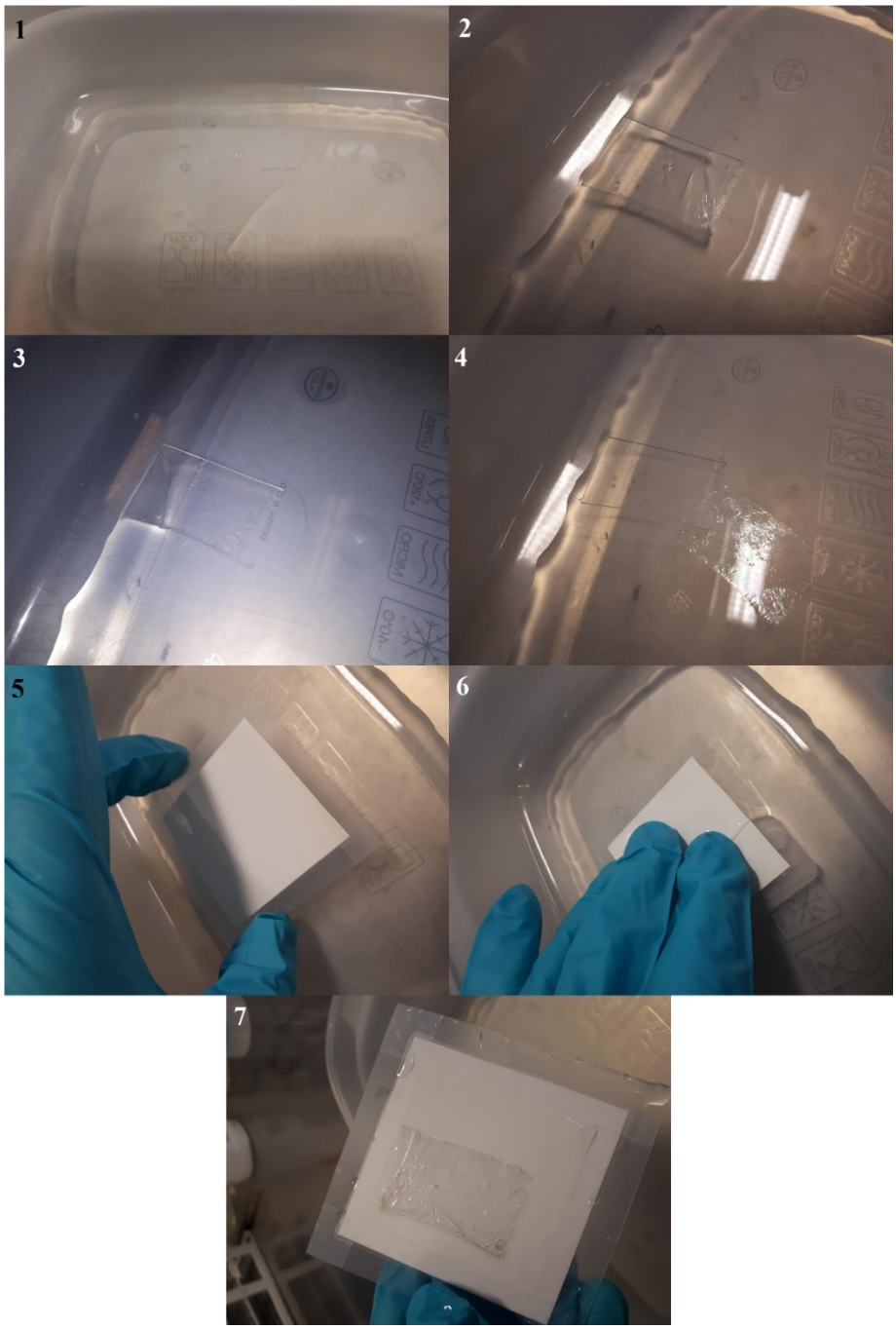

Figure 27. *The process steps of lifting and transferring the spin coated PMMA film on to a piece of tattoo paper.*

The figure above shows the glass slide first floating on the surface of the water in step 1. Then the water starts to lift the PMMA film. This is visible by observing the glass slide in step 2. The PMMA film has partially been lifted from the right side of the glass slide. In step 3, the PMMA film is attached to the glass slide only little from the left side, and in step 4 the whole film floats on the surface, while the glass slide has sunk underwater. Steps 5 to 7 show how the tattoo paper is first placed above the floating film, then pressed against it and finally lifted up to show the PMMA film attached to the tattoo paper. After this, the tattoo paper is dried in an oven for 20 min at 50 °C to remove any water residues.

After removing the water residues, the PMMA film is quite wrinkled. The wrinkles can be removed, at least partially, by heating the film in an oven. The reason in not confirmed, but the straightening of the wrinkles probably results from the PMMA entering a viscous state, after the glass transition temperature is exceeded, and straightening on itself due to the surface tension of the viscous PMMA. However, the glass transition temperature of the used PMMA is not known and thus, the required temperature is not known. Generally, the glass transition temperature of PMMA varies somewhere between 87–157 °C [55]. To make sure that the glass transition temperature was exceeded, the temperature of the oven was set to 180 °C and time to 30 min. This was obviously too high temperature for the tattoo paper not to change color but was done to demonstrate the method's ability to remove the wrinkles. Figure 28 presents the tattoo paper before and after straightening the wrinkles in an oven.

Figure 28. *The tattoo paper before (on the left) and after (on the right) removing wrinkles from the PMMA film in an oven.*

From figure 28, it is visible that some of the wrinkles have been removed. However, there are still some wrinkles left, and it is possible that the release film of the tattoo paper somehow interrupts the viscous flow of the PMMA. This conclusion was made, since another PMMA film, that was transferred on to a piece of PET film, straightened almost completely. On the other hand, the wrinkles remaining on the PMMA film may have been formed during the spin coating process and simply require more time to straighten under the viscous flow.

5.1.4 Spin coating of the AgNW and CNT inks

After concluding that the inkjet printing of the new inks was not possible, it was tested if it was possible to spin coat them. The spin coating was done by drop casting ink on a glass substrate and then using different accelerations and spinning speeds to find out if it was possible to form a thin film on the substrate. The AgNW ink was behaving well on the substrate with multiple accelerations and spinning speeds, but the CNT ink did not

form a continuous film on the substrate, even though there seemed to be no problem with wetting.

After testing the spin coating of the inks on a glass substrate, it was tested if the inks can be spin coated directly on the temporary tattoo paper. However, the inks seemed to break the release film of the paper during the spin coating process ruining the whole paper. It is not possible to confirm the reason, but the breaking of the release film was probably caused by the solid particles in the inks abrading through the thin release film.

Since it was not possible to spin coat the inks directly on the tattoo paper, an alternative method to deposit an ink layer on it using spin coating was developed. First, a PMMA layer was spin coated on the glass substrate and it was tested if the inks can be spin coated on top of the PMMA layer. The AgNW ink formed a continuous thin film on top of the PMMA layer, but the CNT ink was completely removed from the substrate during the spin coating process. It was quite obvious that the reason for the CNT ink's poor behavior was the hydrophobicity of the ink. Clearly, the ink did not wet the surface of PMMA.

The CNT ink has only water as its solvent, and no other solvents to decrease the surface tension of the water. For this reason, the surface tension of the CNT ink is much higher than PMMA's and wetting its surface is difficult. Thus, isopropyl alcohol (IPA) was mixed with the CNT ink to decrease the surface tension. After doing so, the performance during the spin coating increased clearly. However, the result was the same as spin coating the CNT ink directly on glass; there was no continuous film. It was decided that the CNT ink is discarded after this test.

After spin coating the AgNW ink on the PMMA coated glass substrate, it was floated on water. The process is virtually the same as described in chapter 5.1.3. However, in this case the water tends to wet the surface of the AgNW coating in addition to wetting the surface of the glass. As a result, lifting the PMMA–AgNW bilayer is more difficult than lifting the bare PMMA layer, although manageable. After this, the bilayer was dried and wrinkles were removed. However, the problems at this point are basically the same as described in chapter 5.1.3.

5.1.5 Electrical characterization of the AgNW ink

After spin coating the AgNW ink on a glass substrate, the sheet resistance of the formed conductive layer was measured using 4PP method. The formed layers were square shaped due to the shape of the microscope glass slides and thus, it was easy to calculate the sheet resistance after obtaining the measurement results.

Since the expected sheet resistance was not known, the current was first set to 10 µA. It was then raised slowly until a constant voltage-to-current ratio was found. The measured voltage and used current was then used to calculate the sheet resistance of the layer. This

characterization step was done to examine the potential of the AgNW ink as a material to produce electrical conductors.

5.2 Fabrication of screen printed samples

Before the actual screen printing of samples, some preparations were made. The screen printer was first prepared by installing the squeegees and the screen for printing conductive layers. The screen was aligned so that the squeegees were centered between the long edges of the screen to make sure the squeegees covered the whole pattern widthwise. Also, the slide blocks for limiting the length of squeegee movement were set so that both squeegees covered the pattern lengthwise. These two steps were done to make sure the ink is spread over the whole pattern. The layouts that were used to print the conductive and dielectric layers are presented in figure 29. The aqua colored layer is the dielectric layer which is printed on top of the silver colored conductive layer. Figure 29 also shows the alignment of the two layouts. The top row of the complete layout consists of Greek crosses and the pattern below the Greek crosses is referred to as a π-conductor for its resemblance to the Greek letter π. In addition, the layout includes U-conductors and a pattern referred to as a big square.

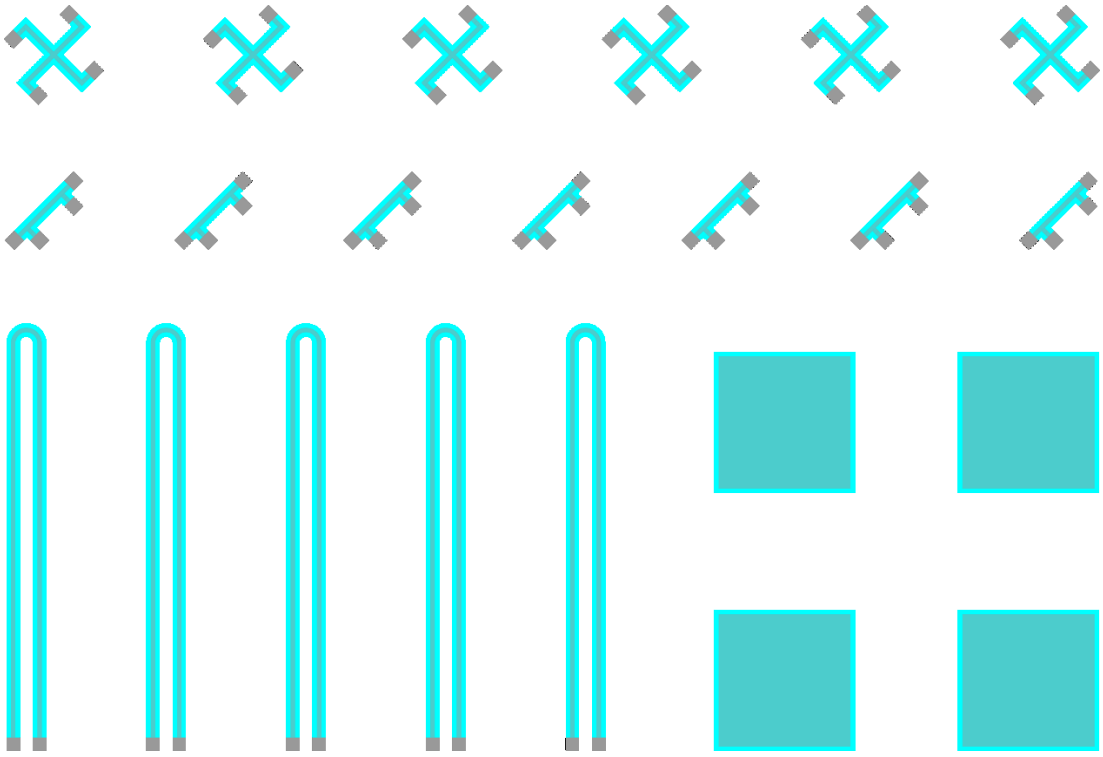

Figure 29. *The layouts for printing the conductive and dielectric layers. The conductor parts in the samples are 1 mm wide and the pads are 3 x 3 mm^2. The big squares are 30 x 30 mm^2. The total length of the U-conductor is 188.4 mm not including the pads. In addition, the dielectric layer has a 1 mm overflow over the edges of the conductors and the big squares.*

After installing the screen and the squeegees, optimal squeegee settings were searched. This is done by following certain procedure for which a process flowchart is presented in figure 30. In addition to the steps in the flowchart, it is possible to encounter a problem where the ink spreads unevenly on the substrate i.e., the quality of the pattern is fine in one area but not in another. In this case, the problem lies with the angle of the rubber squeegee which needs to be readjusted so that the pressure of the squeegee is even along its long side. This problem should not be encountered though if the initial step of adjusting the squeegee angle is followed accurately enough.

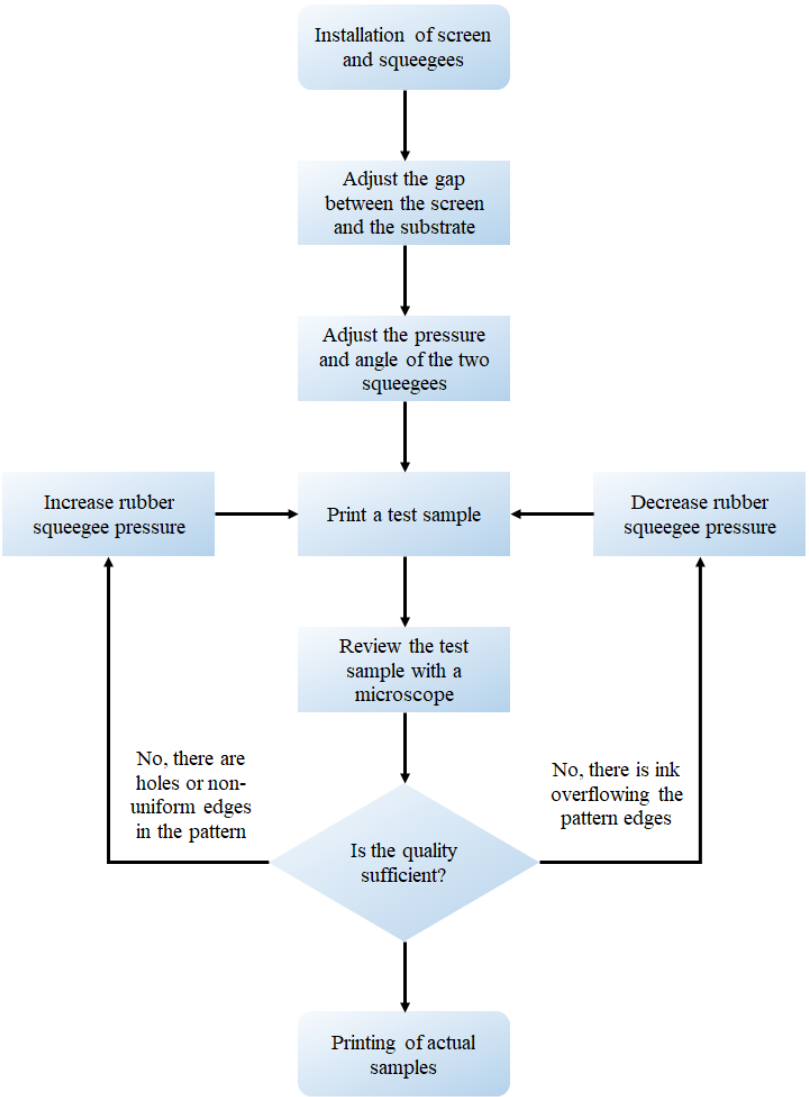

Figure 30. *The process of optimizing print gap and squeegee pressure.*

The first step of the optimization process is to adjust the print gap, or in other words, the gap between the bottom side of the screen and top side of the substrate. This is done by first placing a sheet of tattoo paper on the printing table and lowering the screen on it. Then the operator of the printer can feel the print gap by pressing the screen against the substrate with a finger. It should feel the same as pressing the little finger and thumb

together. If pressing the screen feels softer or harder than pressing the little finger against thumb, the screen needs to be lowered or raised, respectively.

The second step is to adjust the pressure and angle of the two squeegees. The metal squeegee is adjusted so that it is as close to the screen as possible without touching it. The angle is adjusted so that the gap between the screen and the squeegee is uniform along its long side. One practical method of testing whether the gap is good or not is to place a sheet of cleanroom paper between the screen and the squeegee and then pulling the sheet as the squeegee presses it against the screen. The sheet of paper should not move completely freely but the squeegee should hinder its movement as little as possible. Since the cleanroom paper is quite thin, this method makes it possible to find a suitable pressure for the metal squeegee.

The rubber squeegee is adjusted in a different way. When the screen is lowered on the substrate, the pressure of the rubber squeegee is adjusted so that the squeegee can press the screen against the substrate only barely. Whether the pressure is sufficient or not can be tested by pressing the screen against the substrate with a finger while the squeegee is pressing the screen. It should be easy to tell whether there is still a gap between the screen and the substrate. If there is a gap, then the pressure of the squeegee needs to be increased. The size of the gap needs to be tested everywhere along the long side of the squeegee to make sure that the pressure is even along its long side. Otherwise, the angle of the squeegee needs to be adjusted. This step should be done carefully since after adding ink, it is harder to test the pressure. Furthermore, from experience it can be said that when the angle and pressure of the rubber squeegee is adjusted as explained, the pressure should be increased by turning the height adjustment knob by approximately half a turn.

The third step is to print a test sample. For this purpose, a sheet of PET is placed on top of the tattoo paper on the print nest. This ensures that the tattoo paper is not wasted for test purposes as the paper cannot be cleaned without destroying it. After printing the first test sample, it is reviewed with a microscope. The defects that are searched for are non-uniform edges and holes in the pattern, and ink overflowing the pattern edges. In the case of non-uniform edges and holes, the pressure of the rubber squeegee is not high enough to force the ink through every hole in the mesh leaving empty holes in the printed pattern. Thus, the pressure should be increased. On the other hand, if the pressure is too high, it forces the printed pattern to flatten causing the ink to spill over the edges of the pattern and thus, the pressure should be decreased. After readjusting the pressure of the rubber squeegee, another test sample is printed and reviewed. If there are defects, optimization is done again until sufficient quality is achieved. After the optimization is done, the actual samples were printed. In total, four sets were printed. The term set refers to one sheet of the tattoo paper with either the conductive layer or both layers printed on it.

After printing, the samples were cured in an oven for 10 min at 120 °C. Then the sheet resistance was measured from two samples in each set and all the samples were cured for

additional 10 min to see if the sheet resistance dropped. After the additional round of curing, the sheet resistance was measured from the same samples as before the additional curing. The sheet resistance dropped by approximately 10 % and it was concluded that no more additional curing is needed, and that a total of 20 min at 120 °C is a sufficient curing schedule.

After printing the conductive layers, the sheet resistances of the samples were measured, but this is discussed in the next chapter in more detail. After measuring the sheet resistances, dielectric layer was printed on the samples in sets 1 and 2. The method of setting up the printer and printing a test sample is the same as when printing the conductive layers.

Since the screen printer is manually set up, the alignment of the screen needs some consideration. This was simply done by placing the tattoo paper with the conductive layers on the print nest, and the screen was lowered on the tattoo paper. The layout on the tattoo paper was visible through the holes of the stencil on the screen, so it was possible to examine how much the tattoo paper needed to be moved to reach a sufficient alignment. After doing so, the exact spot of the tattoo paper was marked on the print nest with a pencil. All sheets of tattoo paper were then placed inside the marks. The important detail in this alignment method is to do it carefully in the first place because the substrate is not visible through the screen after ink has been spread on it. After printing the layers, the sheets were cured in an UV oven for 45 minutes each. However, the used intensity is not known, and the suitable curing time was found by trial and error. Figure 31 presents one from each type of samples after printing and curing the conductive and dielectric layers.

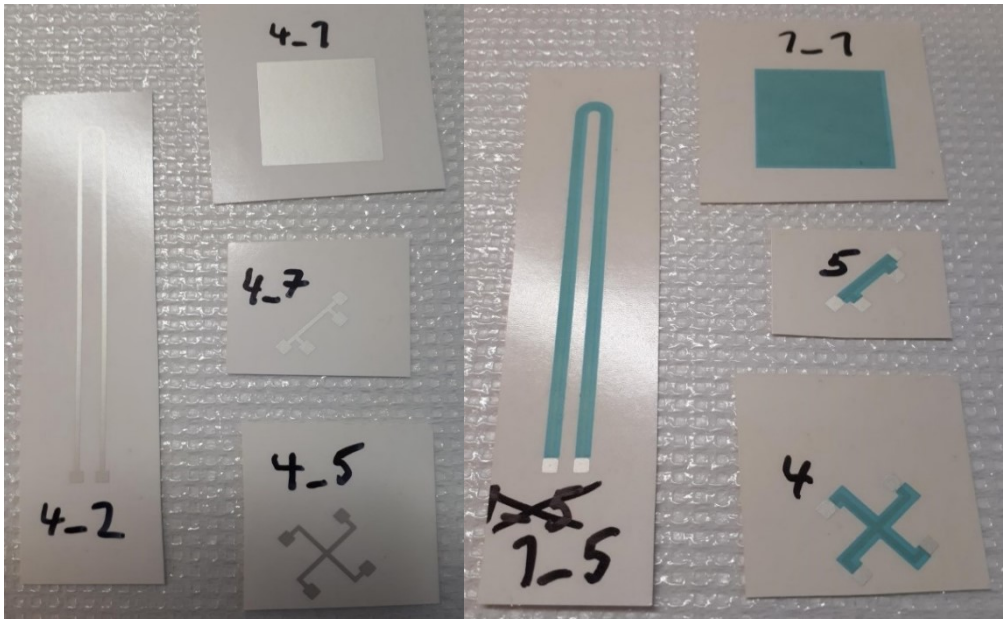

Figure 31. *Some samples after printing and curing the conductive (on the left) and dielectric (on the right) layers.*

By looking at especially the Greek cross sample on the right side of figure 31, the alignment of the dielectric layer is seen. The pads should be open, like they are, and there should be 1 mm of the dielectric layer on both sides of the conductive layer. The alignment could be better, but it is difficult to achieve by alignment by hand.

5.3 Resistance measurements of the screen printed tattoos

After screen printing the conductors on the tattoo paper, the sheet resistances were measured using 4PP method and a regular multimeter. 4PP method was used for the Greek cross, π-conductor and big square patterns, and the regular multimeter was used for the U-conductors. 4PP method measures the voltage across a pattern while known current is fed through the pattern. In the case of the Greek cross and big square patterns, it can be shown that their sheet resistance is

$$R_S = \frac{\pi R}{\ln 2} = \frac{\pi}{\ln 2}\frac{V}{I}, \tag{6}$$

where V is the measured voltage and I is the used current [56, 57]. However, it should be noted that the probes need to be placed to the corners of the big squares and as close to the perimeter as possible for equation (6) to hold. For calculating the sheet resistance of the π-conductor and U-conductor pattern, equation (3) is used. The resistance needed in the equation is measured directly from the U-conductor with a multimeter and can be calculated for the π-conductor by dividing the measured voltage with the used current.

In 4PP measurements, the voltage was measured 2 times from π-conductors and 4 times from Greek crosses and big squares. The patterns with pads numbered are presented in figure 32. The figure helps to understand the probe locations in each measurement.

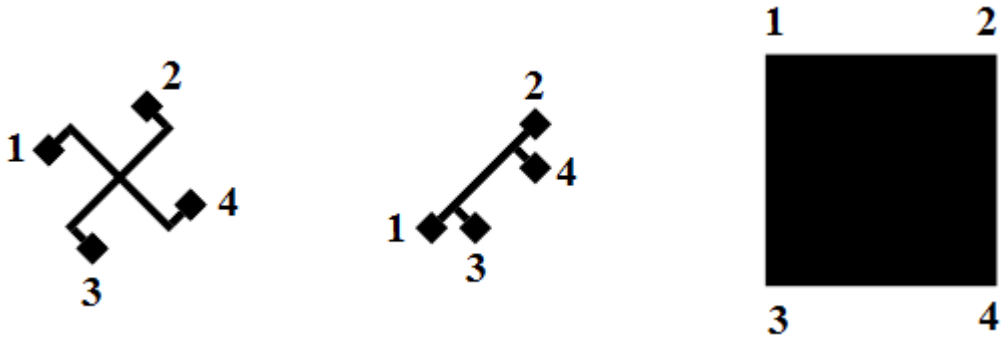

Figure 32. *Patterns, with numbers indicating probe locations, measured using 4PP method.*

Since the big square pattern does not have pads, the probe locations are referred to as "corners" in this pattern. In the first measurements, positive voltage probe was connected to the pad or corner number 3, negative voltage probe to number 4 and positive and neg-

ative current probes to pads or corners numbers 1 and 2, respectively. In the second measurements, the only change done was that the direction of the current was reversed. In other words, positive current probe was connected to pad or corner number 2 and negative current probe to number 1. Order of the voltage probes remained the same. The Greek cross and big square patterns were then measured for the third and fourth time. For these measurements, the patterns were rotated 90 degrees to the clockwise direction and then measurements 1 and 2 were repeated. In reference with figure 35, positive and negative voltage probes were connected to pads or corners 4 and 2, respectively, and positive and negative current probes to numbers 3 and 1, respectively for the third measurement. For the fourth measurement, voltage probes remained the same and positive current probe was connected to pad or corner number 1 and negative current probe to number 3.

After the 4PP measurements, resistances of the U-conductors were measured with a multimeter. After the measurements, five samples of U-conductors were transferred on to a PET film. The PET film had copper tapes placed on it so, that the pads of the U-conductors came in contact with the copper tapes. After transferring the conductors, their resistances were measured again. These measurements were done to find out if mere transferring of the tattoos affects the resistances of the printed conductors.

After the measurements of the printed conductors, dielectric layers were printed on them, as mentioned at the end of chapter 5.2. Then, the same measurements were repeated. The measurements before and after printing the dielectric layers were done to find out if the printing procedure as well as the UV-curing of the dielectric ink has an effect on the resistances of the conductors.

The U-conductors insulated with the dielectric layer were used for the stretching tests on the skin and tensile tests in Instron 4411. When the tests were started, it was observed that the tattoos did not transfer as smoothly as the tattoos with only conductive layer. The most probable reason for this was the additional heating of the insulated tattoos due to the UV-curing. At this point it was necessary to use the adhesive film, that was packed with the tattoo paper, to increase the adhesion of the tattoos. However, removing the tattoos from the skin was extremely difficult and caused strong reddening of the skin.

For the on-skin measurements, copper tapes were placed on the pads of the U-conductors, and the tattoos were transferred on the knee or the forearm of the test person. One such tattoo before transfer, with copper tapes attached, is presented in figure 33.

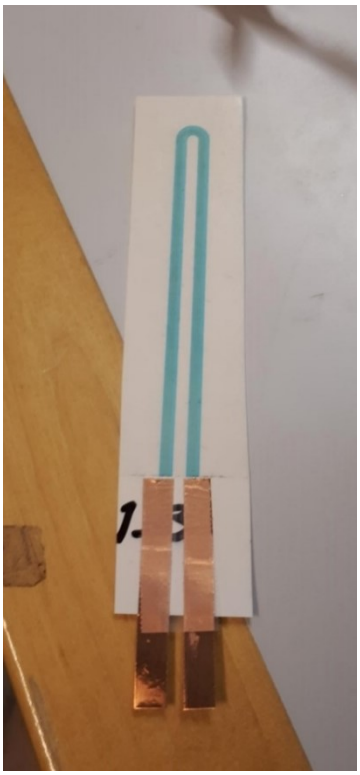

Figure 33. *A sample used in an on-skin stretching test.*

During the test on the knee, the leg of the test person was completely straightened during the transfer. Then, wires from the Keithley 2425 Sourcemeter were connected to the copper tapes and 2-probe measurement was used. In this test, the LabView logger software was used to save the measurement data in real time. After starting the logger software, the test person started to slowly curl his leg, and the logger software saved the measurement data. During the test on the forearm, the test person first had his hand open while transferring the tattoo. Then the wires from Keithley 2425 Sourcemeter were connected and logging of data was started. The test person then repeatedly squeezed his hand in to a fist and then opened it again. The test setup used in both tests is the one described in chapter 4.3.2. Figure 34 presents the tattoos transferred on the forearm and the knee.

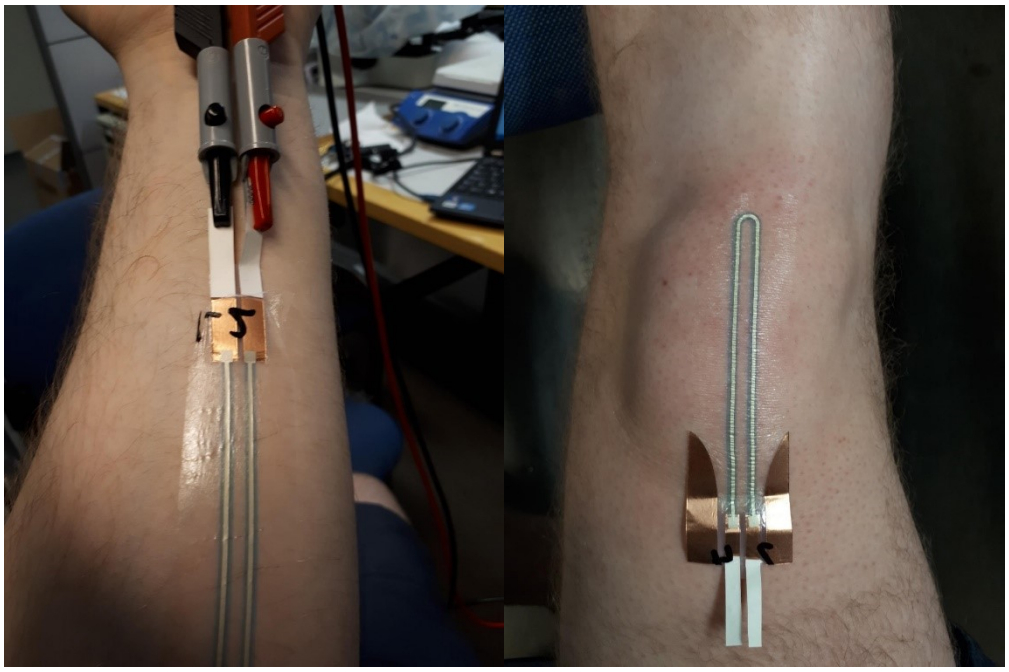

Figure 34. *A transfer tattoo on the forearm and the knee of the test person. The wires connected to the copper tapes are connected to the Keithley 2425 Sourcemeter as described in chapter 4.3.2.*

The copper tapes, that the wires from Keithley 2425 Sourcemeter are connected to, in figure 34 have white backing paper covering the adhesive side (bottom side) of the tape, and the tapes are top side down in the figure. The alligator clips of the wires are connected so, that the metal of the clips makes a contact with the copper side of the tapes. There are also pieces of copper tape visible at the sides of the tattoo near the pads of the conductor on the right side in figure 34. These are attached on the tattoo to dampen the mechanical wave that has a high effect on the tattoo near the copper tapes attached to the pads of the conductor. Without the copper tapes, this mechanical wave tends to tear the tattoo, due to the discontinuity in stretchability, at the edges of the copper tapes connected to the pads. This problem was discovered when the tests were initially started without using the dampening copper tapes.

Strains on the conductors were solved in the following way: First, small pencil marks were drawn below and above the knee of the test person. Second, a long piece of scotch tape was placed on the knee so, that the tape covered the pencil marks, and pencil marks were drawn on the tape on the exact same spots as the pencil marks on the knee below the tape. Third, the tape was removed and placed on a flat surface, and the distance between the pencil marks was measured with a ruler. This was done to define the original length between the marks on the skin along the surface of the knee. Fourth, the test person curled his leg to the extent where the conductor broke, and a long piece of scotch tape was again placed on the knee. Pencil marks were drawn on the tape on the same spots as the pencil marks on the skin, and after that the tape was removed and placed on a flat surface. Fifth, the distance between the marks was measured with a ruler. This was done

to define the distance between the marks on the skin, along the surface of the skin, at the point where the conductor broke. Finally, the difference between the two measurements was used to define how much the marks had moved i.e., how much the skin had stretched. The deformation of the skin is not purely stretching. There is also bending involved and thus, there is also bending involved in the deformation of the tattoos. However, since the tattoos can be considered extremely thin, the bending has virtually no effect on the conductors, and the test method used to solve the strains should be accurate enough.

Instron 4411 was used to get more accurate matching of the resistances to specific strains, and to compare the results with the tests done on the skin. For this test, a tattoo was transferred to a piece of thermoplastic polyurethane (TPU), which was used as a carrier to mount a sample to the Instron 4411. After mounting the sample between the clamps, wires from Keithley 2425 Sourcemeter were connected to copper tapes placed on the pads of the U-conductor in the same manner as in the on-skin measurements. Figure 35 presents the sample mounted to Instron 4411 with the wires connected from Keithley 2425 Sourcemeter.

Figure 35. *A transfer tattoo mounted to Instron 4411 for electromechanical and mechanical testing.*

The LabView logger software was used again to save the measurement data. In this test, the logger software and Instron 4411 were started simultaneously to synchronize the actual tensile test with the resistance measurement. This same setup was also used to measure the forces exerted on the sample during the test. However, as the instrument automatically did the measurement and there was no need to do any additional preparations, this test is not described in detail.

6. RESULTS AND DISCUSSION

This chapter presents and discusses the test results obtained from the experiments. The idea is to use different tools to analyze the reliability of the results where possible, and to make relevant conclusions regarding the different properties of the tattoos and properties of the used methods.

First, the characterization results of the new materials are discussed. Second, the electrical and electromechanical test results of the screen printed tattoos are analyzed. Finally, the mechanical results obtained from tests conducted using Instron 4411 are presented.

6.1 Properties of the new materials

Some results of the new materials were already presented and discussed in chapter 5 since the results were necessary to understand why certain changes were made, or why some other methods were used. There were basically three conductive inks that were considered new materials, and the temporary transfer tattoo paper that was used as a substrate. Also, the PMMA dielectric ink needed some characterization since it was self-made.

The AgNW ink, CNT ink and graphene ink were all purchased as inkjet printable inks. Thus, the primary characterization was to discover the jettability and printability of the inks. The problem with all the inks was the extremely poor jettability. The inks did not even come out of the nozzles, so there was basically no droplet formation. There were several fixations tried, but they did not improve the jettability. It was concluded that the reason for the poor behavior of the inks was probably the length of the particles and water, which was the solvent in all the inks. The reason why water might cause the bad behavior is not known, but there is probably some connection between the wetting properties of the water and wettability of the nozzle plate. Due to the poor jettability, the printability of the inks was not possible to characterize.

After the jettability characterization, the graphene ink ran out and there were no other characterizations done with it. Thus, it remains unknown what kind of electrical and mechanical performance can be achieved with that ink. However, the AgNW ink and the CNT ink were characterized using spin coating. The inks were spin coated on the tattoo paper, but probably due to friction between the inks and the release film of the tattoo paper, the release film was ruined. After this, the inks were spin coated on microscope glass slides, the sheet resistances of the formed coatings were measured and the coatings were also visually inspected.

The CNT ink did not form a uniform coating and it had no conductivity even with varied spin coating settings. The CNT ink spin coated on two microscope glass slides is presented on the left in figure 36.

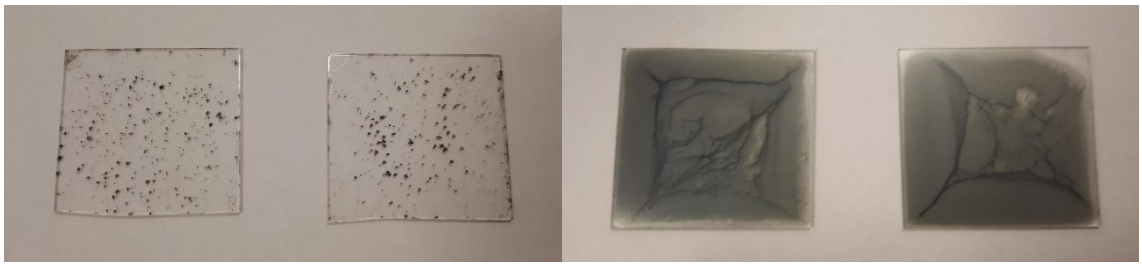

Figure 36. *CNT ink from NanoLab spin coated on microscope glass slides on the left. The black dots are actual ink with slight conductivity. Drop cast AgNW ink from Novarials on microscope glass slides on the right. For some reason, the ink tends to form a network resembling a human nervous system.*

The black dots on the glass slides are the CNT ink with slight conductivity, and the transparent areas have no conductivity at all. The CNT ink was also drop casted on glass slides to ensure uniform coating, but there was still very low conductivity even though the layer was quite thick. Considering these results and the fact that even the manufacturer of the ink has provided some resistance measurement results [39], which indicate high resistances, it is safe to say that the ink has a very low conductivity and poor jettability with DMP-2850 inkjet printer. The CNT ink also does not seem to be suitable for spin coating.

The AgNW ink formed a highly transparent coating on the glass slide, but it had a high sheet resistance of 1.3 MΩ/□. The reason for such high sheet resistance could be the thickness of the coating. Unfortunately, no actual thickness measurements were conducted for the spin coated layers in this thesis, but the transparency of the coating was extremely high, which could indicate a low thickness. There is also another possibility. According to Ossila, spin coating nanoparticle-based solutions need special requirements, and normally spin coated nanoparticles tend to form uneven coatings [58]. So, it is possible that the AgNWs; even though they are not exactly nanoparticles, but nano-sized fibers; did not form a mesh-like structure in the first place and thus, the sheet resistance was so high. In the future, scanning electron microscope (SEM) images could be taken from the spin coated layers to make sure if a mesh-like structure is formed or not. Nevertheless, to get some estimates of the potential electrical performance of the AgNW ink, drop casting of the ink was also done. The drop cast AgNW layers are presented on the right in figure 36.

The sheet resistance of the layers was difficult to measure reliably with 4PP. This could be due to the high non-uniform thickness of the spin coated layers which is not suitable for 4PP measurements. Also, silver is susceptible to migration creating short circuits between the nanowires and thus, increasing the conductivity [59]. The layer also exhibits

Joule heating which causes AgNWs to break and create discontinuities in the AgNW network [60]. With increased current, it was discovered that the conductivity suddenly disappeared and was not regained even after long periods. Thus, the heating of the layer probably broke the silver nanowires resulting in the loss of conductivity. Only three drop cast samples were prepared, and after discovering the need to use low current, and by estimating the average measurement reading, one sample gave an approximate sheet resistance of 3.4 Ω/□. This sheet resistance is quite low and could be used in applications demanding high conductances. However, the thickness of the drop cast layers is also unknown, and it is possible that the conductance of the layer is too low when layer thicknesses suitable for the transfer tattoos are used. The ink also needs a reliable deposition method, since spin coating seems to produce thin layers with too high resistances, even though highly transparent.

The PMMA ink was characterized by spin coating it on a glass substrate and lifting it with water. The spin coated PMMA film was highly transparent, and there were no problems observed during the spin coating. Lifting the PMMA film was mostly easy but sometimes the film broke during the lifting or was already discontinuous after spin coating. These are probably due to varied spin coating speeds and variations in the composition of the PMMA ink since multiple portions of the ink was made. However, it was confirmed that it is possible to formulate a functional PMMA ink for spin coating a thin film which can be lifted from the glass substrate. This characterization was done since originally the film was supposed to be used as a carrier for lifting and transferring a spin coated AgNW layer on the transfer tattoo paper. It was also confirmed, that it is possible to spin coat a AgNW layer on a PMMA layer spin coated on glass. However, lifting of AgNW–PMMA bilayer with water proved a little difficult since water tends to wet the AgNW coating causing the glass to sink and the actual lifting of the bilayer becomes impossible. In principle, lifting the AgNW layer by using a PMMA layer as a carrier film is possible, but there are difficulties and the method for depositing a AgNW layer on the transfer tattoo paper is too complicated to be efficient. Additionally, since the AgNWs did not work in a desirable way, these tests including lifting of the spin coated layers was not continued any further.

The transfer tattoo paper was used in multiple tests as a substrate, so its performance was mostly observed during other tests. The only individual characterization test made to the paper was baking it in an oven to see if any color changes were observed. The pieces of the tattoo paper baked at 100 °C and 120 °C for 20 min showed no visible color change. The piece baked at 140 °C for 20 min showed slight color change, and the piece baked at 160 °C for 20 min had clearly changed color to yellow-brownish. It was concluded that 20 minutes or even 30 minutes at 120 °C or less should not affect the properties of the tattoo paper.

6.2 Electrical performance of the screen printed tattoos

Screen printed tattoos were electrically characterized by 4PP method and a multimeter. Initial resistance measurements were done after printing the conductive layers, and second measurements after printing the dielectric layers. Electromechanical measurements were done on the skin and with Instron 4411.

There were also some measurements done with U-conductors that were transferred on a PET film. These measurements were done to observe the possible effects of the actual transfer process. Since the surface of the PET film was quite smooth, this test was used to see if even a surface with virtually no surface roughness causes changes in the resistances of the conductors. However, practically no change at all was observed. Thus, it was concluded that transferring a tattoo on to a smooth surface does not have an effect on the properties of the tattoo.

6.2.1 Initial resistance measurements

The initial resistances of the tattoos were measured after printing and curing them in an oven. The printed patterns measured using 4PP were used to analyze two main factors: the quality of the printed patterns between different print sets and the quality of different patterns inside the sets. These factors are analyzed to investigate how changing the substrate after each print cycle affects the quality, and how uniform the quality of each individual print is around the printing area. The latter is important when printing large patterns or if multiple patterns cover large area of the screen. If the screen is not straight or if the print nest is not balanced, the quality of a large pattern or the quality between smaller patterns is not uniform.

The sheet resistances of the Greek cross patterns were measured in two positions: 0° and 90°, two measurements were taken in both positions and the arithmetic mean of the two measurements was used as the result. Ideally, the position does not affect the measurement result, since ideally the Greek cross pattern is completely symmetrical. However, in reality there are differences in the results. A scatterplot of the sheet resistances measured in both positions for each sample in each set is presented in figure 37.

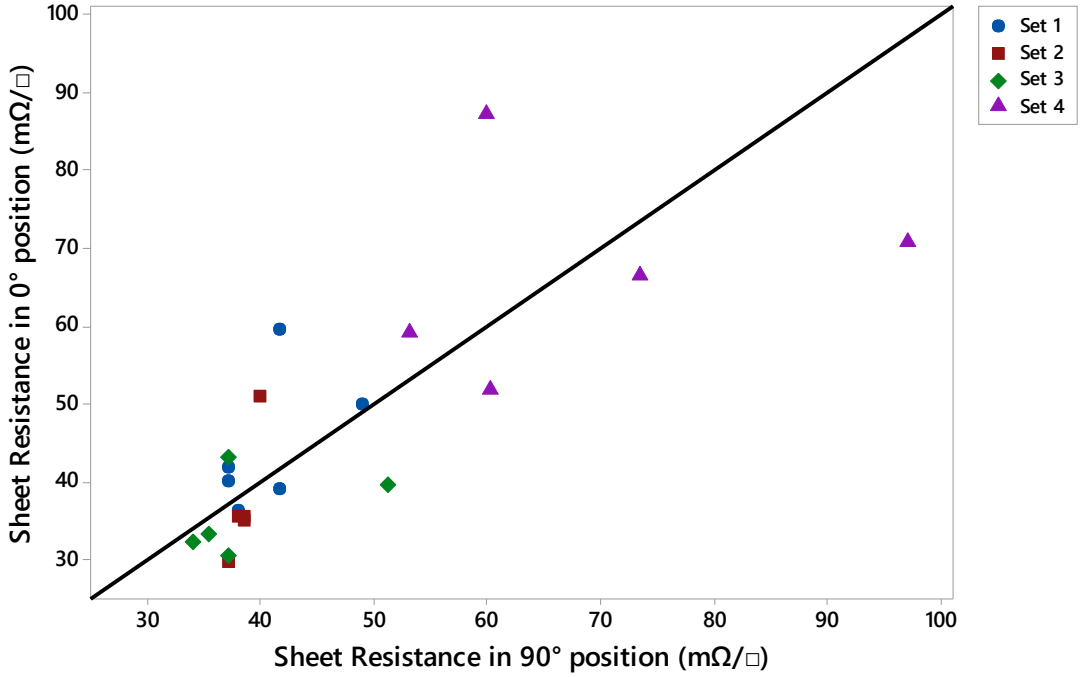

Figure 37. *A scatterplot of the sheet resistances of the Greek cross pattern samples in 0° and 90° positions. All points on the line have the same value in x and y directions.*

The scatterplot above has the measurement result in 0° position and 90° position on the *y*- and *x*-axis, respectively, for each sample in each set. There is also a line drawn in the graph so that all data points on the line have the same value in both directions. Thus, if a data point diverges from the line, that data point has different measurement result in the two measurement positions. Furthermore, the larger the divergence of the data point from the line, the larger the difference between the measurement results. In addition, if the data point is below the line, the result in 90° position is larger than in 0° position. If the data point is above the line, the result in 0° position is larger than in 90° position. It is also easy to see from the figure if the measurement results between different samples diverge from each other. In an ideal case, two similar samples fabricated in the same process should have the same sheet resistance.

From figure 37 it can be seen, that the measurement results in each set divide quite evenly on both sides of the line and/or are close to the line. In sets 1–3, the samples are close to each other and close to the line. There is one sample in each of sets 1–3, that is a little farther from the line than the other samples in those sets. In set 4 however, the samples are far from the samples in other sets and there are also two samples that are far from the line. In fact, those two samples are farther from the line than any other sample in any set.

To get more insight into the total deviations and average sheet resistances in both positions, an interval plot of the sheet resistances in both measurement positions is presented in figure 38.

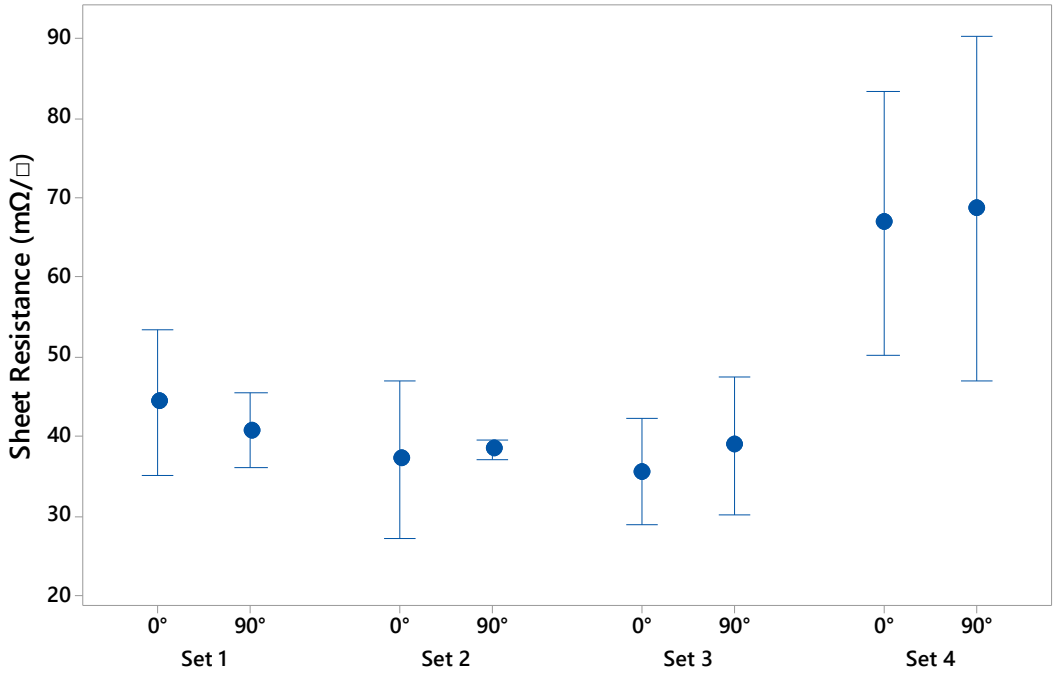

Figure 38. *An interval plot of the sheet resistances of the Greek cross pattern samples. 95 % confidence interval (CI) is used for the mean values.*

The mean values of sets 1–3 are close to each other. Additionally, it can be seen that the intervals are similar except for 90° position of set 2, which seems to be much smaller. So, the sheet resistance in that direction in set 2 is extremely uniform. However, with such a low number of intervals and low sample size in each mean value, it cannot be concluded that these differences are not normally distributed. Set 4 differs from the others in both mean values and intervals, just as expected based on the scatterplot in figure 37.

According to these observations, something could have happened while printing set 4. Sets 1–3 seem to have quite uniform quality in both directions and between each other. However, it is not possible to analyze with these results alone, what has happened while printing set 4. Thus, further analysis is needed. It should be noted at this point, that when comparing the results between individual samples, the average sheet resistance over the total pattern area should be used since there are deviations, even if small in sets 1–3, in the two measurement positions. This is especially important when comparing samples in set 4. For example, the two samples that are the farthest from the line in figure 37, have sheet resistances of 87.0 mΩ/□ and 70.7 mΩ/□ in 0° position and 59.8 mΩ/□ and 97.0 mΩ/□ in 90° position, respectively. If only the sheet resistance in 90° position was used as the result, it would not represent the average sheet resistance of the samples as well as

an average of the two measurements would. In addition, in 90° position there would be a difference of 37.2 mΩ/□ in the sheet resistance of the two samples, but only a difference of 10.5 mΩ/□, if the average sheet resistance is used. Thus, from here on, the sheet resistance of the Greek cross pattern samples is the arithmetic mean of the sheet resistances measured in 0° and 90° position.

Analyzing the quality further, the big square patterns were measured in 0° and 90° positions, and two measurements were done in both. The sheet resistance of each sample in each position is again the arithmetic mean of the two measurements done in that position. A scatterplot of the sheet resistances in both positions for each sample is presented in figure 39.

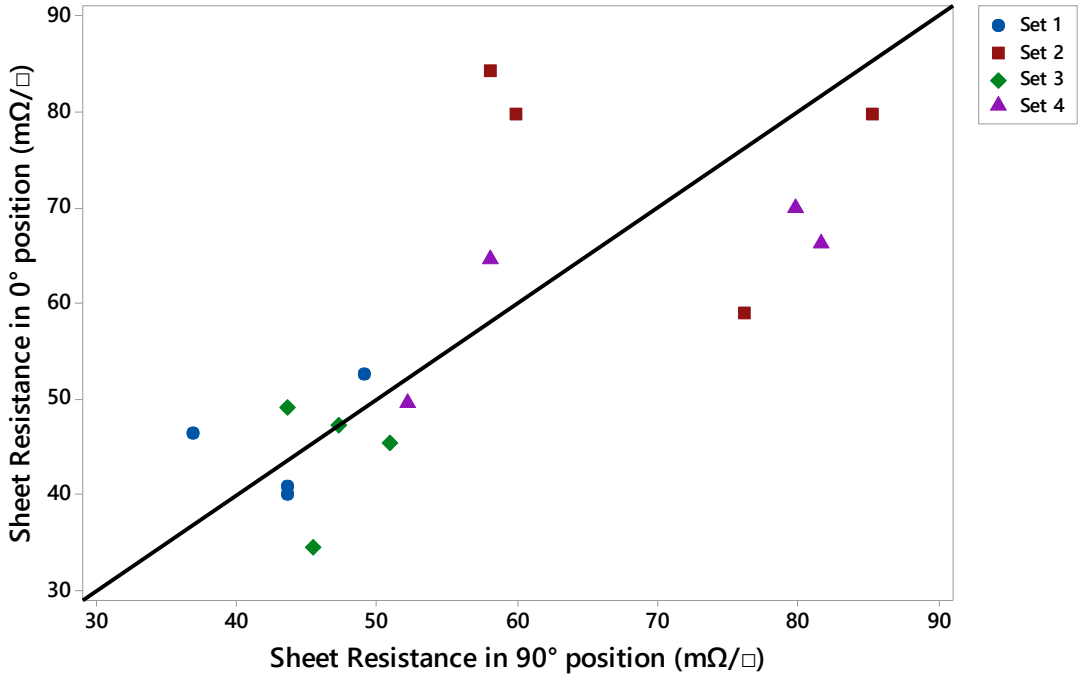

Figure 39. *A scatterplot of the sheet resistances of the big square pattern samples in 0° and 90° positions. All points on the line have the same value in x and y directions.*

Similar observations can be made from the scatterplot above as was made with the Greek crosses. However, something has happened with the big squares in set 2. Sets 1 and 3 have samples close to the line with an even distribution on both sides, and there seems to be one sample in both sets a little farther from the line than the other samples in these sets. Again, set 4 has higher sheet resistances, and there is one, maybe two, samples farther from the line than in sets 1 and 3. Set 2, however, has three samples farther from the line than any other sample in any set. In addition, the sheet resistances are higher than in the other sets.

Again, to see the mean values and deviations of the sets and measurement positions, an interval plot of the sheet resistances of the big square pattern samples in both positions is presented figure 40.

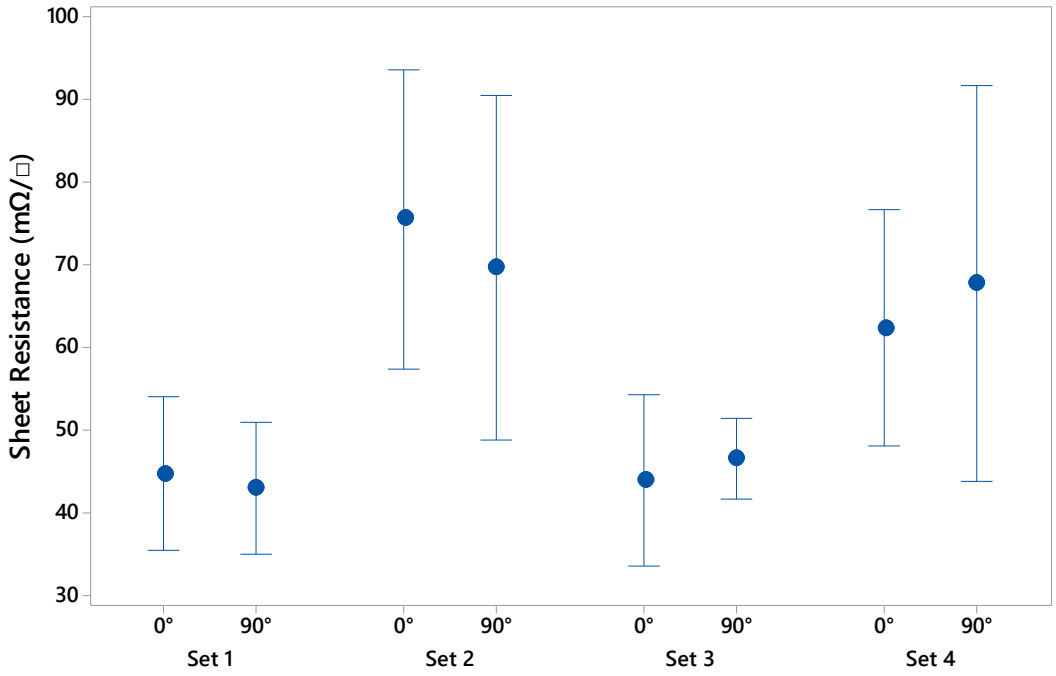

Figure 40. *An interval plot of the sheet resistances of the big square pattern samples. 95 % CI is used for the mean values.*

The figure above confirms the previous observations. Sets 1 and 3 seem to have equal sheet resistances and intervals, and set 4 has higher sheet resistances and intervals. However, set 2, as expected, has the highest sheet resistances and high intervals. So, sets 1 and 3 seem to have uniform quality with low deviation, whereas set 4 has more deviation in the quality between the samples. When looking at the scatterplot, all values are quite close to the line, but they are far from each other. In set 2, there seems to be high deviations between the samples and measurement positions. Due to the deviations, arithmetic mean of the sheet resistances measured in the two positions is used as the sheet resistance for the big squares from now on.

Nevertheless, the results so far indicate that the quality is quite uniform in both directions. There are some deviations, and arithmetic means of the measurements in the two positions are used. However, since for sets 1–3, with the exception of the big squares in set 2, the deviations are not very high, and it would not be completely wrong to use only one measurement position. Even so, if only one measurement position is used, large deviations would go unnoticed, and the results would not represent the truth very well. Basically, the farther the sample from the line in the scatterplots, the larger the difference in the

sheet resistances in the two positions, and the more the sheet resistance in one position deviates from the average.

The large deviations appear in samples belonging to set 4 and the big squares in set 2. In addition, set 4 and big squares in set 2 have larger sheet resistances anyway, so it is possible that there is a connection between the large variations and large sheet resistances. It seems, that printing of set 4 and the big squares in set 2 have failed somehow. The reason for the possible failure of set 4 could be a critical decrease in the amount of used ink, since that set was printed last. To get a better understanding of the effects related to the geometry of the pattern, figure 41 presents an interval plot of the sheet resistances of the Greek crosses, big squares, π-conductors and U-conductors in each set.

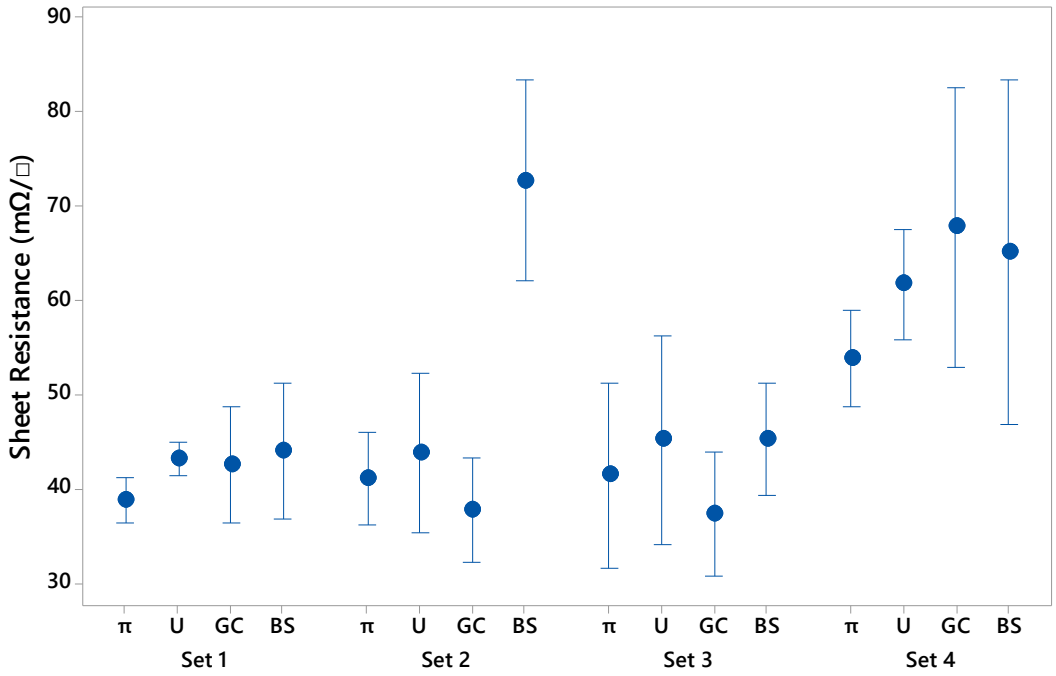

Figure 41. *An interval plot of the sheet resistances of the π-conductors (π), U-conductors (U), Greek crosses (GC) and big squares (BS) in each set.*

The figure above amplifies two suspicions; the big squares in set 2 have failed and set 4 as a complete set has somewhat failed. In sets 1–3, the mean values and intervals are close to each other, and in set 4 the mean values are higher than in other sets. There also seems to be somewhat higher deviation between the mean values in set 4 than in other sets. Based on the figure above, the big squares in set 2 are a clear anomaly in the data and will be discarded from the results from now on. In addition, set 4 will be analyzed individually.

The reason for the big squares in set 2 failing is probably the following: In the used screen printer, the ink tends to flow toward the back edge of the screen. This occurs probably due to a tilted holder of the screen on the printer. The back edge is the long edge where

the Greek crosses are located on the layout. So, the ink flows away from the squares. In addition, the ink was spread with the metal squeegee from left to right, and the amount of ink in front of the squeegee decreases when the ink is spread. Thus, it is possible that the amount of ink that was spread on the big squares, located in the front-right corner of the screen, had reduced critically due to the decrease in ink and the ink flowing away from them. This problem was noticed during the printing, and ink was either added to the front of the screen or scraped with a spatula from the back edge toward the front edge. This is probably why the big squares in the other sets succeeded. Nevertheless, the printer should be balanced or replaced.

Appendix A presents a one-way analysis of variance (ANOVA) -test for the means in sets 1–3 in figure 41 (the big squares in set 2 now removed). The p-value in the test is 0.093, which is higher than the α-level (α = 0.05). This implies that all the means are equal for the patterns in sets 1–3. In this test (and in the other upcoming ANOVA -tests), equal variances were not assumed, since it is not known whether they are equal or not, the number of means tested is small and there is variation in the intervals in figure 41. Similarly, appendix B presents ANOVA -test for the patterns in set 4. The p-value in this test is 0.060 barely indicating equal means between the patterns. To see if the set number has some effect on the results, figure 42 presents an interval plot of the sheet resistance of each set.

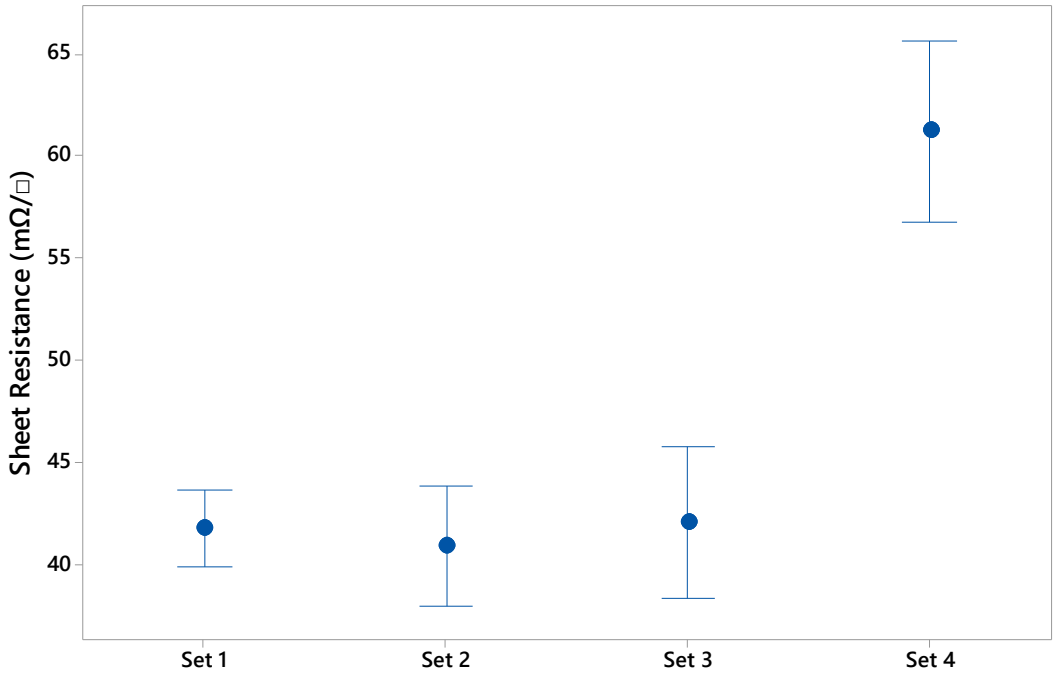

Figure 42. *An interval plot of the sheet resistance of each set.*

It was already expected that sets 1–3 are close to each other in both mean values and intervals and set 4 deviates from the others. To see how close the sets 1–3 are, appendix

C presents ANOVA -test of the sets 1–3. The p-value in the test is 0.842 strongly indicating equal means in the sets. From this result, it looks like the set number has little to no effect on the sheet resistances.

Next, to see if the pattern or location has some effect on the sheet resistances, figure 43 presents an interval plot of the sheet resistances of the different patterns. The patterns from set 4 and the big squares from set 2 have been obviously excluded. ANOVA -test for the patterns is also presented in appendix D.

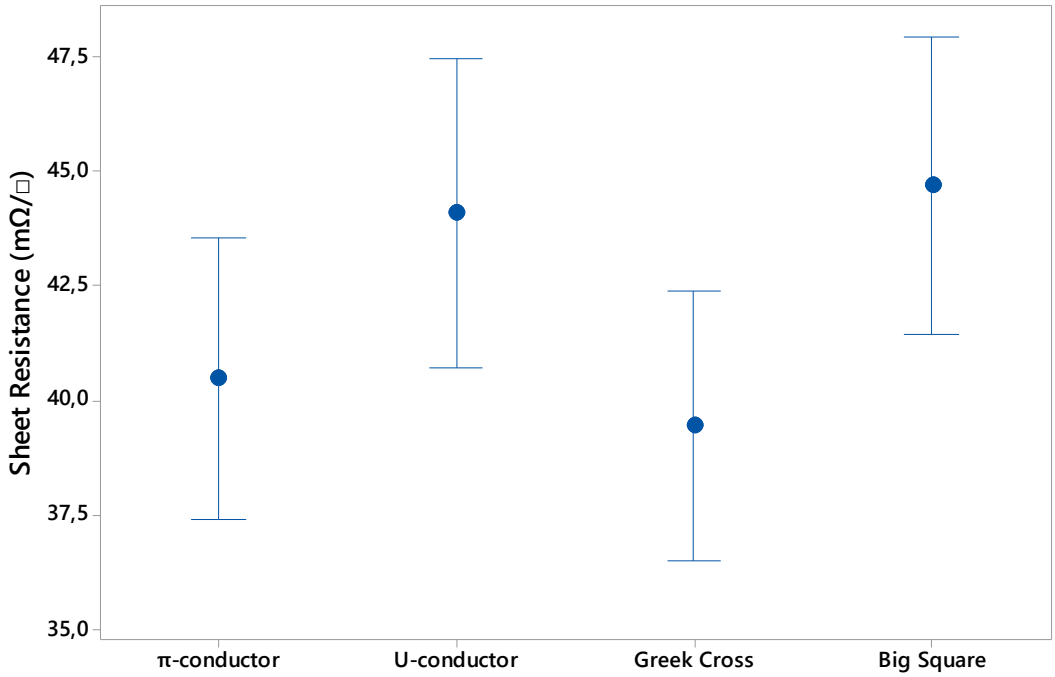

Figure 43. *An interval plot of the sheet resistances of the different patterns.*

The p-value in the ANOVA -test is 0.039, which is lower than $\alpha = 0.05$. It is also visible in figure 43 that there are quite large variations in the means. If equal variances are assumed in the test, which is somewhat reasonable since the intervals look extremely equal to each other, the p-value is 0.066, which is a little above the α-level. Still, it seems that the pattern or location has a larger effect than the set number. This was also visible from the ANOVA -tests in appendices A and B where different patterns were compared. It is not known at this point whether it is the pattern or the location on the screen that causes the deviations since all patterns were printed in different location from each other. However, it can be analyzed by comparing the sheet resistances of individual samples in each set. Figure 44 presents scatterplots of the sheet resistances of individual samples in sets 1–3.

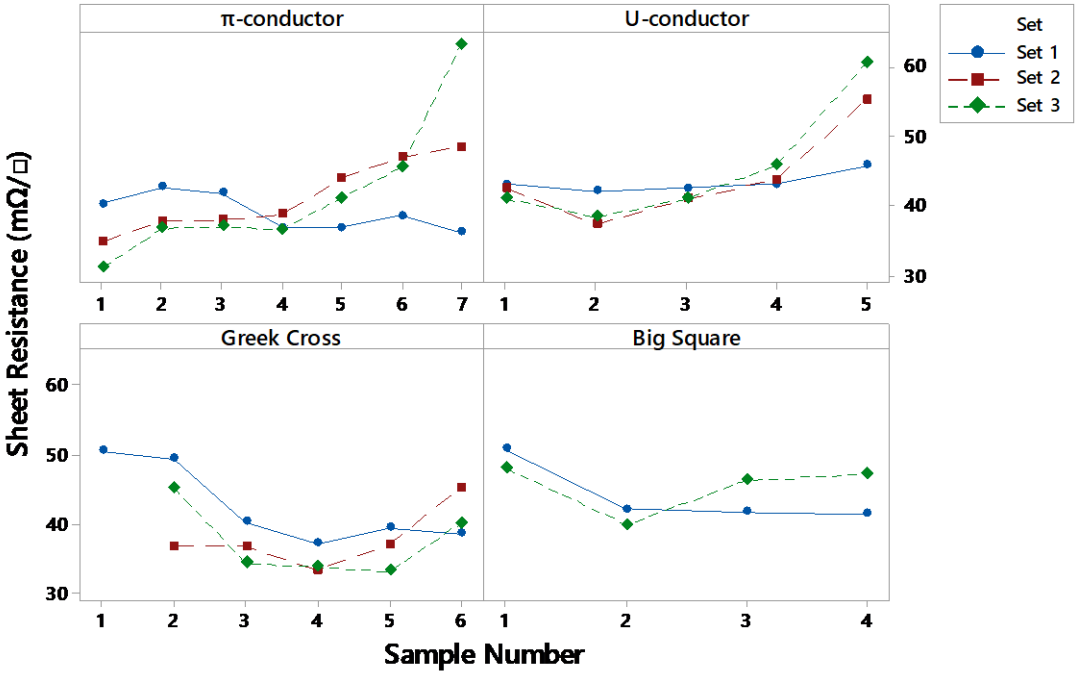

Figure 44. *Scatterplots of the sheet resistances of individual samples in sets 1–3.*

The scatterplots have the same scaling on the *y*-axis, so it is easier to compare different patterns as well as location. All samples, except the big squares, were numbered from left to right on the layout, so each sample with the same number was on the exact same spot on the screen. However, there was six succeeded Greek cross samples in set 1 and only five in the other sets, so there is only one Greek cross sample with sample number '1'. Since the big squares were arranged in a square-like configuration on the layout, their location should be used to analyze only the difference in the sheet resistance produced at a specific location between the sets.

From figure 44 it looks like the Greek cross samples in the middle of the screen in longitudinal direction (sample numbering runs in the longitudinal direction) have lower sheet resistance than the samples near the edges. In addition, the sheet resistances of the π- and U-conductors increase from left to right, and the differences between samples with the same number are the largest on the right side of the screen. There does not seem to be large differences between the sheet resistances of different patterns. However, the U-conductors and big squares show lightly higher sheet resistances when figures 41 and 43 are also considered.

The above results imply, that the pattern does not have much effect on the sheet resistance, but the location does. Especially so, since there are clear trends in the curves when moving in the longitudinal direction rather than the differences being random. Since the location seems to affect the sheet resistances in a trend like manner, it could also explain the differences in the uniformity of the samples when measured in two positions.

The sheet resistance seems to increase from left to right, at least when observing the π- and U-conductors. It is possible that spreading the ink in that direction might have something to do with it. Especially, the speed of the metal squeegee was slow, so the ink had much time to stand on the screen and possibly flow through the holes to the substrate. This could have caused thicker layers with lower sheet resistances to form on samples near the left edge. Also, the Greek crosses show an upward parabolic-like curve in figure 44. One explanation could be that, since the screen mesh is bound to the frame, the screen mesh flexes more near the middle, less near the edges and the least near the corners, and the squeegee presses samples with higher pressure near the middle of the screen. The Greek cross samples 1 and 6 are located near the corners. In addition, the high sheet resistance of the π-conductors near the right edge could be explained with this. This is a problem that cannot be fixed with a practical solution. That is, the quality is probably reasonably uniform inside a specific area near the middle of the screen and thus, increasing the size of the screen and placing the patterns inside that area allows printing of patterns of any size. However, this is not very practical solution if the area that produces high quality is relatively small to the size of the screen.

The previous phenomenon does not explain why the U-conductor sample number 5 in each set has a high sheet resistance, since those samples were located near the middle of the screen in the longitudinal direction. It is possible that the measurement method is one cause, since the U-conductors were measured with a multimeter, which has higher contact resistances than 4PP. In addition, the overall sheet resistance, according to figures 41 and 43, is also slightly higher.

The big square pattern also produced a slightly higher sheet resistance than the π-conductors and Greek crosses. According to Michael B. Heaney, the positions of the probes are critical in 4PP measurements and they should be completely independent of each other [61]. In big square measurements, the probes are placed inside the actual measurement area. On the contrary, in Greek cross and π-conductor measurements, the probes are connected to the actual measurement areas by pads and short sections of conductor. Thus, the probe locations in big square measurements could be the reason for slightly higher sheet resistance. Also, according to Miccoli et al. [57], the probes in the configuration used in this thesis should be exactly in the corners of the big squares. In reality, they were a little closer to the center to make sure a proper contact to the conductive layer was made. However, there should be virtually no difference if the probes are close to the corners [57, p. 10]. It is also possible that large patterns that are continuous in all directions are more difficult to print, or in other words, non-uniformities are emphasized more in these kinds of patterns. That is, there could be spots in the screen causing higher sheet resistances, and patterns with large surface area, that is continuous in all directions, have higher probability of being on those spots than smaller patterns.

To see if the samples do not follow a normal distribution, probability plots are presented in figure 45. The first plot includes the samples from sets 1–3. From the fixed plot, the π-

conductor sample number 7 in set 3 has been removed due to the large deviation and clear change in trend when compared to the other samples with the same number. The last plot has the samples from set 4 to see if the samples do not follow a normal distribution.

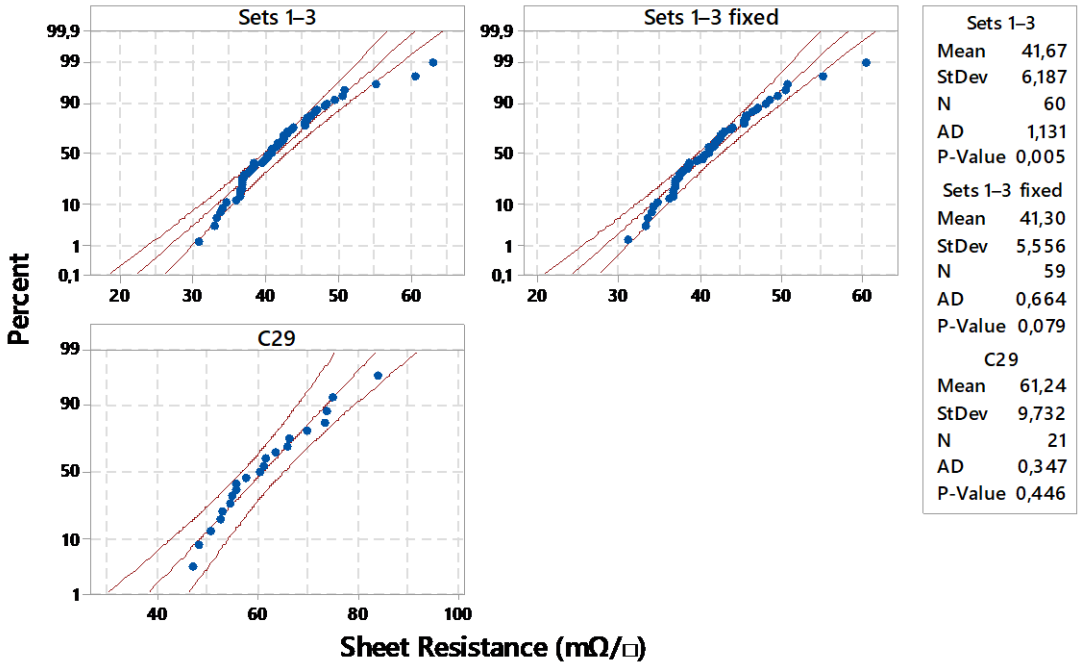

Figure 45. *Probability plots of the sheet resistances of the samples in sets 1-3, sets 1–3 fixed and set 4.*

The p-value of the first plot is 0.005, which is below the used α-level (0.05). From this, it can be concluded that the samples do not follow a normal distribution. However, when the one π-conductor sample is removed, the fixed plot has a p-value of 0.079, which is above the α-level. Thus, it cannot be concluded that the samples do not follow a normal distribution. However, it cannot be concluded that they do follow a normal distribution either. Similarly, the samples in set 4 might or might not follow a normal distribution. This means that overall, the above result looks quite good. In sets 1–3, there are 60 samples and all but one fit inside the 95 % CIs, and in set 4, all samples fit inside the 95 % CIs. When a large number of samples is produced, it is always possible that one or two samples fail due to an unknown reason.

In general, it looks like the fabrication of the samples is quite reliable in terms of the uniformity of samples. Set 4 could have failed due to critical decrease in the amount of ink, but the samples were still somewhat uniform when compared to each other. In addition, the big squares in set 2 failed and the reason was already discussed. There were some random variations in the quality, and one reason could be that the ink had to be spread by moving the metal squeegee by twitching. The speed of the squeegee had to be low, but it

was not possible to adjust the speed with the speed control screws. The twitching movement caused the ink to be spread a little non-uniformly, which could have caused the small variations in the sheet resistances. However, the rubber squeegee, that was used to press the ink through the screen, moved with stable speed.

In addition, there are some general problems with the printer. The screen printer is semi-automatic and setting up the printer is done by hand. There are no clear methods of measuring the settings such as pressures of the squeegees or the print gap and thus, no way of confirming whether the settings are the same each time the printer is set up. In addition, if some non-uniformities are observed while printing, and settings are changed after a printed set, the samples in the next sets could become skewed. Furthermore, usually the test print cycles are performed using different substrate than what the actual samples are printed on, to save expensive materials and clean the test substrate easily for multiple test prints. This means, that if there are differences in the properties, such as thickness, of the substrates for testing and actual printing, and there usually are, the optimized settings for the test substrate are not optimum for the actual substrate. This usually causes changing of settings between printed sets resulting in variation in quality. Overall, an automatic printer would give a huge advantage, because settings would need to be optimized only once for each substrate and then saved on the computer controlling the printer. This way, the exact same settings could be used every time eliminating many of the mentioned problems.

6.2.2 Resistance measurements of the insulated tattoos

After measuring the sheet resistances of the printed patterns, a dielectric ink was printed on the samples in sets 1 and 2. Then the sheet resistances of the insulated samples were measured again. However, similar analysis as above will not be done for the samples. This analysis concentrates on the differences between the non-insulated and insulated samples to see if the insulator layer, or the printing and curing of it, has some effect on the sheet resistances of the samples. Ideally, an insulator layer on a conducting layer should not have an effect on the conductivity. Also, it should be noted that it is not possible to measure the sheet resistances of the big square pattern samples since they were completely covered with the insulator. However, using the analysis of the following results, it is possible to estimate the sheet resistance of the big squares. This estimate could then be used to verify whether a contactless sheet resistance measurement method, that might be available for use in the future, is giving accurate values.

Figure 46 presents a scatterplot of the initial sheet resistances of the samples in sets 1 and 2 as a function of the sheet resistances after insulation. Figure 47 in turn presents a scatterplot of the initial sheet resistances of the samples in set 3 as a function of the sheet resistances after UV-curing.

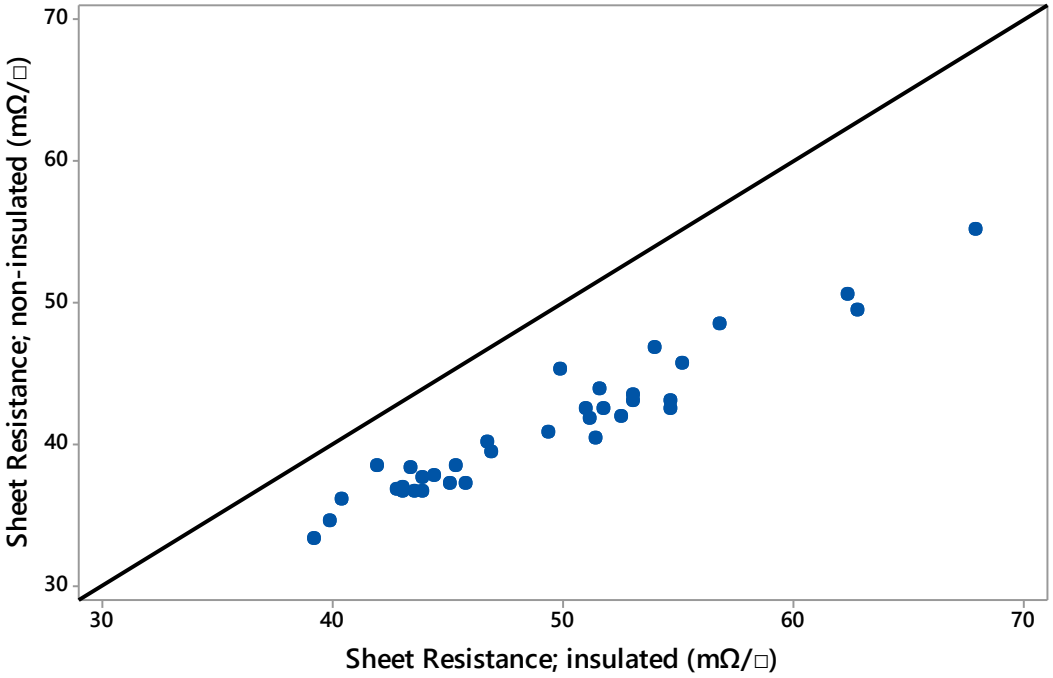

Figure 46. *A scatterplot of the initial sheet resistances of the samples in sets 1 and 2 as a function of the sheet resistances after insulation.*

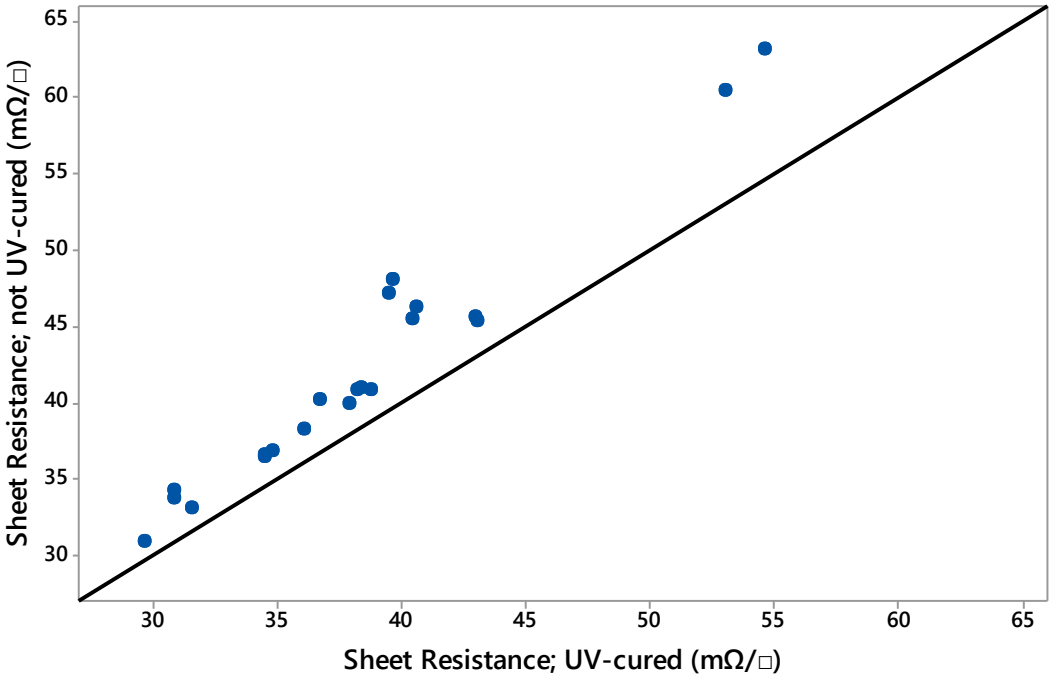

Figure 47. *A scatterplot of the initial sheet resistances of the samples in set 3 as a function of the sheet resistances after UV-curing.*

The figures above show that UV-curing decreases the sheet resistance of the samples and printing an insulator layer increases the sheet resistance of the samples without an exception. The mean values of the sheet resistances of the non-insulated and insulated sets 1 and 2 are 41.1 mΩ/□ and 49.2 mΩ/□, respectively. Thus, there is a 19.7 % increase in the sheet resistance after insulation. In addition, bare UV-curing of set 3 decreases the initial mean sheet resistance from 42.1 mΩ/□ to 38.4 mΩ/□. Thus, there is an 8.8 % decrease. Now, assuming the same decrease in the mean value of sets 1 and 2, and then calculating the 19.7 % increase due to printing the insulator layer, the total increase in resistance would be 31.2 %.

The decrease in the sheet resistance after UV-curing results from the conductive layers heating. It should also be noted that the decrease in sheet resistance after UV-curing depends on how well the conductive layers have been thermally cured in the first place. The most probable reason for the increased sheet resistance after insulation results from the characteristic of screen printing. Since the printing always has a contact with the substrate and ink is mechanically pushed on it, it is possible that the dielectric ink gets pushed inside the rather soft conductive layer made of silver–polymer composite. This decreases the effective thickness, or on the other hand, increases the total resistivity of the conductive layer that, according to equation (2), increases the sheet resistance of the layer. It has been already noted that screen printing produces rather thick layers for electronic transfer tattoos, but the phenomenon described above gives another reason to consider other, especially contactless, printing methods. When printing thin conductive layers, sheet resistance increases rapidly as thickness decreases, and dielectric ink getting pushed inside the layers might cause critical increase in sheet resistance.

6.2.3 Electromechanical performance

The electromechanical measurements were conducted using Instron 4411 tensile strength tester. The results will be used in comparison with the results from on-skin tests, which will be discussed in chapter 6.2.4. Figure 48 presents a scatterplot of the normalized resistance of a U-conductor as a function of strain. This U-conductor was printed on the tattoo paper, insulated and transferred on to a piece of TPU.

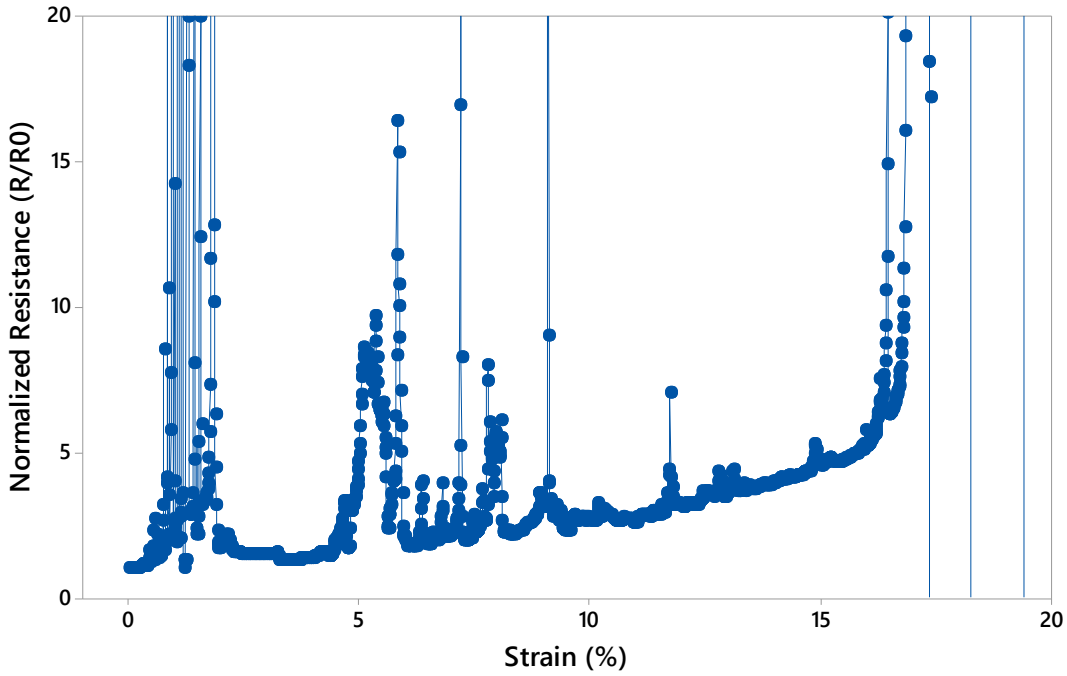

Figure 48. *A scatterplot of the normalized resistance of a U-conductor as a function of strain.*

Figure 48 shows that there is some large variation in the resistance of the U-conductor at the beginning and at the end of the test. The normalized resistance i.e., the resistance in respect to the initial resistance, increases to almost 300 at these spikes. The variation at the end is normal due to the fracturing of the conductor that happens in stages. The variation at the beginning is more interesting. It is not known what causes such large variation, but it could be due to the interaction between the tattoo and the piece of TPU. Since the tattoo is actually stretched through the TPU, and not directly by moving the clamps, there could happen some variation in the uniformity of the stretch. The same reason could be causing the smaller sudden spikes in the resistance throughout the test. The reason for the rather large variation at the beginning could be due to the fact, that initially the stretching of the tattoo is stopped and then it is suddenly started. The discontinuity in the strain rate could cause the variation to be greater than later during the test.

The test shows that the final breaking of the conductor is reached at the strain of 19.4 %, although the conductor starts to fracture already approximately at the strain of 16 %. At this strain the resistance of the conductor is approximately six times the initial resistance. These results indicate that using these tattoos on body parts where the stretchability is the highest is not possible. However, this test was conducted using only one sample, so reliability of the result cannot be confirmed. On the other hand, assuming that the quality of the sample used in the test represents the average quality of all samples fabricated in the screen printing process, there are too much problems with either the measurement setup

(the tattoo had to be laminated on the TPU) or using the tattoo as a stretchable platform (large variations in the resistance).

6.2.4 On-skin resistance measurements

Two different on-skin measurements were done: measurements on the forearm and measurements on the knee. Figure 49 presents a scatterplot of the normalized resistance of a U-conductor laminated on the forearm as a function of time as the test person repeatedly squeezed his hand in to a fist.

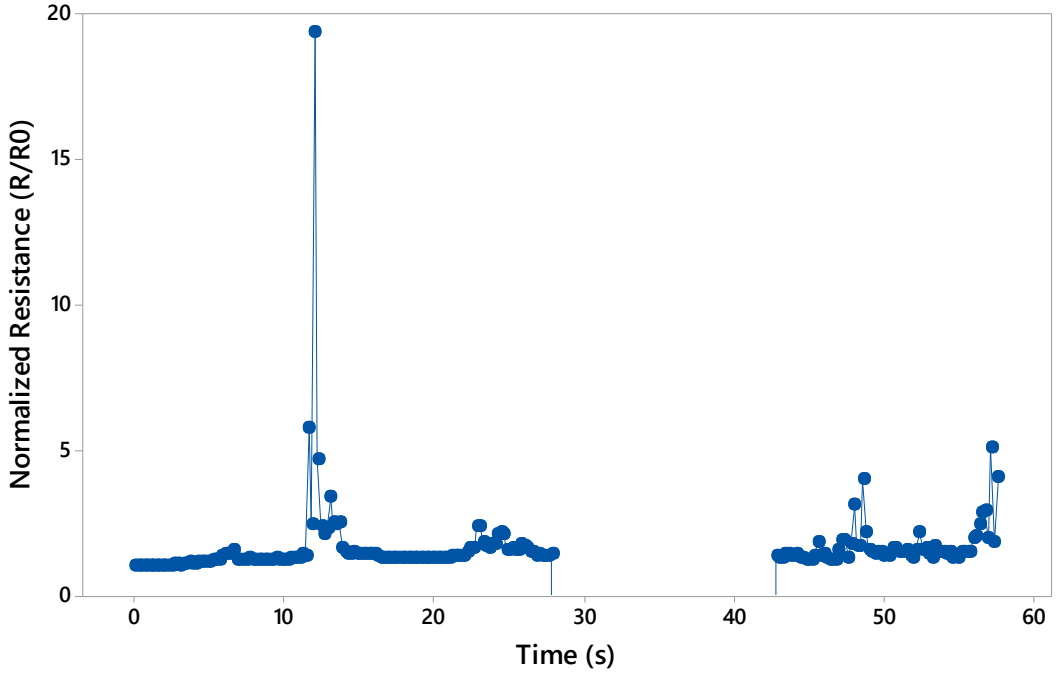

Figure 49. *A scatterplot of the normalized resistance of a U-conductor laminated on the forearm of a test person as a function of time.*

The figure above shows that there is not much variation in the resistance of the conductor. However, this is to be expected since squeezing hand to a fist produces very little strain to the tattoo laminated on the forearm. The large spike after the 10 second mark was caused by the test person waving his hand, but this actually caused the contact between the measurement instrument and the tattoo to weaken. In addition, the loss of data before the 30 second mark was caused by disconnecting the measurement instrument, and the regaining of the data after the 40 second mark was due to reconnecting the instrument. This disconnection–reconnection was done just to make sure that the same data was measured even after something temporary happened to the measurement instrument.

Multiple samples were measured while laminated on the knee of the test person. However, due to the difficulties concerning the measurement setup, there were only a couple

of somewhat successful samples. Figure 50 presents a scatterplot of the normalized resistance of the most successful sample as a function of time.

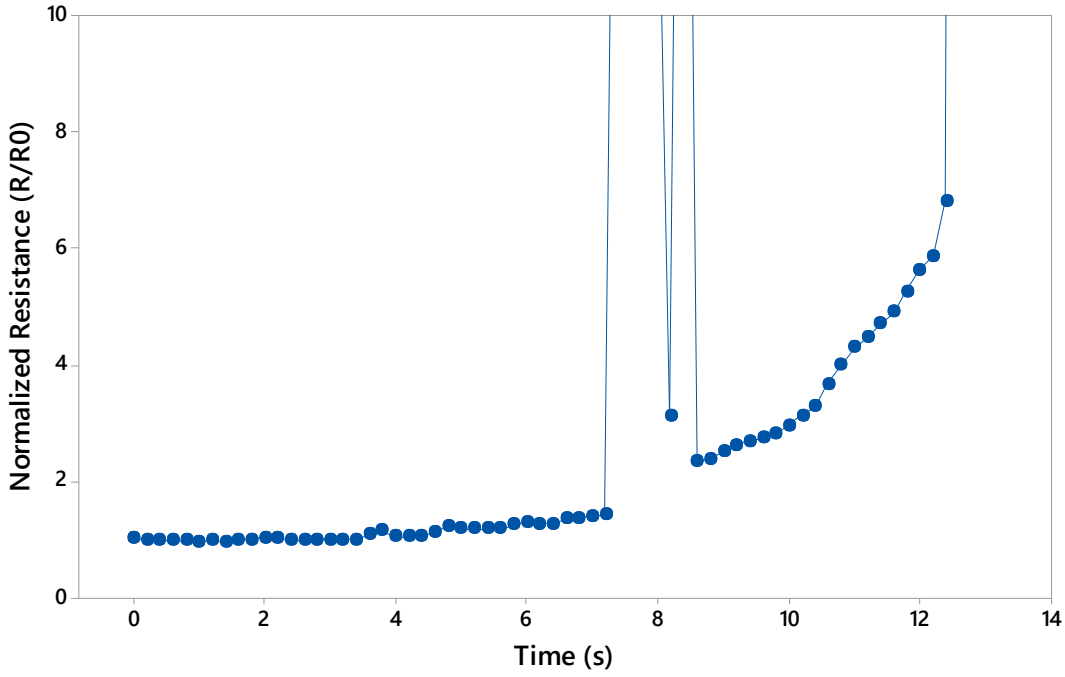

Figure 50. *A scatterplot of the normalized resistance of a tattoo laminated on the knee as a function of time.*

In the figure above, the normalized resistance increases to 50 at the 8 second mark. The conductor cannot be considered broken, but there is a clear change in the performance. Other than that, the resistance of the conductor increases smoothly until it breaks at the 12.4 second mark. It is interesting that until the sudden change in the resistance around the 8 second mark, the resistance is quite constant and only after the sudden change, the resistance starts to increase more rapidly. It is possible that the sudden change triggered some major changes in the structure of the tattoo that caused the resistance to start increasing. Using the method to solve the elongation at break described in chapter 5.3, the conductor in figure 50 broke approximately at a strain of 19.4 %.

Using the method to solve for different strains, the following results were obtained: distance of the pencil marks, when the leg was straight, i.e. at an angle of 0°, was 97 mm, 114 mm when the leg was at an angle of 45° and 131 mm at an angle of 90°. Using the distances at angles of 45° and 90° and dividing them with the distance at 0° angle, the strains are 17.5 % at 45° and 35.1 % at 90°. In other words, while the 90° angle is double the 45° angle, the strain at 90° angle is also double the strain at 45° angle. Using this information and assuming, that the strain increases linearly with increasing angle of the leg, and the leg was curled at a constant speed during the test, different strains at different times can be solved. It was already mentioned that the strain, when the conductor in figure

50 broke, was 19.4 % and this occurred at the 12.4 second mark. Assuming linear increase of strain with time, figure 51 presents the same scatterplot as figure 50, except the normalized resistance is as a function of strain, which has been calculated from the known information.

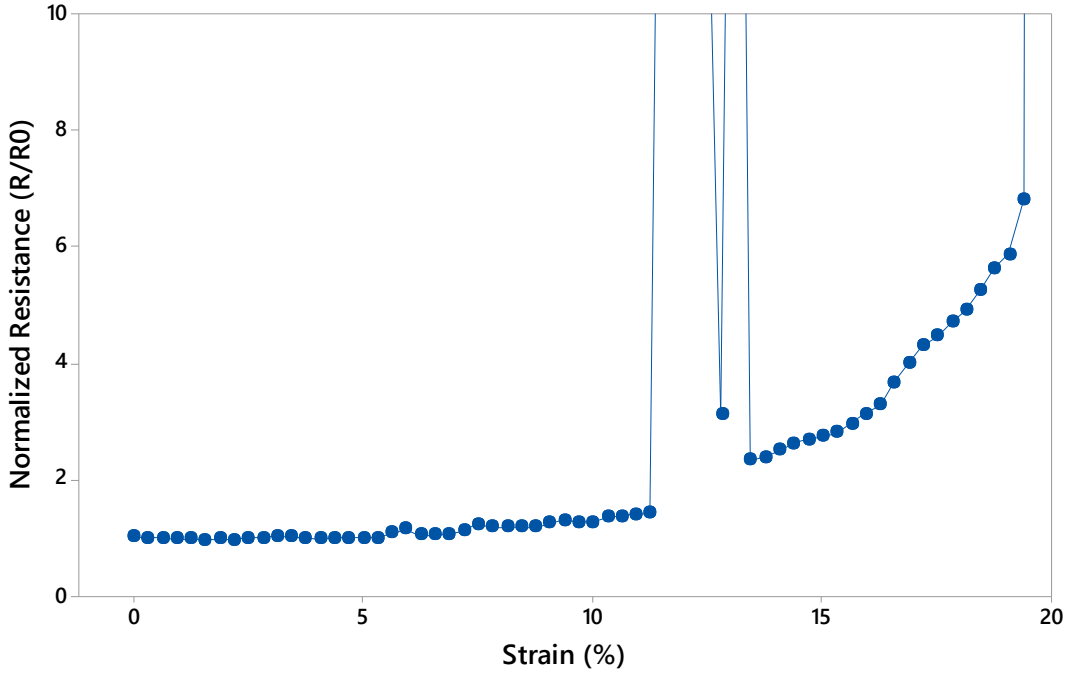

Figure 51. *A scatterplot of the normalized resistance of a tattoo laminated on the knee as a function of strain.*

The figure above shows similarities to figure 48. If the sudden changes in the resistance in figure 48 are not considered, both figures have quite constant resistances until strains of 10 % and after that the resistances start to increase. Moreover, the elongation at break is 19.4 % in both figures. However, due to the extremely small sample sizes, the reliabilities of the results are not known. Anyway, it looks like the maximum strain the conductors can take without losing conductivity is around 15–20 %, which is too small to be used effectively on the skin at locations with high maximum strains such as the knee or elbow. On the other hand, locations where the strains are less than or equivalent to 10 %, should be suitable for mounting the tattoos.

6.3 Mechanical performance of the screen printed tattoos

The mechanical properties of the tattoos were characterized using Instron 4411 tensile strength tester simultaneously with the electromechanical measurements. Figure 52 presents a scatterplot of the force of the sample used in the mechanical characterization as a function of strain. As a comparison, figure 53 presents a scatterplot of force as a function

of strain from Jari Suikkola's Master of Science thesis [51]. The sample used in Suikkola's work is a similar U-conductor using the same ink printed directly on the same TPU material that was used in this thesis. So, the only difference is that in this thesis there is the release film of the tattoo laminated on the TPU and the conductor is printed on the release film.

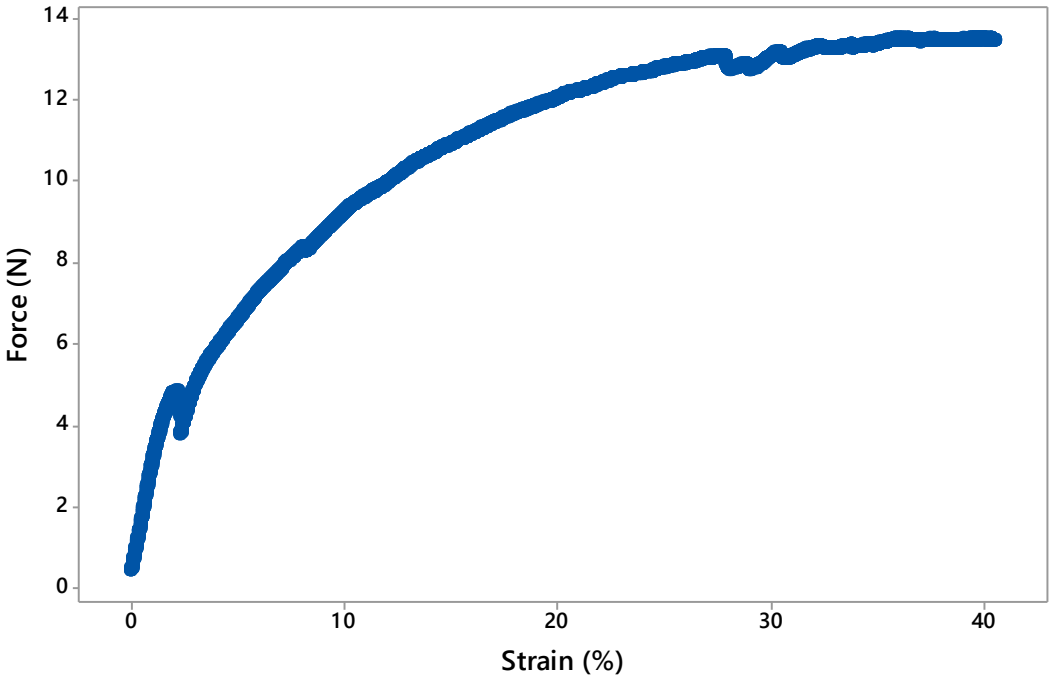

Figure 52. *A scatterplot of the force of the sample used in electromechanical characterization test as a function of strain.*

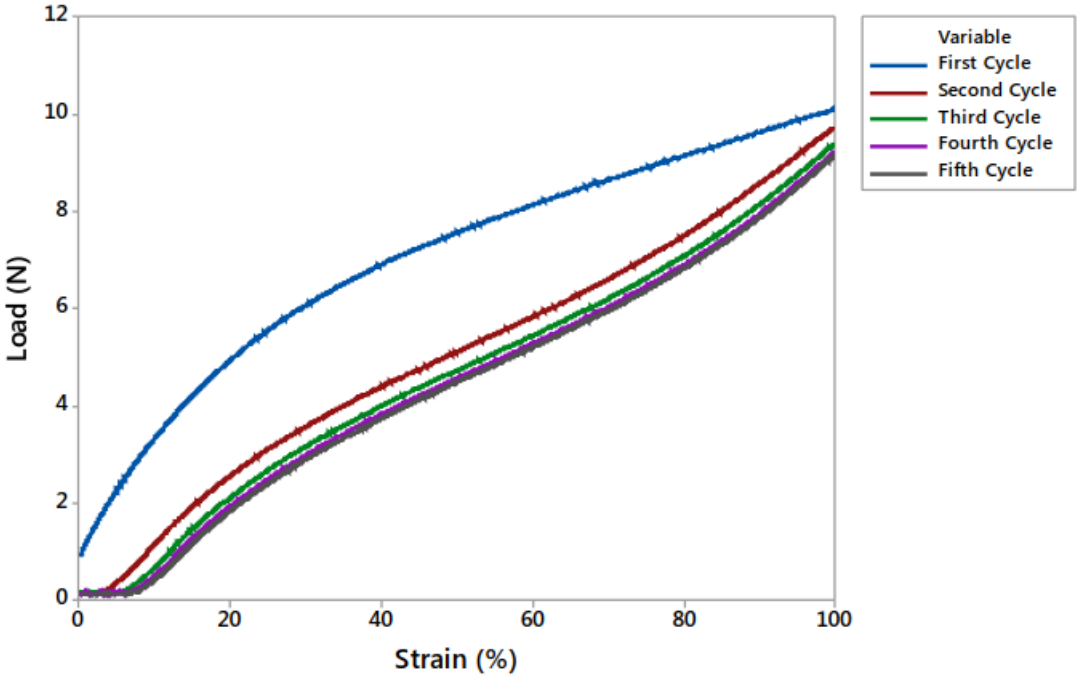

Figure 53. *A scatterplot of the force of one sample, used in Jari Suikkola's Master of Science thesis, as a function of strain [51, p. 50].*

While comparing the two figures above, the first cycle curve in figure 53 is the one used in the comparison. The stiffness of the tattoo–TPU bilayer used in this thesis seems to be much higher than the stiffness of Suikkola's sample, even though the release film is extremely thin and feels soft. However, the reason for such a difference in the stiffness' might not be due to the release film, but rather due to the adhesive layer used to laminate the release film on the TPU. During the measurements on the skin, it was observed that the adhesive was quite strong, which means that the chemical bonds between molecules in the adhesive are strong. This ultimately means that the adhesive layer is quite stiff after drying. Probably this stiffness causes the difference in the stiffness' in the above figures. This large stiffness could be also a reason for the large variations in the resistance in the electromechanical test in Instron 4411. The tattoos should be soft to feel comfortable to the user, and the above observations give another reason, in addition to a number of others already mentioned, not to use chemical adhesives.

In addition, conformability of the tattoos was observed by transferring a tattoo on the back of the hand of the test person. Since it is not simple to actually measure the conformability, it was only visually observed. Figure 54 presents a transfer tattoo on the test person's backhand.

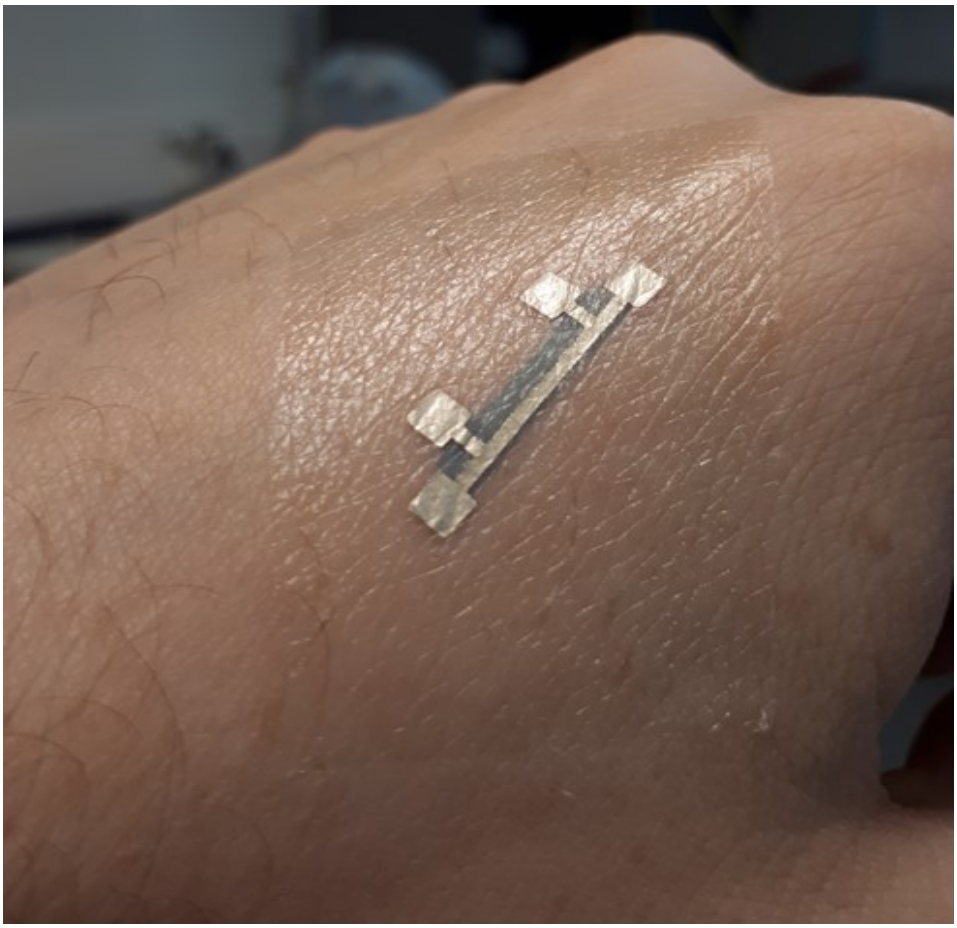

Figure 54. *A transfer tattoo on the back of the test person's hand.*

Examining the figure above, the surface features of the skin are visible. Furthermore, the conductor and the dielectric layer seem to have at least partially conformed to the skin since the surface features are visible on the printed layers. In addition, the conformability of the printed layers is important for minimizing the contact impedances, as discussed in chapter 3.1.3. This means that the conductors do not necessarily have to conform to the skin where there is a dielectric layer between the conductive layer and the skin, but only outside the dielectric layer areas. Observing the pads of the π-conductor, they seem to have conformed quite well. However, since it was necessary to use the adhesive film, the observed result could be biased if compared to the conformability of the tattoo without the adhesive. The adhesive film also insulates the conductive layer from the skin and thus, it would not be possible to use the adhesive layer in real applications.

7. CONCLUSIONS

This thesis focused on fabrication of electronic transfer tattoos by printing technologies. The aim was to achieve thin, stretchable, transparent, biocompatible, conformable and highly conductive structures. However, most of these were not achieved.

There was no specific target value set for the sheet resistance of the fabricated tattoos, but the calculated mean value for the sheet resistance, with the big squares from set 2 and the samples from set 4 excluded, was 41.7 mΩ/□ with a 6.2 mΩ/□ standard deviation. This sheet resistance can be considered quite low and is suitable for many high-frequency applications and communication circuits. However, in Jari Suikkola's thesis, the achieved sheet resistance with the same conductive ink and the same screen printer was 36.3 mΩ/□ with a 4.5 mΩ/□ standard deviation [51]. In addition, according to the technical datasheet of the CI-1036 ink, the sheet resistance should be less than 10 mΩ/□ [42]. However, since the thickness of the printed layer is inversely proportional to the sheet resistance, it is possible that the layers printed in this thesis were thinner than the advised thickness. Furthermore, the tattoo paper could have an effect on the sheet resistance.

The fabricated tattoos were supposed to be thin to be comfortable and to conform to the skin, which would allow mounting without adhesives. Unfortunately, due to the limited time and resources, thickness measurements were not done. However, the advised layer thickness, according to the datasheet of the CI-1036 ink, was 8 µm [42]. Using equation (2) to calculate the theoretical resistivity with the sheet resistance and target film thickness in the datasheet, and then inserting that resistivity and the sheet resistance obtained in this thesis back to equation (2), the thickness of the screen printed tattoos would be 1.9 µm on average.

The elongation at break achieved during the electromechanical tests was approximately 19.4 %. It was stated that the maximum strain that the human skin experiences is around 30 % and thus, using the fabricated tattoos on anatomic locations with high strains would not be possible. In his thesis, Suikkola has reported interconnects with elongations at break of over 70 %, and strains on the order of 30–40 % were easily reached without the interconnects breaking. However, Suikkola printed his interconnects directly on TPU, and it has been stated that the behavior of the interconnect–substrate interface has an effect on the resistance of the interconnect. [51] In addition, the reliability of the results cannot be guaranteed due to the small sample sizes used in the measurements.

Biocompatibility is not easy to measure and is a somewhat subjective concept. The used materials did not cause allergic reactions, itching, tearing or any other harsh body reactions. It was also tested with the tattoo paper alone that transferring and removing it from the skin is pain free. However, probably due to the tattoo paper being exposed to too high

temperatures for long periods of time, the transferability of the tattoos suffered, and it was necessary to use an adhesive film. Thus, removing the tattoos became quite difficult, painful and caused reddening of the skin.

Measuring conformability is also not simple. In this thesis, conformability was only observed visually. Conformability depends on the thickness along with various other properties of the thin film. However, it is not possible to tell, since it was not studied, that how thin the screen printed layers would have to be to fully conform. There was some conforming observed, but the adhesive film probably improved it.

Transparency was one of the objectives for the fabricated tattoos. Unfortunately, this was not achieved at all due to the flake-like particles in the CI-1036 ink. It is simply not possible to achieve transparent layers with that ink. Originally, the new inks were acquired due to their theoretical potential to produce transparent layers. However, the inks did not perform the way they should have. Nevertheless, it was confirmed by spin coating that the AgNW ink produces transparent layers, although the thickness and uniformity of the layers are not known.

In addition to the properties of the tattoos, the new conductive inks were characterized and analyzed. It was concluded that they do not work properly. The reasons are probably too long particles and poor wetting of the nozzle plate by water. The length of the 1D materials used in the AgNW and CNT inks are in the micrometer range, and the largest recommended particle size for the Dimatix printer is approximately 200 nm. Thus, clogging of the nozzles was possible. In addition, during the drop casting test of the AgNW ink, there was patterns resembling the human nervous system observed. Those dark patterns could have been formed by agglomerated AgNWs. If this is the case, then the AgNWs could have agglomerated also in the ink cartridge increasing the probability of the nozzle clogging. The graphene ink has a particle size of 80–500 nm according to the supplier of the ink. The particle size might not be the cause of the poor jettability in this case, but the water as a solvent could.

The tattoo paper was also characterized throughout the tests. It was concluded that the heat resistance of the paper is not sufficient for the process steps used. Even though low curing temperatures were used, they were still too high, or the curing times too long, for the tattoo paper. During printing, there seemed to be no problems. However, the stretchability of the release film is also concerning if the 19.4 % maximum strain, obtained from the mechanical tests, is reliable.

There were also some observations made about the fabrication and characterization methods. First, the screen printing process produces uniform quality overall, but there are some problems concerning the printer. The screen holder is tilted causing the ink to flow away from the front edge toward the back edge of the screen. The printing quality along the screen is also not completely uniform but seems to change in the longitudinal direction

of the screen. The printer being semi-automatic and not completely automatic is also a concern since there are too many variables with this printer.

In addition, it seems that designing patterns for 4PP measurements needs more attention. The big squares produced a little larger sheet resistance than the Greek crosses and π-conductors. Thus, the big squares were either difficult pattern to print or were designed poorly for 4PP measurements. However, since the deviations were quite small, and the sheet resistance of the big squares was basically equal to the sheet resistance of the U-conductors, the measurement setup is the more probable cause. The big squares probably should have had pads outside the measurement area, connected to the corners with short conductive traces, in a similar manner as the Greek crosses and π-conductors had. It was also stated that the slightly larger sheet resistance of the U-conductors compared to the Greek crosses and π-conductors was probably caused by the contact resistances of the used multimeter. This is one downside of 2-probe method.

The measurement setups used during the electromechanical and mechanical tests were also problematic. The problem actually arises from the fact that a contact needs to be made to the thin film. The contacts cause discontinuities in the stretchability of the film causing its premature breaking. In addition, mounting a thin film to the Instron 4411 is difficult without a carrier film. Furthermore, the carrier film produces biased data, and even if the mechanical properties of the carrier film are known, calculating the mechanical properties of the thin film from the biased data in not straightforward.

In general, the main problems during this thesis were the new materials and the measurement setups. The formulation of the inks need consideration, or alternatively inkjet printing needs development. The length of the 1D materials should not be decreased since longer particles allow higher conductivity. To avoid the clogging of the nozzles, the cavities should be larger. However, this would cause the jetted droplet size to increase causing the layer thicknesses to increase. This problem should be avoided if the wettability of the substrate and jetting velocity of the droplets can be increased. In addition, decreasing the inks' viscosity should provide lower layer thicknesses.

The resistance measurement setups caused problems in stretching tests due to the mechanical contacts that were necessary for sufficient electrical contacts. However, contactless sheet resistance measurement instruments, which could provide the solution, have been developed. Although, integrating such devices to tensile testers or using them in on-skin measurements needs consideration. In addition, tensile testing instruments for thin films need also development due to the encountered problems. However, one such device that utilizes buoyancy of water to support the thin film, and polydimethylsiloxane (PDMS) coated grips to make soft contacts via van der Waals forces to the surface of the thin film, has already been developed and demonstrated by Jae-Han Kim et al. [62]. Finally, due to the low sample sizes used in this thesis in the stretching tests, the reliability

of the results is unknown, and to get reliable results, the tests conducted should be repeated with higher sample sizes in the future.

REFERENCES

[1] D.-. Kim, N. Lu, R. Ma, Y.-. Kim, R.-. Kim, S. Wang, J. Wu, S.M. Won, H. Tao, A. Islam, K.J. Yu, T.-. Kim, R. Chowdhury, M. Ying, L. Xu, M. Li, H.-. Chung, H. Keum, M. McCormick, P. Liu, Y.-. Zhang, F.G. Omenetto, Y. Huang, T. Coleman, J.A. Rogers, Epidermal electronics, Science, Vol. 333, Iss. 6044, 2011, pp. 838–843.

[2] W.-. Yeo, Y.-. Kim, J. Lee, A. Ameen, L. Shi, M. Li, S. Wang, R. Ma, S.H. Jin, Z. Kang, Y. Huang, J.A. Rogers, Multifunctional epidermal electronics printed directly onto the skin, Advanced Materials, Vol. 25, Iss. 20, 2013, pp. 2773–2778.

[3] A.J. Casson, R. Saunders, J.C. Batchelor, Five Day Attachment ECG Electrodes for Longitudinal Bio-Sensing Using Conformal Tattoo Substrates, IEEE Sensors Journal, Vol. 17, Iss. 7, 2017, pp. 2205–2214.

[4] S. Kabiri Ameri, R. Ho, H. Jang, L. Tao, Y. Wang, L. Wang, D.M. Schnyer, D. Akinwande, N. Lu, Graphene Electronic Tattoo Sensors, ACS Nano, Vol. 11, Iss. 8, 2017, pp. 7634–7641.

[5] Electrical Resistivity; definition, formula & units, Electronics Notes, website. Available (accessed on 13.6.2018): https://www.electronics-notes.com/articles/basic_concepts/resistance/electrical-resistivity.php.

[6] Sheet Resistance: A Guide to Theory, Ossila, website. Available (accessed on 30.8.2018): https://www.ossila.com/pages/sheet-resistance-theory.

[7] Poisson's ratio, Engineering ToolBox, website. Available (accessed on 30.8.2018): https://www.engineeringtoolbox.com/poissons-ratio-d_1224.html.

[8] M.D. Dickey, Stretchable and Soft Electronics using Liquid Metals, Advanced Materials, Vol. 29, Iss. 27, 2017.

[9] Mercury and health, World Health Organization, website. Available (accessed on 2.7.2018): http://www.who.int/mediacentre/factsheets/fs361/en/.

[10] R. Balint, N.J. Cassidy, S.H. Cartmell, Conductive polymers: Towards a smart biomaterial for tissue engineering, Acta Biomaterialia, Vol. 10, Iss. 6, 2014, pp. 2341–2353.

[11] K.S. Novoselov, V.I. Fal'Ko, L. Colombo, P.R. Gellert, M.G. Schwab, K. Kim, A roadmap for graphene, Nature, Vol. 490, Iss. 7419, 2012, pp. 192–200.

[12] A.K. Geim, Graphene: Status and prospects, Science, Vol. 324, Iss. 5934, 2009, pp. 1530–1534.

[13] Y. Wyser, C. Pelletier, J. Lange, Predicting and determining the bending stiffness of thin films and laminates, Packaging Technology and Science, Vol. 14, Iss. 3, 2001, pp. 97–108.

[14] W. Dang, V. Vinciguerra, L. Lorenzelli, R. Dahiya, Printable stretchable interconnects, Flexible and Printed Electronics, Vol. 2, Iss. 1, 2017.

[15] D.-. Kim, J. Xiao, J. Song, Y. Huang, J.A. Rogers, Stretchable, curvilinear electronics based on inorganic materials, Advanced Materials, Vol. 22, Iss. 19, 2010, pp. 2108–2124.

[16] K.-. Kim, K.-. Jung, S.-. Jung, Design and fabrication of screen-printed silver circuits for stretchable electronics, Microelectronic Engineering, Vol. 120, 2014, pp. 216–220.

[17] Y. Zhang, H. Fu, Y. Su, S. Xu, H. Cheng, J.A. Fan, K. Hwang, J.A. Rogers, Y. Huang, Mechanics of ultra-stretchable self-similar serpentine interconnects, Acta Materialia, Vol. 61, Iss. 20, 2013, pp. 7816–7827.

[18] J. Suikkola, T. Björninen, M. Mosallaei, T. Kankkunen, P. Iso-Ketola, L. Ukkonen, J. Vanhala, M. Mäntysalo, Screen-Printing Fabrication and Characterization of Stretchable Electronics, Scientific Reports, Vol. 6, 2016.

[19] S. Yao, Y. Zhu, Nanomaterial-enabled stretchable conductors: Strategies, materials and devices, Advanced Materials, Vol. 27, Iss. 9, 2015, pp. 1480–1511.

[20] Y. Zhu, F. Xu, Buckling of aligned carbon nanotubes as stretchable conductors: A new manufacturing strategy, Advanced Materials, Vol. 24, Iss. 8, 2012, pp. 1073–1077.

[21] B. McGinty, Column Buckling, Continuum Mechanics, website. Available (accessed on 1.9.2018): http://www.continuummechanics.org/columnbuckling.html.

[22] K.-. Kim, D.-. Jeong, N.-. Jang, S.-. Ha, J.-. Kim, Extremely stretchable conductors based on hierarchically-structured metal nanowire network, RSC Advances, Vol. 6, Iss. 62, 2016, pp. 56896–56902.

[23] Daniel Langley, Silver nanowire networks: effects of percolation and thermal annealing on physical properties, Doctor of Science thesis, Université de Grenoble, 2014, 152 p. Available (accessed on 1.9.2018): https://tel.archives-ouvertes.fr/tel-01133345/document.

[24] T. Araki, M. Nogi, K. Suganuma, M. Kogure, O. Kirihara, Printable and stretchable conductive wirings comprising silver flakes and elastomers, IEEE Electron Device Letters, Vol. 32, Iss. 10, 2011, pp. 1424–1426.

[25] N. Matsuhisa, M. Kaltenbrunner, T. Yokota, H. Jinno, K. Kuribara, T. Sekitani, T. Someya, Printable elastic conductors with a high conductivity for electronic textile applications, Nature Communications, Vol. 6, 2015.

[26] CLIP COMPEX ELECTRODES, SIZE 5X5, Biomedical Therapy, website. Available (accessed on 4.7.2018): http://www.biomedical-therapy.com/area-medica_1/electrodos-compex-de-clip-tamano-5x5_1.

[27] A.J. Gallagher, A. Ní Anniadh, K. Bruyere, M. Otténio, H. Xie, M.D. Gilchrist, Dynamic tensile properties of human skin, 2012 IRCOBI Conference Proceedings - International Research Council on the Biomechanics of Injury, 12–14 September, 2012, Dublin, Ireland, pp. 494–502.

[28] D. Williams, Concepts in biocompatibility: new biomaterials, new paradigms and new testing regimes, in: J. Boutrand (ed.), Biocompatibility and Performance of Medical Devices, Woodhead Publishing, Cambridge, UK, 2012, pp. 3–17.

[29] L. Wang, N. Lu, Conformability of a thin elastic membrane laminated on a soft substrate with slightly wavy surface, Journal of Applied Mechanics, Transactions ASME, Vol. 83, Iss. 4, 2016.

[30] X. Zhang, Van der Waals Forces, in: Q.J. Wang, Y. Chung (ed.), Encyclopedia of Tribology, Springer US, Boston, MA, 2013, pp. 3945–3947.

[31] C.P. Hendriks, S.E. Franklin, Influence of Surface Roughness, Material and Climate Conditions on the Friction of Human Skin, Tribology Letters, Vol. 37, Iss. 2, 2010, pp. 361–373.

[32] A. Ram, Fundamentals of Polymer Engineering, Springer US, Boston, MA, 1997, 237 p.

[33] D.S. Hecht, L. Hu, G. Irvin, Emerging transparent electrodes based on thin films of carbon nanotubes, graphene, and metallic nanostructures, Advanced Materials, Vol. 23, Iss. 13, 2011, pp. 1482–1513.

[34] J.A. Soares, Introduction to optical characterization of materials, in: M. Sardela (ed.), Practical Materials Characterization, Springer, New York, NY, 2014, pp. 43–92.

[35] R.R. Nair, P. Blake, A.N. Grigorenko, K.S. Novoselov, T.J. Booth, T. Stauber, N.M.R. Peres, A.K. Geim, Fine structure constant defines visual transparency of graphene, Science, Vol. 320, Iss. 5881, 2008, pp. 1308.

[36] Temporary Tattoo, Advameg, website. Available (accessed on 2.9.2018): http://www.madehow.com/Volume-4/Temporary-Tattoo.html.

[37] How small can the naked eye see?, Immediate Media Company, website. Available (accessed on 1.9.2018): https://www.sciencefocus.com/the-human-body/how-small-can-the-naked-eye-see/.

[38] Silver Nanowire Coating Ink A30, Novarials Corporation, website. Available (accessed on 3.5.2018): http://www.novarials.com/ProductsAgNWCIA30.html.

[39] Technical Data Sheet Nink-1000, NanoLab Incorporation. Available (accessed on 8.5.2018): https://sep.yimg.com/ty/cdn/nanolab2000/Nink1000-TDS-2017.pdf?t=1511629666&.

[40] Graphene ink in water, Sigma-Aldrich Incorporation, website. Available (accessed on 8.5.2018): https://www.sigmaaldrich.com/catalog/product/aldrich/808288?lang=fi&region=FI.

[41] NANOPASTE® series, Harimatec Incorporation, sales brochure. Available (accessed on 9.5.2018): http://harimatec.com/wp/pdf/NANOPASTE_series.pdf.

[42] Technical Data Sheet CI-1036, Engineered Materials Systems Incorporation, 2017.

[43] Technical Data Sheet DI-7540, Engineered Materials Systems Incorporation, 2014.

[44] Poly(methyl methacrylate), Alfa Aesar, product specification datasheet. Available (accessed on 14.5.2018): https://www.alfa.com/en/prodspec/043982.

[45] Tolueeni, VWR Chemicals, website. Available (accessed on 14.5.2018): https://fi.vwr.com/store/catalog/product.jsp?catalog_number=28681.295.

[46] Printable Tattoo Paper, Silhouette Europe, website. Available (accessed on 14.5.2018): http://www.silhouettecameoeurope.com/printable-tattoo-paper.html.

[47] V. Sanchez-Romaguera, M.A. Ziai, D. Oyeka, S. Barbosa, J.S.R. Wheeler, J.C. Batchelor, E.A. Parker, S.G. Yeates, Towards inkjet-printed low cost passive UHF RFID skin mounted tattoo paper tags based on silver nanoparticle inks, Journal of Materials Chemistry C, Vol. 1, Iss. 39, 2013, pp. 6395–6402.

[48] Dimatix Materials Printer DMP-2850, Fujifilm, website. Available (accessed on 9.7.2018): http://www.fujifilmusa.com/products/industrial_inkjet_print-heads/deposition-products/dmp-2800/index.html.

[49] M. Singh, H.M. Haverinen, P. Dhagat, G.E. Jabbour, Inkjet printing-process and its applications, Advanced Materials, Vol. 22, Iss. 6, 2010, pp. 673–685.

[50] K.-. Sung, J. Park, H. Kang, Multi-Layer Inkjet Printing of Ag Nanoparticle Inks and Its Sintering with a Near-Infrared System, International Journal of Precision Engineering and Manufacturing, Vol. 19, Iss. 2, 2018, pp. 303–307.

[51] J. Suikkola, Printed Stretchable Interconnects for Wearable Health and Wellbeing Applications, Master of Science thesis, Tampere University of Technology, 2015, 59 p. Available: https://dspace.cc.tut.fi/dpub/handle/123456789/23448.

[52] M. Hösel Screen printing, DTU Energy, website. Available (accessed on 2.9.2018): http://plasticphotovoltaics.org/lc/lc-fabrication/lc-printing/lc-screen.html.

[53] Spin Coating Theory, University of Louisville, 2013. Available (accessed on 28.8.2018): https://louisville.edu/micronano/files/documents/standard-operating-procedures/SpinCoatingInfo.pdf.

[54] WS-650-8B Spin Coater, Laurell Techologies Incorporation, website. Available (accessed on 24.8.2018): http://www.laurell.com/spin-coater/?model=WS-650-8B.

[55] Polymethacrylates, Polymer Properties Database, website. Available (accessed on 29.8.2018): http://polymerdatabase.com/polymer%20classes/Polymethacrylate%20type.html.

[56] Performing van der Pauw Sheet Resistance Measurements Using the Keithley S530 Parametric Tester, Keithley Instruments, Inc, Application Note Series, 2012. Available (accessed on 3.9.2018): download.tek.com/document/S530_VanDerPauwSheetRstnce.pdf.

[57] I. Miccoli, F. Edler, H. Pfnür, C. Tegenkamp, The 100th anniversary of the four-point probe technique: The role of probe geometries in isotropic and anisotropic systems, Journal of Physics Condensed Matter, Vol. 27, Iss. 22, 2015, pp 29.

[58] Spin Coating: A Guide to Theory and Techniques, Ossila, website. Available (accessed on 3.9.2018): https://www.ossila.com/pages/spin-coating.

[59] H.R. Patil, H.B. Huntington, Electromigration and associated void formation in silver, Journal of Physics and Chemistry of Solids, Vol. 31, Iss. 3, 1970, pp. 474.

[60] H.H. Khaligh, I.A. Goldthorpe, Failure of silver nanowire transparent electrodes under current flow, Nanoscale Research Letters, Vol. 8, Iss. 1, 2013, pp. 235.

[61] M.B. Heaney, Electrical Conductivity and Resistivity, in: J.G. Webster (ed.), Electrical Measurement, Signal Processing, and Displays, CRC Press, 2003, pp. 14.

[62] J.-. Kim, A. Nizami, Y. Hwangbo, B. Jang, H.-. Lee, C.-. Woo, S. Hyun, T.-. Kim, Tensile testing of ultra-thin films on water surface, Nature Communications, Vol. 4, 2013.

APPENDIX A: ONE-WAY ANOVA: PATTERNS IN SETS 1–3

Method

Null hypothesis	All means are equal
Alternative hypothesis	Not all means are equal
Significance level	α = 0,05
Rows unused	17

Equal variances were not assumed for the analysis.

Factor Information

Factor	Levels	Values
Factor	11	π_set1; U_set1; GC_set1; BS_set1; π_set2; U_set2; GC_set2; π_set3; U_set3; GC_set3; BS_set3

Welch's Test

Source	DF Num	DF Den	F-Value	P-Value
Factor	10	18,0439	2,02	0,093

Model Summary

R-sq	R-sq(adj)	R-sq(pred)
17,94%	1,19%	0,00%

Means

Factor	N	Mean	StDev	95% CI
π_set1	7	38,908	2,620	(36,485; 41,331)
U_set1	5	43,206	1,434	(41,425; 44,987)
GC_set1	6	42,57	5,84	(36,44; 48,70)
BS_set1	4	44,02	4,50	(36,85; 51,19)
π_set2	7	41,09	5,28	(36,22; 45,97)
U_set2	5	43,84	6,79	(35,41; 52,28)
GC_set2	5	37,80	4,47	(32,25; 43,35)
π_set3	7	41,46	10,55	(31,71; 51,22)
U_set3	5	45,22	8,96	(34,10; 56,34)
GC_set3	5	37,30	5,29	(30,73; 43,87)
BS_set3	4	45,32	3,70	(39,44; 51,21)

APPENDIX B: ONE-WAY ANOVA: PATTERNS IN SET 4

Method

Null hypothesis	All means are equal
Alternative hypothesis	Not all means are equal
Significance level	α = 0,05
Rows unused	7

Equal variances were assumed for the analysis.

Factor Information

Factor	Levels	Values
Factor	4	π_set4; U_set4; GC_set4; BS_set4

Analysis of Variance

Source	DF	Adj SS	Adj MS	F-Value	P-Value
Factor	3	653,3	217,76	2,98	0,060
Error	17	1241,0	73,00		
Total	20	1894,3			

Model Summary

S	R-sq	R-sq(adj)	R-sq(pred)
8,54399	34,49%	22,93%	0,00%

Means

Factor	N	Mean	StDev	95% CI
π_set4	7	53,92	5,58	(47,11; 60,73)
U_set4	5	61,78	4,73	(53,72; 69,85)
GC_set4	5	67,80	11,97	(59,74; 75,87)
BS_set4	4	65,15	11,43	(56,14; 74,17)

Pooled StDev = 8,54399

APPENDIX C: ONE-WAY ANOVA: SETS 1–3

Method

Null hypothesis	All means are equal
Alternative hypothesis	Not all means are equal
Significance level	α = 0,05
Rows unused	24

Equal variances were assumed for the analysis.

Factor Information

Factor	Levels	Values
Factor	3	Set 1; Set 2; Set 3

Analysis of Variance

Source	DF	Adj SS	Adj MS	F-Value	P-Value
Factor	2	13,59	6,794	0,17	0,842
Error	57	2245,00	39,386		
Total	59	2258,58			

Model Summary

S	R-sq	R-sq(adj)	R-sq(pred)
6,27582	0,60%	0,00%	0,00%

Means

Factor	N	Mean	StDev	95% CI
Set 1	22	41,812	4,212	(39,133; 44,491)
Set 2	17	40,93	5,72	(37,89; 43,98)
Set 3	21	42,10	8,21	(39,36; 44,85)

Pooled StDev = 6,27582

APPENDIX D: ONE-WAY ANOVA: DIFFERENT PATTERNS

Method

Null hypothesis	All means are equal
Alternative hypothesis	Not all means are equal
Significance level	α = 0,05
Rows unused	24

Equal variances were not assumed for the analysis.

Factor Information

Factor	Levels	Values
Factor	4	π; U; GC; BS

Welch's Test

Source	DF Num	DF Den	F-Value	P-Value
Factor	3	27,2495	3,19	0,039

Model Summary

R-sq	R-sq(adj)	R-sq(pred)
11,93%	7,21%	0,18%

Means

Factor	N	Mean	StDev	95% CI
π	21	40,49	6,72	(37,43; 43,55)
U	15	44,09	6,12	(40,70; 47,48)
GC	16	39,43	5,52	(36,49; 42,37)
BS	8	44,67	3,88	(41,43; 47,91)